TRANSPORTATION RESEARCH RECORD 852

Strength and Deformation Characteristics of Pavements

TRANSPORTATION RESEARCH BOARD

NATIONAL RESEARCH COUNCIL

NATIONAL ACADEMY OF SCIENCES
WASHINGTON, D.C. 1982

Transportation Research Record 852
Price $8.80
Edited for TRB by Naomi Kassabian

modes
1 highway transportation
4 air transportation

subject areas
24 pavement design and performance
62 soil foundations

Library of Congress Cataloging in Publication Data
Strength and deformation characteristics of pavements.

(Transportation research record; 852)
Reports presented at the 61st annual meeting of the Transportation Research Board.
1. Pavements—Testing—Addresses, essays, lectures. I. National Research Council (U.S.). Transportation Research Board. II. Series.
TE7.H5 no.852 [TE250] 380.5s [625.8'028'7] 82-14449
ISBN 0-309-03356-X ISSN 0361-1981

Sponsorship of the Papers in This Transportation Research Record

GROUP 2—DESIGN AND CONSTRUCTION OF TRANSPORTATION FACILITIES
R.V. LeClerc, consultant, Olympia, Washington, chairman

Pavement Design Section
W. Ronald Hudson, University of Texas at Austin, chairman

Committee on Pavement Condition Evaluation
K.H. McGhee, Virginia Highway & Transportation Research Council, chairman
Doyt Y. Bolling, Michael I. Darter, Karl H. Dunn, Asif Faiz, Robert H. Gietz, Wouter Gulden, Lawrence F. Hart, William H. Highter, W. Ronald Hudson, Don H. Kobi, Scott A. Kutz, J.W. Lyon, Jr., Robert L. Novak, Richard D. Pavlovich, William A. Phang, Freddy L. Roberts, Albert F. Sanborn, Lawrence L. Smith, Herbert F. Southgate, Elson B. Spangler, Shiraz D. Tayabji, Loren M. Womack

Committee on Strength and Deformation Characteristics of Pavement Sections
Amir N. Hanna, Portland Cement Association, chairman
Richard D. Barksdale, Stephen F. Brown, George R. Cochran, Gaylord Cumberledge, Jim W. Hall, Jr., R.G. Hicks, Robert K.H. Ho, Ignat V. Kalcheff, William J. Kenis, Thomas W. Kennedy, Erland Lukanen, Kamran Majidzadeh, Lufti Raad, J. Brent Rauhut, Quentin L. Robnett, Jatinder Sharma, Gary Wayne Sharpe, James F. Shook, Eugene L. Skok, Jr., T. Paul Teng, Mian-Chang Wang

Lawrence F. Spaine, Transportation Research Board staff

Sponsorship is indicated by a footnote at the end of each report. The organizational units, officers, and members are as of December 31, 1981.

Contents

Authors of the Papers in This Record

Freeme, C.R., National Institute for Transport and Road Research, Council for Scientific and Industrial Research, P.O. Box 385, Pretoria, 0001, South Africa
Heisey, J.S., Woodward-Clyde Consultants, 201 Willowbrook Boulevard, Wayne, NJ 07470
Hoffman, Mario S., Department of Civil Engineering, Louisiana State University, Baton Rouge, LA 70803
Kallas, Bernard F., The Asphalt Institute, Asphalt Institute Building, College Park, MD 20740
Kenis, William J., Federal Highway Administration, 400 7th Street, S.W., Washington, DC 20590
Maree, J.H., National Institute for Transport and Road Research, Council for Scientific and Industrial Research, P.O. Box 385, Pretoria, 0001, South Africa
McCullough, B. Frank, Center for Transportation Research, University of Texas at Austin, Austin, TX 78712
Meyer, A.H., University of Texas at Austin, Austin, TX 78712
Rada, Gonzalo, Department of Civil Engineering, Building J, Room 2125, University of Maryland, College Park, MD 20742
Sherwood, James A., Federal Highway Administration, 400 7th Street, S.W., Washington, DC 20590
Shook, James F., The Asphalt Institute, Asphalt Institute Building, College Park, MD 20740
Stokoe, K.H. II, University of Texas at Austin, Austin, TX 78712
Taute, Arthur, 202 Roos Street, Meyerspark, Pretoria 0184, South Africa
Thompson, Marshall R., Department of Civil Engineering, University of Illinois at Urbana-Champaign, 104 South Wright Street, Urbana, IL 61801
Van Zyl, N.J.W., National Institute for Transport and Road Research, Council for Scientific and Industrial Research, P.O. Box 385, Pretoria, 0001, South Africa
Witczak, Matthew W., Department of Civil Engineering, Building J, Room 2125, University of Maryland, College Park, MD 20742

Ordway Colorado Experimental Base Project

JAMES F. SHOOK AND BERNARD F. KALLAS

The Ordway Colorado Experimental Base Project was a full-scale field experiment constructed with various thicknesses of two full-depth hot-mix sand asphalt bases, one full-depth asphalt concrete base, and one thickness of a standard design with untreated base and subbase layers and two different subgrades (A-6 and A-7-6). The project was planned as an American Association of State Highway Officials (AASHO) Road Test satellite project to be useful in extending the AASHO Road Test findings to Colorado conditions. The primary objectives were (a) to determine relative thicknesses of one asphalt concrete base, two hot-mix sand asphalt bases, and one standard design with untreated base and subbase required to give an equal level of pavement performance and (b) to relate certain measured properties of the pavement and the pavement components to observed levels of performance by using both empirical and theoretical models for pavement behavior. Performance data indicated that the different base types had different abilities to resist various forms of distress: (a) the asphalt concrete base mixture provided the best resistance to rutting and to all forms of cracking, (b) both hot-mix sand asphalt bases provided good resistance to alligator cracking but the low-stability hot-mix sand asphalt mix provided less resistance to rutting than the other bases, (c) the untreated standard base and subbase provided the best resistance to rutting but the least resistance to alligator or load-associated cracking. All base types exhibited severe transverse shrinkage cracking conditions. Analysis of rut depth and deflection data produced the following average layer coefficients: asphalt concrete surface course, 50 mm (2 in) thick, >0.44; asphalt concrete base course, 0.34; hot-mix sand asphalt base, 0.24-0.28; and untreated aggregate base and subbase, 0.16.

The Colorado Experimental Base Project was a full-scale field experiment constructed with various thicknesses of two full-depth hot-mix sand asphalt bases, one full-depth asphalt concrete base, and one thickness of a standard design with untreated base and subbase layers. The project was opened to traffic in 1965; routine measurements were discontinued in 1976. A final set of measurements was made in 1978.

The Colorado Experimental Base Project was planned as an American Association of State Highway Officials (AASHO) Road Test satellite project to be useful in extending the AASHO Road Test findings to Colorado conditions. The primary objectives were as follows:

1. To determine relative thicknesses of one asphalt concrete base, two hot-mix sand asphalt bases, and one standard design with untreated base and subbase required to give an equal level of pavement performance and
2. To relate certain measured properties of the pavement and the pavement components to observed levels of performance by using both empirical and theoretical models for pavement behavior.

The experiment was planned, designed, and constructed by the Colorado Department of Highways with the cooperation of the Federal Highway Administration and the Asphalt Institute. Continued surveillance and an extensive testing program were conducted by research personnel of the Department.

Several reports have been released to date on the project; they include summarized construction test data, field-performance measurements made during the first year, a subgrade moisture study, a deflection-temperature study, laboratory-determined mechanical properties of materials for elastic analysis, and a study of mechanical properties by using field dynamic-testing techniques (1-7). This report summarizes the field-performance data obtained during the period 1965-1978 and reports the results of analyses of the performance data. The final report (8) includes additional details of these analyses and tables of test data.

EXPERIMENT DESIGN

Two soil types, an A-7-6 with a California bearing ratio (CBR) of 2.6 and an A-6 with a CBR of 3.4, were included in the experiment, as shown in Table 1. Test sections were located within each soil type by a random process. There was a total of 20 test sections; each test section had a westbound and an eastbound lane. Test sections were 137.2 m (450 ft) long with an additional 15.2-m (50-ft) transition section at each end of the test section reserved for destructive testing.

Thicknesses were selected to give a maximum design life of approximately 20 years. Two thinner levels were selected in an attempt to obtain earlier failures. Traffic estimates made in 1978 indicated that the accumulated number of equivalent 80-kN (18 000-lbf) single-axle load applications (ESALs) applied between 1965 and 1978, when the last series of field measurements was made, totaled approximately 140 000.

MATERIALS AND CONSTRUCTION

The asphalt concrete surfacing had a well-graded aggregate and an asphalt content of 5.6 percent. The coarse aggregate contained at least 60 percent crushed material with at least two crushed faces. The asphalt concrete base contained slightly less fine aggregate than the surfacing but approximately the same percentage of asphalt. The aggregate used for the asphalt concrete base was similar to that used on the AASHO Road Test and was not crushed. The hot-mix sand asphalts contained 8 percent asphalt and 3-6 percent air voids. Average Marshall stability values for the sand asphalts were 2.0 kN (451 lbf) for the low-stability mix and 3.4 kN (770 lbf) for the high-stability mix. The higher stability of the high-stability mix was obtained by adding additional mineral filler to the low-stability mix. The Marshall stability of the asphalt concrete base was 5.2 kN (1170 lbf). The asphalt used for all three bases was a 60-70 penetration-grade asphalt with a mean penetration of 67.

The test sections identified as Colorado Standard were constructed by using an uncrushed gravel base and subbase. The base had a maximum size of 12.7 mm (0.5 in) and 9 percent passing the 75-μm (No. 200) sieve. The -425-μm (No. 40) sieve fractions were nonplastic. The subbase had a maximum size of 76.2 mm (3 in) and 5 percent passing the 75-μm sieve. It was nonplastic.

FIELD INSTRUMENTATION AND MEASUREMENTS PROGRAM

The objective of the field-measurement program was to determine the performance and load-response characteristics of the test section. Present serviceability index (PSI) was measured with the CHLOE profilometer developed on the AASHO Road Test (9,10). PSI was calculated by using the following formulas. The initial formula was as follows:

$$PSI = 5.03 - 1.91 \log(SV - 2.0) - 0.01(C + P)^{1/2} - 1.38\,\overline{RD}^2 \quad (1)$$

where terms are defined as they were on the AASHO Road Test (9,10) and

Table 1. Experiment design.

	Soil Type				
	A-7-6			A-6	
	Base Thickness (in)				
Base Type[a]	140	178	216	140	178
Asphalt concrete (AC)	X	X	XX	X	X
Hot-mix sand asphalt					
Low stability (LSS)	X	X	XX	X	XX
High stability (HSS)	X	X	X		
Standard Design[b]		XXX			X

Note: 1 mm = 0.04 in.
X = one test section.

[a] Uniform 50-mm asphalt concrete surface course on all sections.
[b] 102-mm untreated base and 356-mm untreated subbase.

SV = slope variance from the CHLOE profilometer,
C + P = amount of class 2 and class 3 cracking plus patching (m^2/1000 m^2 of pavement), and
$\overline{RD}$ = average rut depth (mm/25.4).

Beginning in 1972, PSI was also corrected for texture by using the texturemeter described by Scrivner (10). A correction term was determined from tests on pavements that had a range in textures (11). A slight modification was also made in the PSI equation. The modified PSI equation used was as follows:

$$PSI = 4.85 - 1.91 \log(SV - 2.0) - 0.01(C + P)^{1/2} - 1.38\,\overline{RD}^2 \quad (2)$$

The texture correction was made as follows:

$$PSI\ (corrected) = PSI + 0.140(T)^{0.560} \quad (3)$$

where T is average texture determined with the texturemeter.

Rut depths were measured with the AASHO Road Test (9) rut-depth gauge for the routine-measurement program. The device measures the depth of rut over a 1.22-m (4-ft) span. Several randomly located spots were measured.

Cracking maps were prepared for each test section and updated periodically. Class 2 and class 3 cracks, identified as alligator cracks, were reported in square meters per 100 square meters of pavement. Class 2 cracks were defined (9,10) as cracking that has progressed to the stage at which the cracks become connected to form a grid-type pattern. Class 3 cracking was defined as that in which segments of the pavement surface have become loose. The number of transverse cracks and the total linear meters of all cracks, both longitudinal and transverse, also were reported.

The procedure adopted for the Benkelman-beam deflection measurement was the pavement-rebound procedure by using a 40-kN (9000-lbf) wheel load as published by the Canadian Good Roads Association (12) and the Asphalt Institute (13). For each test series, five locations in the outer wheel path of each lane of each test section were selected at random for testing. Thus, a total of 10 deflections was obtained for each test section.

Benkelman-beam deflection data were reported as recorded and as corrected to a standard temperature of 21.1°C (70°F). Temperature corrections were made by using curves developed in part from data collected on the project as described by Kingham (14) and which had been included in the Asphalt Institute publication (13) for many years. Temperatures were measured by using thermocouples until 1971, when the imbedded thermocouples were no longer giving satisfactory service. Afterwards the procedure described in the Asphalt Institute publication (13, Chap. XII) was used to estimate pavement temperatures. This procedure uses the pavement surface temperature and the preceding five-day mean air temperature.

Radius of curvature was determined by using the Dehlen curvature meter (15). Curvature data were not used in the analysis of performance data and are not reported in this paper.

LABORATORY MATERIALS CHARACTERIZATION STUDIES

The objective of the laboratory materials characterization program was to obtain data that could be used to apply elastic theory to a study of the pavement performance data. The tests included (a) triaxial compression resilient modulus M_r tests on the subgrade soils and untreated base and subbase materials, (b) unconfined dynamic modulus $|E^*|$ on the asphalt concrete surface and base mixtures and the two hot-mix sand asphalt base mixtures, and (c) repeated-load flexural fatigue tests on the asphalt concrete surface and base mixtures and the two hot-mix sand asphalt base mixtures. The tests were performed in the Asphalt Institute laboratory.

Repeated-load triaxial compression tests were performed to determine the resilient modulus M_r of the subgrade soils and the untreated granular subbase and base materials. Procedures and equipment for M_r determinations are described by Kallas and Riley (2) and in the Asphalt Institute Soils Manual (16). The data showed that the M_r of the subgrade soil--depending on soil type, water content, density, and the deviator stress and confining pressure test conditions--ranged between 27.6 and 227.5 MPa (4000 and 33 000 psi). The M_r of both the gravel aggregate base and subbase, depending on water content, density, and deviator stress and confining pressure test conditions, varied between 82.7 and 448 MPa (12 000 and 65 000 psi).

Dynamic modulus $|E^*|$ and phase lag ϕ were determined on laboratory-prepared samples of the asphalt concrete surface and base-course mixtures and on the low-stability and high-stability hot-mix sand asphalt base-course mixtures at temperatures of 4.4, 21.1, and 37.8°C (40, 70, and 100°F). Loading frequencies of 1, 4, and 16 Hz were used at each test temperature. Equipment and procedures for these tests have been described elsewhere (2).

Dynamic-modulus tests also were performed on cores to obtain information on modulus changes of the asphalt base courses with aging and traffic and for comparison with the modulus of laboratory-prepared specimens. Cores were obtained in 1965 shortly after the project was opened to traffic, in 1971 after the first pavement cracking was observed, and in 1976 at the time the final field measurements were made. Cores were obtained from wheel-path locations but not from the same test section at each sampling. Thus, modulus test results for cores include any variations due to the sampling location. Dynamic modulus $|E^*|$ and phase lag ϕ were determined at the same temperature and loading frequencies used for laboratory specimens except that the 1971 and 1976 core tests were also made with loading frequencies of 0.01 and 0.1 Hz at temperatures of -12.2 and 4.4°C (10 and 40°F) to obtain modulus data at lower temperatures and longer loading times.

Average values of $|E^*|$ for loading frequencies of 1, 4, and 16 Hz at each test temperature of 4.4, 21.1, and 37.8°C are shown in Figure 1. Average $|E^*|$ values for the asphalt concrete base show an increasing trend from 1965 to 1976. Average $|E^*|$ values for both low-stability and high-

stability sand asphalt bases increased from 1965 to 1971 and then decreased from 1971 to 1976 to slightly below the 1965 levels. Average |E*| levels of asphalt concrete base were considerably above those of the sand asphalt base course.

Relationships between |E*| at 4 Hz and temperature for laboratory-prepared specimens and the 1965, 1971, and 1976 cores are shown in Figures 2 and 3, respectively, for the asphalt concrete base and the low-stability sand asphalt base. The |E*| of the laboratory specimens was about 12-33 percent greater than that for the 1965, 1971, and 1976 core specimens. Based on core test results, the modulus changes in all the asphalt base courses are relatively small and generally less than the difference between the modulus of laboratory-prepared specimens and the modulus of the cores.

Repeated-load flexure tests were made to determine constant stress fatigue behavior of the asphalt concrete surface and base courses and the high-stability and low-stability sand asphalt base courses. Equipment and procedures for the fatigue tests have been described by Kallas and Puzinauskas (17). Constants, correlation coefficients, and standard errors are given in Table 2 for the least-squares regression equation $N_f = k_1(1/\epsilon)^n$ for log-log plots of initial bending strain ϵ versus number of load applications to fracture N_f for the asphalt courses.

Test properties of the original asphalt and of asphalt extracted from the 1976 asphalt base and surface course cores are given in Table 3. Compared with the test properties of the original asphalt, there was little change in the consistency of the asphalt in the asphalt base courses from 1965 to 1976. The asphalt hardened slightly more in the asphalt concrete base than in the sand asphalt base courses. The asphalt hardened considerably more in the asphalt concrete surface course than in the base course.

ANALYSIS OF ROUTINE FIELD-PERFORMANCE DATA

An overall picture of the relative performance of different test sections at the end of the measurement period can be found in Table 4, a summary of measurements made in September 1978. The 1978 data were the last set obtained on the project. Measurements included in Table 4 are PSI, rut depth, cracking, and deflection. Averages for both eastbound and westbound roadways are given.

In 1976 and 1977, a preliminary study was made of selected data collected between 1970 and 1976 by using analysis-of-variance (ANOVA) techniques. The following measurements were included in the study: PSI, corrected for texture; rut depth; linear meters of cracking per 1000 square meters of pavement; alligator cracking; number of transverse cracks; linear meters of transverse cracking; and Benkelman-beam deflection, corrected for temperature. The purpose of the analysis was to determine base type or base thickness effects as measured by these parameters, one of the major objectives of the project. The analysis was made for the test sections on the A-7-6 soil type (Sections 1 through 14) and for each year and each lane, where data permitted. A conventional two-way ANOVA with a single observation per cell and partial replication was used (18).

Figure 1. Average dynamic modulus of cores.

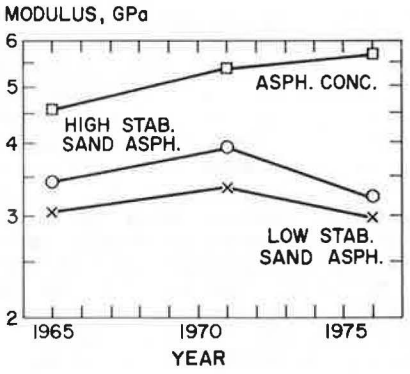

Figure 2. Temperature versus dynamic modulus: asphalt concrete base.

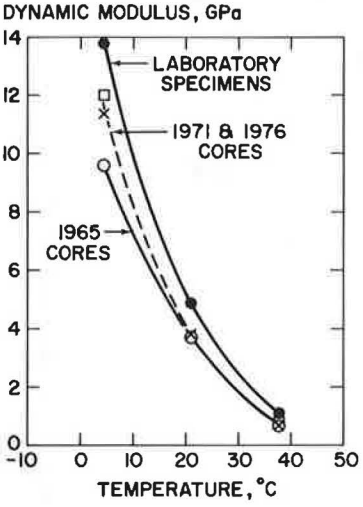

Figure 3. Temperature versus dynamic modulus: low-stability sand asphalt base.

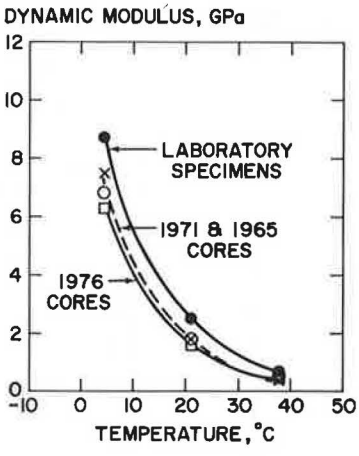

Table 2. Results of flexural fatigue tests on asphalt mixtures as function of strain.

Course	No. of Specimens	Temperature (°C)	Constant k_1	Constant n_1	Correlation Coefficient	SDE
AC surface	9	21	2.73×10^{-7}	3.25	0.91	0.52
AC base	8	21	2.01×10^{-5}	2.69	0.98	0.18
LSS asphalt	3	21	8.97×10^{-7}	3.25	0.99	0.13
HSS asphalt base	2	21	2.82×10^{-11}	4.60	-	-

Note: $t°C = (t°F - 32)/1.8$.

Results of the ANOVA indicated that, in general, there were no highly significant differences between base types or base thicknesses for most of the measurements and years included in the analysis. No significant differences in PSI could be attributed to either base type or base thickness. Visual inspection of the 1978 data summarized in Table 4 confirms this observation. A regression analysis of the PSI trend data also confirmed the conclusion, although there was a slight effect of thickness in this study.

The fact that there is almost no effect of base thickness on PSI loss indicates that most of the loss in PSI observed after 12 years of traffic was not load associated. The absence of alligator cracking in the sections with thin treated bases also supports this thesis. Surface erosion of the matrix from the surface of the pavement had a large effect on the PSI measurements made with the CHLOE profilometer and indicates that most of the PSI loss can be laid to environmental influences. The presence of alligator cracking in the standard sections with thin asphalt surfacing and untreated bases and the presence of a small amount of rutting in all sections indicates that axle loads did have an effect on the pavements, however.

A considerable amount of transverse cracking, possibly a low-temperature cracking phenomenon, was observed on the project. However, there does not appear to be any relationship between this cracking and PSI. Transverse cracking was first observed on the project in 1971 after a particularly severe winter. Some longitudinal cracking was observed prior to this in untreated base section 20 and in the paved shoulders, but it was not extensive.

Three major types of cracking were logged in a study of the cracking maps: alligator cracking, transverse linear cracking, and longitudinal linear cracking. The distribution of the three types of cracking is summarized below:

Base Type	Percentage of Cracking by Type (1978)		
	Alligator	Transverse	Longitudinal
AC	2	70	28
LSS	4	70	26
HSS	3	73	24
Standard	30	38	32

Percentage of cracking is defined in this study as the percentage of blocks, or arbitrary units of area, 0.61 m (2 ft) long (direction of traffic) and 0.3 m (1 ft) wide (transverse direction) that exhibit cracking of the type indicated.

It is apparent that alligator cracking distress was a major factor only in the untreated base test section. In 1978 these sections averaged 9 percent alligator cracking after 140 000 load repetitions. Alligator cracking is usually associated with pavements that exhibit fatigue distress.

By far the most prevalent form of cracking in the asphalt base sections was transverse and longitudinal linear cracking. The extent of this cracking can be observed in Figure 4. The first analysis of this type of cracking was made by Kingham in 1972 shortly after it was observed. Kingham observed that the transverse orientation of the cracks ob-

Table 3. Test properties of original asphalt and asphalt recovered from 1976 base and surface-course cores.

Test Property	Asphalt Extracted from 1976 Cores				
	Original	AC Base	HSS Base	LSS Base	AC Surface
Viscosity					
15.5°C (Mpoises)	26				
60°C (poises)	2546	3499	3147	3001	11 023
135°C (cSt)	427	545	478	459	800
Penetration, 100 g, 5 s, 0.1 mm	60	55	55	60	31
Softening point (ring and ball) (°C)		53.9	53.3	52.8	59.4
Ductility, 25°C (5 cm/min) (cm)	150+				
Specific gravity, 25°C	1032				
Thin-film oven residue:					
Penetration, 25°C (100 g, 5 s)	40				
Viscosity, 60°C (poises)	5636				
Viscosity, 135°C (cSt)	627				

Notes: $t°C = (t°F - 32)/1.8$; 1 mm = 0.04 in; 1 cm = 0.39 in.

Table 4. Summary of measurements made September 1978.

Section No.	Base Type	Pavement Thickness (mm)		PSI	PSI Corrected[a]	Rut Depth (mm)	Percentage of Cracking[b]		Deflection[c] (mm)
		Asphalt Surface and Base	Untreated Base and Subbase				Alligator	Total	
7	AC	201		1.6	2.5	5	1	22	0.36
12	AC	234		1.7	2.7	5	1	26	0.25
4	AC	279		1.8	2.6	3	1	18	0.15
8	AC	269		1.6	2.4	5	1	20	0.30
16	AC	190		1.9	3.0	5	0	7	0.40
15	AC	254		1.8	2.5	5	1	8	0.30
17	AC	236		1.6	2.5	5	0	7	0.30
10	LSS	196		1.6	2.5	10	1	10	0.46
2	LSS	239		1.8	2.6	10	1	12	0.33
3	LSS	297		2.0	2.6	10	1	16	0.25
13	LSS	269		1.6	2.5	8	1	15	0.30
18	LSS	193		2.0	2.4	13	1	15	0.38
19	LSS	234		2.0	2.3	10	1	7	0.36
5	HSS	198		1.6	2.5	8	1	25	0.41
9	HSS	226		1.7	2.7	5	1	19	0.33
6	HSS	274		1.7	2.4	8	1	14	0.30
1	Standard	71	404	1.7	2.7	3	2	25	0.41
11	Standard	66	442	1.9	2.4	3	12	35	0.30
14	Standard	56	422	1.8	2.5	3	16	36	0.33
20	Standard	71	409	1.9	2.6	3	7	22	0.25

Note: 1 mm = 0.04 in; $t°C = (t°F - 32)/1.8$.

[a] Corrected for texture.
[b] Percent total area cracked.
[c] Benkelman-beam deflection taken after spring thaw, corrected to 21.1°C.

Figure 4. Transverse shrinkage cracking.

served after the severe winter pointed to the likelihood that they resulted from thermal shrinkage, a phenomenon that at that time was attracting considerable attention in Canada and in parts of the United States. Kingham used techniques in his investigation subsequently reported by Haas (19). He used the results of original tests on the asphalt from the project and data obtained from asphalt concrete core samples obtained from the roadway. Critical temperatures when cracking first appeared were of the order of -21.7°C (-7°F) for the asphalt pavement. A -30°C (-22°F) air temperature was observed. By using properties of the asphalt cement and the core samples, Kingham was able to conclude that the pavements would be expected to crack at these temperatures. He stated, however, that his investigation was limited and that further investigations should be made.

In subsequent years, the amount of linear cracking increased, even though winter temperatures never were as low as those observed at the time the cracking was initiated. In general, the greatest amount of cracking in test sections constructed with hot-mix sand asphalt bases occurred in 1971, whereas the greatest amount occurred in the asphalt concrete base and standard sections in 1974 or in later years. These differences were not great, however.

Rut-depth data from Table 4 for the asphalt base sections of approximately equal thickness are summarized below for comparison (1 mm = 0.004 in; range is distance between sections):

Base		Rut Depth (mm)		Approximate Base
Type	Location	Avg	Range	Thickness (mm)
AC	West	5	0	165
LSS	West	10	0	165
HSS	West	8	3	165
AC	East	5	0	165
LSS	East	13	3	165

The summary indicates that, when compared on the basis of equal thickness, the hot-mix sand asphalt bases deformed more than the asphalt concrete base did and that the high-stability hot-mix sand asphalt mix was more resistant to deformation than was the low-stability mix. The rut depths observed for the standard untreated base sections were less than any observed for the asphalt-treated base sections, except Section 4 (279 mm of asphalt concrete).

An attempt was made to investigate the relative resistance to rutting of the different bases through the application of linear regression techniques. Two analyses were made: a comparison between the asphalt-treated bases and a comparison between the asphalt concrete base and the standard base. Unfortunately, the analysis between the asphalt bases was not successful because of the large amount of scatter in the data. However, the results did confirm the fact that the different bases performed differently, and they were useful in calculating the layer equivalency values reported later.

Routine Benkelman-beam deflection data, taken in the spring after thaw, and radius-of-curvature data are summarized in Table 4 for 1978. A simple linear regression analysis and 1978 data were used to determine whether there was a significant effect of base thickness or base type on deflection. The following model was used in analysis:

$$\text{deflection} = a_0 + a_1 T + a_2 C \quad (4)$$

where

a_0, a_1, a_2 = regression coefficients,
T = base thickness,
C = base code = 0 for asphalt concrete, and
C = base code = 1 for LSS and HSS bases.

The 1978 data points and a plot of the derived curves can be seen in Figure 5.

In this analysis both the base-thickness term and the base-type code term were statistically significant from zero; i.e., deflection reflected both base type and base thickness. Comparisons on the basis of equal deflection were made from the equations. Approximate ratios of 1.1 to 1.2 were obtained for thickness of low-stability and high-stability sand asphalt compared with asphalt concrete. A similar comparison was made between the average thickness of standard untreated base and the calculated thickness of asphalt concrete for the average deflection of the untreated base. The deflection value in this case was 0.33 mm (0.013 in) and the thickness ratio was 1.9 (419/216).

SPECIAL STUDIES

Several special field studies, not considered part of the routine measurement program, were made during the life of the project: These included a continuing study of subgrade moisture conditions, special deflection studies, and a trench study.

Subgrade moisture studies were made in a number of test sections in 1965, 1966, 1967, 1968, 1969, 1971, 1972, and 1974. Figure 6 shows schematically the distribution of moisture content obtained in 1968 test sections 3 and 7. Table 5 summarizes moisture data obtained from sections 3, 7, and 11 on a routine basis in the years 1967, 1968, 1969, 1971, 1972, and 1974 for the top 305 mm (1 ft) and second 305 mm on the centerline and approximately 3.05 m (10 ft) on either side of the pavement centerline. From earlier studies of data such as those presented in Figure 6, it appeared that the subgrade under the full-depth asphalt sections was drying out, whereas under the untreated base sections the subgrade was getting wetter. This appears to be the case from Figure 6, but it is not clearly evident from the data in Table 5.

Large seasonal variations in deflection were observed in the full-depth asphalt sections, which appeared to be related to differences in temperature rather than moisture or frost effects. A study of temperature effects was initiated in 1966. The study was designed to measure pavement deflections over a temperature range of -1°C to 37.8°C (30-100°F). Two levels of subgrade strength, temperature, and thickness were included. Low subgrade strength conditions were evaluated in the spring and

high strength conditions were evaluated in the late summer or fall. The program was completed over a two-year time period, 1966-1968. These data along with similar data collected on the San Diego County Experimental Base Project (20) were used to develop temperature-deflection correction curves (13).

In late 1976, trenches were cut in the eastbound lanes of Sections 10 and 18 to study more closely the rutting that had occurred in these sections. Sections 10 and 18 consisted of a nominal 140-mm (5.5-in) thickness of low-stability hot-mix sand asphalt base. Rut-depth data from the trench study indicated that the change in thickness of the surface course was approximately 5 percent, or about 13 percent of the total rut depth. The hot-mix sand asphalt base was reduced in thickness about 10 percent or about 73 percent of the rut depth. About 14 percent of the rut was attributed to the subgrade.

Since the above study involved only one base type and one base thickness, no comparisons can be made with other base types or thicknesses. However, the data do confirm that the source of the rut is primarily the base and that from a structural viewpoint the subgrade was not significantly overstressed.

Figure 5. Deflection versus base thickness.

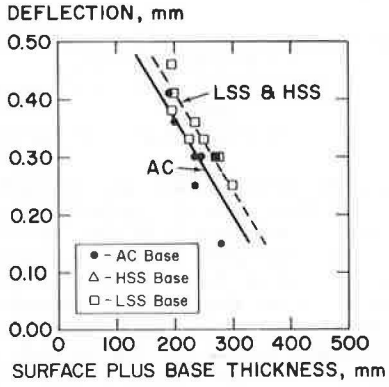

Figure 6. Results of moisture study.

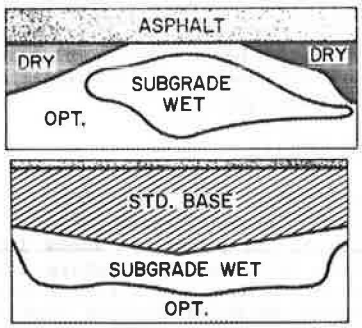

RELATIVE THICKNESS REQUIREMENT OF PAVEMENT MATERIALS

In the American Association of State Highway and Transportation Officials (AASHTO) Interim Guide (21) and the Colorado Roadway Design Manual (22), the relative contributions of different types of base and subbase are expressed as coefficients in an equation of the form shown below:

$$SN = aD_1 + bD_2 + cD_3 \quad (5)$$

where

SN = structural number, obtained from the design method for a given design situation;
a, b, c = coefficients that vary with material type; and
D_1, D_2, D_3 = thickness of surface, base, and subbase layers, respectively.

A list of coefficients used in the AASHTO and Colorado design methods is given in Table 6.

Two of the analyses presented in this report, the rut-depth analysis and the deflection analysis, produced results that were used to estimate material coefficients for the materials used as base on the project. These values are given in Table 7.

In addition to the coefficients for the base materials, there are indications from the analysis of rut depth presented earlier and from an analysis of deflection data not included that the coefficient for the asphalt surface course should be higher than 0.44. The values obtained were 0.94 and 0.48, respectively. It would seem, however, that the frequently used value of 0.44 would be more reasonable for use in routine design.

Table 5. Summary of routine subgrade moisture measurements.

Year	Subgrade Depth[a] (mm)	Percentage of Moisture									Avg All Sections
		Section 3			Section 7			Section 11			
		N[b]	C	S[c]	N	C	S	N	C	S	
1967	Top 0.3 m	15	21	15	11	14	15	20	20	20	17
	Next 0.6 m	16	20	14	14	17	17	18	18	18	17
1968	Top 0.3 m	18	21	15	11	10	15	7	10	9	13
	Next 0.6 m	17	21	19	14	18	17	19	21	21	19
1969	Top 0.3 m	13	21	20	19	19	18	19	19	18	18
	Next 0.6 m	15	21	20	20	19	20	22	22	22	20
1971	Top 0.3 m	15	19	18	16	16	16	16	20	17	17
	Next 0.6 m	20	22	21	20	20	21	23	24	23	22
1972	Top 0.3 m	13	11	13	15	16	13	14	15	17	14
	Next 0.6 m	19	21	21	20	21	19	22	22	22	21
1974	Top 0.3 m	20	19	20	19	9	18	19	20	19	18
	Next 0.6 m	20	20	19	21	14	20	24	23	23	20
Avg	Top 0.3 m	16	19	17	15	14	16	16	17	17	16
	Next 0.6 m	18	21	20	18	18	19	21	22	22	20
Section avg	Top 0.3 m		17			15			17		
	Next 0.6 m		20			18			22		
	Top 0.9 m		18			16			19		

Note: 1 mm = 0.04 in.

[a]Approximate depth. [b]N = approximately 3 m north of centerline of roadway. [c]S = approximately 3 m south of centerline of roadway.

Table 6. Comparison of layer coefficients.

Material	AASHTO Guide Coefficients[a]	Colorado Method Coefficients[b]
AC surfacing (D_1)	0.44	0.25-0.44
AC base (D_2)	0.34	0.22-0.34
LSS base (D_2)	0.30	Not included
HSS base (D_2)	0.30	Not included
Standard base (D_2)	0.14[c]	0.10-0.14
Standard subbase (D_3)	0.11	0.10-0.14

[a] Adopted in 1961; values used by many individual states are different.
[b] Functions of strength of material as measured by R_t-values for asphalt mixes and R-values for aggregate bases.
[c] Normally applied to crushed stone.

Table 7. Estimated layer coefficients.

Base Material	Rut-Depth Analysis		Deflection Analysis		Average	
	Ratio	Coefficient	Ratio	Coefficient	Ratio	Coefficient
AC	1.0	0.34	1.0	0.34	1.0	0.34
LSS	1.8	0.19	1.2	0.28	1.5	0.24
HSS	1.2	0.28	1.2	0.28	1.2	0.28
Standard[a]	2.4	0.14	1.9	0.18	2.2	0.16

[a] Includes base and subbase.

RESISTANCE TO RUTTING AND CRACKING

Based on information reported in Table 4, it is possible to rank the base types in order of their resistance to a given form of distress or performance variable; i.e., roughness (PSI), rut depth, alligator cracking, and transverse shrinkage cracking. The results of this ranking process are given below (0 = equal, 1 = best, etc.):

Base Type	Rank by Performance Variable			
	Roughness (PSI)	Rut Depth	Alligator Cracking	Transverse Cracking
AC	0	2	0	1
HSS	0	3	0	4
LSS	0	4	0	3
Standard	0	1	4	2

CONCLUSIONS

The different base types included in the Ordway Colorado Experimental Base Project exhibited different abilities to resist various forms of distress:

1. The asphalt concrete base mixture provided the best resistance to rutting and to all forms of cracking,
2. Both hot-mix sand asphalt bases provided equally good resistance to alligator cracking, but the low-stability hot-mix sand asphalt mix provided less resistance to rutting than the other bases, and
3. The untreated base and subbase provided the best resistance to rutting but the least resistance to alligator or load-associated cracking.

After 12 years of traffic without major maintenance, all test sections were exhibiting substantial erosion of the matrix from the asphalt concrete surface course and severe transverse shrinkage cracking conditions. These conditions were somewhat more severe than was observed on pavements on adjacent highways. Also, some of these conditions may have been partly overcome by normal maintenance procedures; however, because of the experimental nature of the project, no maintenance was permitted.

Analysis of rut-depth and deflection data produced the following average layer coefficients: asphalt concrete surface course, 50 mm (2 in) thick, >0.44; asphalt concrete base course, 0.34; hot-mix sand asphalt base, 0.24-0.28; and untreated aggregate base and subbase, 0.16.

ACKNOWLEDGMENT

The contents of this report reflect our views and we are responsible for the facts and accuracy of the data presented here. The contents do not necessarily reflect the official views of the Asphalt Institute, the Colorado Department of Highways, or the Federal Highway Administration. This report does not constitute a standard, specification, or regulation.

The facilities of the University of Maryland Computer Science Center were used in the analysis of performance data described in this report. The assistance of the Colorado Department of Highways also is gratefully acknowledged.

REFERENCES

1. R.I. Kingham and T.C. Reseigh. A Field Experiment of Asphalt-Treated Bases in Colorado. Proc., 2nd International Conference on the Structural Design of Asphalt Pavements, Univ. of Michigan, Ann Arbor, 1967.
2. B.F. Kallas and J.C. Riley. Mechanical Properties of Asphalt Pavement Materials. Proc., 2nd International Conference on Structural Design of Asphalt Pavements, Univ. of Michigan, Ann Arbor, 1967, pp. 791-814.
3. C.T. Metcalf. Field Measurement of Elastic Moduli of Materials in Flexible Pavement Structures. Proc., 2nd International Conference on Structural Design of Asphalt Pavements, Univ. of Michigan, Ann Arbor, 1967.
4. Ordway Experimental Project Post-Construction Field Measurements: Interim Report. Colorado Department of Highways, Denver, Oct. 1969.
5. T.C. Reseigh and B.B. Gerhardt. The Ordway Colorado Experimental Base Project. Presented at the 52nd Annual Meeting, TRB, 1973.
6. B.B. Gerhardt. Ordway After Ten Years. Presented at Asphalt Paving Conference, Colorado State Univ., Fort Collins, Dec. 11, 1975.
7. B.A. Brakey and J.A. Carroll. Experimental Work--Design and Construction of Asphalt Bases and Membranes in Colorado. Proc., AAPT, Vol. 40, 1971, pp. 30-63.
8. J.F. Shook and B.F. Kallas. Ordway Colorado Experimental Base Project Performance Studies: Final Report. Colorado Department of Highways, Denver, Rept. FHWA-CO-80-8, 1980.
9. The AASHO Road Test: Report 5--Pavement Research. HRB, Special Rept. 61E, 1968.
10. F.H. Scrivner and W.M. Moore. Standard Measurements Program for Satellite Road Test Programs. NCHRP, Rept. 59, 1968.
11. R.L. Hayden. Calibration of Colorado's Texturemeter. Colorado Division of Highways, Denver, Rept. CDOH-P & R-R & SS-72-12, Dec. 1972.
12. Canadian Good Roads Association. Pavement Evaluation Studies in Canada. Proc., International Conference on the Structural Design of Asphalt Pavements, Univ. of Michigan, Ann Arbor, 1962.
13. Asphalt Overlays and Pavement Rehabilitation (MS-17), 1st ed. The Asphalt Institute, College Park, MD, Nov. 1969.
14. R.I. Kingham. A New Temperature Correction Procedure for Benkelman Beam Rebound Deflections. The Asphalt Institute, College Park, MD, Res. Rept. 69-1 (RR-69-1), 1969.

15. G.L. Dehlen. A Simple Instrument for Measuring the Curvature Induced in a Road Surface by a Wheel Load. Civil Engineer in South Africa, Vol. 4, No. 9, Sept. 1962, pp. 189-194, and Vol. 5, No. 3, March 1963, pp. 72-73.
16. Soils Manual (MS-10). The Asphalt Institute, College Park, MD, March 1978.
17. B.F. Kallas and V.P. Puzinauskas. Flexural Fatigue Tests on Asphalt Paving Mixtures. Symposium on Fatigue of Compacted Bituminous Aggregate Mixes, American Society for Testing and Materials, Philadelphia, PA, STP 508, July 1971.
18. V.L. Anderson and R.A. McLean. Design of Experiments. Marcel Dekker, New York, 1974, pp. 102-103.
19. R.C.G. Haas. A Method for Designing Asphalt Pavements to Minimize Low-Temperature Shrinkage Cracking. The Asphalt Institute, College Park, MD, Res. Rept. 73-1 (RR-73-1), Jan. 1973.
20. J.F. Shook. San Diego County Experimental Base Project: Analysis of Performance. Proc., AAPT, Vol. 45, 1976.
21. AASHTO Interim Guide for the Design of Pavement Structures. American Association of State Highway and Transportation Officials, Washington, DC, 1974.
22. Roadway Design Manual. Colorado Division of Highways, Denver, 1980.

Publication of this paper sponsored by Committee on Strength and Deformation Characteristics of Pavement Sections.

Use of Deflection Measurements for Determining Pavement Material Properties

B. FRANK McCULLOUGH AND ARTHUR TAUTE

This paper develops and describes models and constraints for using Dynaflect measurements to obtain the elastic-modulus inputs for layered theory. A nomograph is provided for determining the subgrade modulus of elasticity by using the sensor-1 and sensor-5 deflections. A graph and equations for correcting these modulus properties based on the thickness of the subgrade are also provided. In addition, problems associated with the modulus predictions considering stress sensitivity of pavement materials, variations of subgrade stiffness with depth, seasonal effects, and discontinuities in the pavement structure are described. A step-by-step summary procedure is provided to permit a designer to readily utilize the information presented in the body of the report.

Mechanistic design procedures require the use of a suitable theory and model to analyze the behavior of a pavement structure. Plate, layered, and finite-element theories have been used for this purpose. Typically, these theories are used to compute the tensile stresses in the upper, bound pavement layers, which are then input into a fatigue equation to predict the life of the pavement. Use of one of these theories requires that the materials that make up the pavement be suitably characterized.

Plate theory is often used for rigid pavement design; if so, the concrete layer is represented by a relatively stiff plate and the lower layers are characterized as a bed of linear springs. Elastic-layered and finite-element theories have also been used with success for rigid pavement design. These last two theories use Young's modulus and Poisson's ratio to characterize the stress-strain behavior of the pavement materials.

Taute, McCullough, and Hudson (1) have shown that plate and layered theories predict similar tensile stresses in the bottom of a concrete pavement layer when the supporting structure consists of granular material. The spring constant K used in the plate-theory calculations is equated to the layer moduli used in layered-theory calculations by computing the deflection of the subbase under a plate load with layered theory. This deflection is used to obtain the equivalent k-value of the supporting structure.

Layered-theory computer programs that can predict the state of stress, strain, and deflections of pavement structures at minimal cost are freely available. For this reason, layered theory is often used in mechanistic design procedures. Shortcomings of the theory, such as the inability to predict pavement stresses under an edge-loading condition, can be overcome by using stress-modification factors. These factors can be calculated by using plate or finite-element theories.

OBJECTIVE

Because layered-theory analysis is often used for mechanistic pavement analysis, the material properties most often required for the pavement layers are Young's modulus and Poisson's ratio. Both laboratory and in situ methods are available for determining these material characteristics. The objective of this paper is to develop and describe the techniques, models, and constraints involved in using deflection measurements to obtain the inputs to layered theory.

DEFLECTION MEASUREMENTS

The use of deflection measurements for the estimation of pavement layer stiffnesses is rapidly gaining popularity and application. Computer programs that model the pavement layers as homogeneous, isotropic, elastic layers provide reasonable estimates of pavement behavior under loading. A Dynaflect is at present used in Texas to obtain pavement deflection measurements. Thus, the developments in this paper are based on Dynaflect loadings, but the concepts are applicable to any deflection-measuring device.

The Dynaflect uses two masses rotating in opposite directions to apply a cyclic load to the pavement surface. The cycle frequency used is typically 8 Hz and the peak-to-peak load applied is 1000 lb on two steel load wheels placed at 20-in centers. The peak-to-peak deflections are measured by five geophones at 1-ft intervals; the first one is placed

Figure 1. Effect of layer moduli on Dynaflect deflection basins for typical rigid pavement structure.

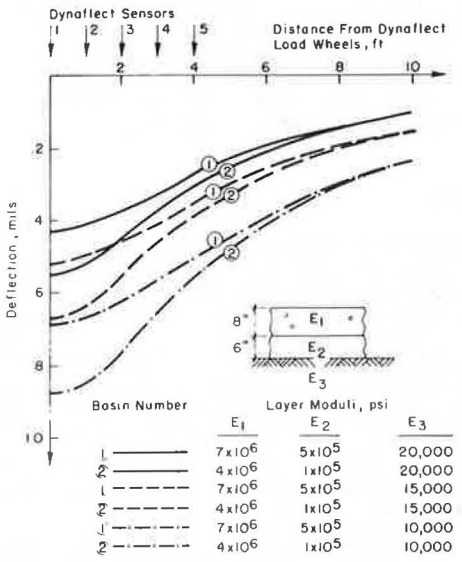

Figure 2. Relationship between Dynaflect sensor-5 modulus and subgrade modulus for different rigid pavement thicknesses.

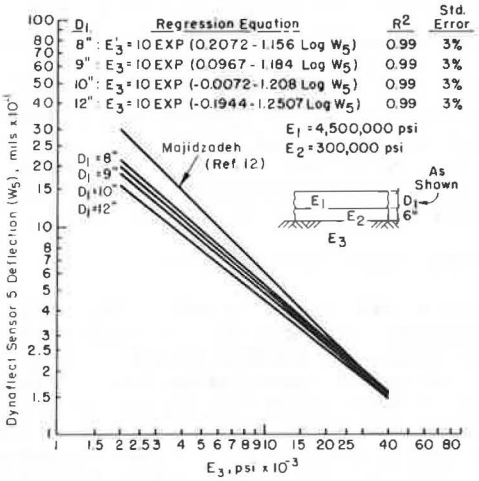

directly between the wheels. This device thus provides an indication of the displacement and shape of the deflected surface within 4 ft of the load wheels. In the following sections, procedures for estimating material properties from Dynaflect deflections and problems associated with these predictions are discussed.

Estimation of Material Properties from Dynaflect Deflections

The pavement layer stiffnesses may be estimated from Dynaflect deflection measurements by using elastic-layered theory as follows:

1. Pavement layer thicknesses, initial estimates of the pavement layer moduli, and the loading and deflection measurement configuration are input into the computer program.
2. The computed deflections at the five geophone positions can be compared with those actually measured in the field.
3. The layer moduli used in the computer program can now be adjusted to improve the fit of the predicted and actual deflection basins.
4. This process is repeated until the two deflection basins are virtually the same. The process may have to be repeated several times before a reasonable fit is obtained.

Knowledge of the effects of changes to the various layer moduli on the shape and position of the deflection basin may speed the process considerably. Some of the terms commonly used with deflection basins are as follows:

1. Sensor-i deflection, Wi;
2. Surface curvature index (SCI), W1-W2;
3. Base curvature index (BCI), W4-W5;
4. Spreadability, (W1 + W2 + W3 + W4 + W5)/5W1; and
5. Slope of the deflection basin, W1-W5.

These parameters are related to the stiffness of one or more of the pavement layers in varying degrees. This factor is illustrated in Figure 1, in which deflection basins predicted by layered theory for different layer moduli are presented. Typical concrete pavement structures consist of a concrete pavement layer, a stabilized subbase layer, and a subgrade.

A large number of layered-theory computations were made by using this type of pavement structure, and the following conclusions have been drawn:

1. As illustrated in Figure 1, changes to the surface or stabilized subbase modulus result in significant changes to the sensor-1 deflections and only minor changes to sensor-5 deflections. These correspond to a change in the deflection basin slope.
2. Changes to the subgrade moduli result in significant changes to both sensor-1 and sensor-5 deflections. Both these deflection parameters are affected approximately proportionally by changes to the subgrade modulus, and there is little change to the deflection basin slope.

Therefore, it can be hypothesized with the use of interior measurements on a concrete pavement that the subgrade modulus may be predicted from the deflection at any sensor and that the slope of the basin may be used to predict the surface and subbase moduli. However, the prediction of the subgrade modulus from the sensor-5 deflection will be fairly accurate for a wide range of surface and subbase moduli because of the small effect that these moduli have on this deflection parameter. In the case of the basin slope, however, an infinite number of combinations of surface and stabilized subbase moduli exist that, when used in layered-theory analysis, will predict approximately the same basin slope.

A number of figures have been prepared to simplify the calculation of layer moduli from Dynaflect deflections. Because the pavement stiffness has a minor effect on the fifth sensor deflection, Figure 2 shows the subgrade modulus as a function of sensor-5 deflection and the rigid pavement thickness. Both the layer modulus and the thickness of the layer affect the stiffness of the layer, but the latter variable is much more important.

The relationship in the figure was obtained by regression analysis of data obtained from layered-theory computations. In the log-log form presented in Figure 2 and for constant upper-layer moduli and thicknesses, the subgrade modulus is very highly correlated to deflection at any point on the pavement surface. The regression equations used in Figure 2 and their correlation coefficients and standard errors are shown on the figure. With these

Figure 3. Nomograph for predicting Dynaflect deflection basin slope ($W_1 - W_5$) for rigid pavements.

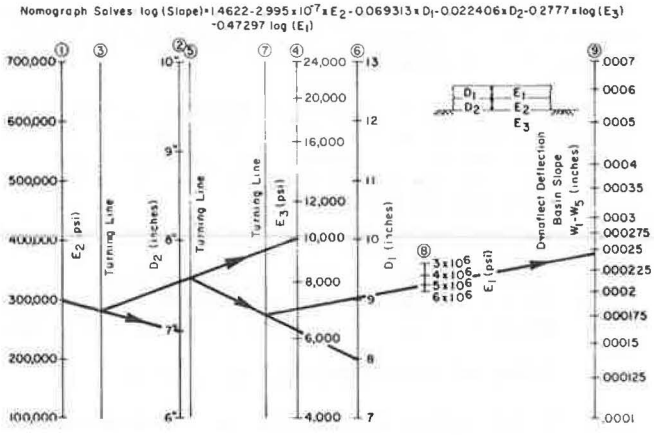

equations, the subgrade modulus may be estimated with the sensor-5 reading.

The upper-layer moduli-deflection basin slope relationships may be developed for different subgrade moduli for typical conditions by using numerous layered-theory computations. From such a study it was noted that a number of combinations of surface and subbase modulus values can result in a given basin slope.

A nomograph has also been prepared for trial-and-error calculations of deflection-basin slopes from estimates of layer moduli. The equation used for the development of the nomograph in Figure 3 was obtained from regression analysis of layered-theory results. The correlation coefficient of this equation is 0.98 and the standard error of the residuals is 8 percent.

The upper-layer thicknesses and estimates of the layer moduli are used in the nomograph to obtain a prediction of the deflection basin slope under a Dynaflect load. The selected moduli can be modified until the basin slope obtained in the nomograph coincides with the slope obtained in the field. The numbers above each scale on the nomograph indicate the sequence at which the lines should be crossed. From the nomograph, it is apparent that the basin slope is extremely sensitive to surface and subbase layer thicknesses and moduli. Thus, whenever possible, laboratory testing should be used to corroborate moduli obtained from this procedure.

In the past, the surface curvature index (SCI) has often been correlated to layer stiffnesses for asphalt pavements (2). As shown in Figure 1, a typical deflection basin for rigid pavements is very flat with a large radius of curvature. Thus, for rigid pavements, the SCI is a very small quantity and any small measurement inaccuracies in the Dynaflect may result in a considerable change in SCI. This may be the cause of the larger average coefficient of variation of the SCI (50 percent) than of the basin slope (30 percent), as found in numerous field studies (1). For this reason, the slope of the basin (sensor 1 minus sensor 5) has been correlated to the upper layer stiffnesses rather than to SCI.

Problems Associated With Predictions of Deflection Modulus

A number of factors exist that may result in inaccurate predictions of moduli from deflection measurements: (a) stress sensitivity of pavement materials, (b) variation of subgrade stiffness with depth, (c) seasonal effects, and (d) discontinuities in the pavement structure. All these factors lead to significant changes in the deflection measurements and consequently to the moduli predicted from these deflections. If these problems are recognized, deflection measurements or calculated moduli can be adjusted to account for them. In the following paragraphs, methods of accounting for these problems are discussed.

Stress Sensitivity

The fact that pavement materials do not behave in a linear-elastic fashion has long been established. In May 1962 at the St. Louis conference on the AASHO Road Test (3), data were presented that showed that deflections were not proportional to load. In the discussions that followed, Hveem stated that deflection-load relationships depended on the nature of the subgrade soil. Subsequent resilient-modulus tests of subgrade soils have shown that the stress-strain relationship depends to a large degree on soil type (4,5). Most pavement materials are not linearly elastic and the moduli may vary with stress. Clayey soils may be stress softening (i.e., result in reduced modulus with increased stress), whereas granular materials may be stress hardening (have increased modulus with increased stress). The Texas overlay design procedure takes only the stress sensitivity of the subgrade into account by using the slope of the resilient modulus--principal stress difference line.

Dynaflect deflections do not provide any indication of the stress sensitivity of the pavement material. Deflection devices that are capable of applying different loads to the pavement may provide some indication of the stress sensitivity of the material. Generally, at this stage of development, an indication of the stress sensitivity of the subgrade is obtained from resilient-modulus tests.

Variation of Subgrade Stiffness With Depth

Deflection measurements provide an indication of the pavement's response to loading. Layered-theory modeling of the pavement structure typically assumes that the subgrade has a semiinfinite depth. Very little of the pavement deflection is due to compression of the surface layers; it is due mostly to compression of the subgrade. For the same subgrade stiffness, loading an infinitely thick subgrade would result in much larger deflections than loading a shallow subgrade supported by a more rigid foundation. This factor is illustrated in Figure 4, in which a number of deflection basins obtained by using the BISAR and ELSYM5 elastic-layered theory programs are plotted. The structures used as inputs to the program are indicated in the figure.

This indicates that if samples of the subgrade from immediately below the subbase layer are tested for modulus, use of this modulus in layered-theory computations with an infinite subgrade depth will overpredict the surface deflections. McCullough has demonstrated this (6); computed deflections by using moduli from material tests as inputs were greater than the field deflections. In reality, infinitely thick subgrades and homogeneous subgrades with a well-defined depth supported by a rigid foundation seldom exist in the field.

Field conditions will most often be somewhere between these two extremes. A granular subgrade whose stiffness gradually increases with depth or a clayey subgrade that, due to desication, may be stiffer at the surface than lower down may be more likely to occur in practice. Furthermore, this condition may change along the length of the road.

Figure 4. Deflection basins obtained from ELSYM5 and BISAR for two different loads and subgrade thicknesses.

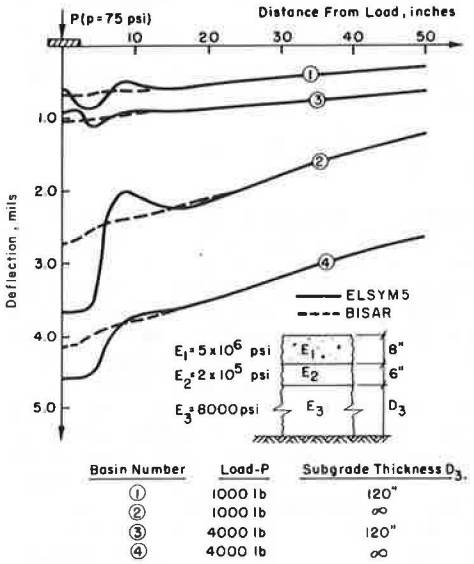

Basin Number	Load-P	Subgrade Thickness D_3
①	1000 lb	120"
②	1000 lb	∞
③	4000 lb	120"
④	4000 lb	∞

Figure 5. Reduction in subgrade modulus predicted by using Dynaflect measurements at sensor 5 when subgrade is supported by rigid foundation at depth D_3.

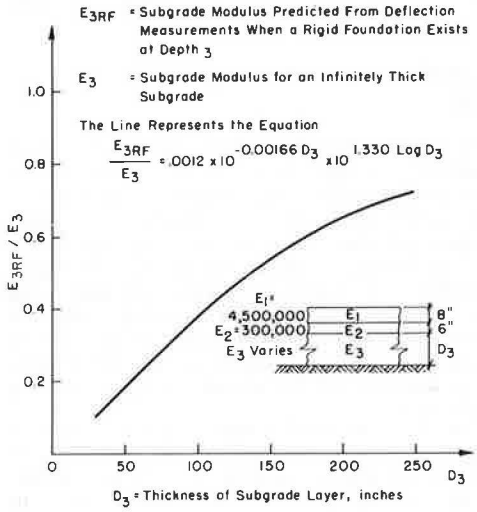

Cut-and-fill areas, for example, may have extremely different subgrades. Seismic testing or deep probing may provide some information to the designer in this regard. If no information is available, engineering judgment should be used for an approximation of the change in subgrade stiffness with depth.

Furthermore, from Figure 4 it is apparent that layered-theory programs, such as ELSYM5, that are based on the CHEVRON 5 program predict unrealistic deflections in the vicinity of the load. For predictions of Dynaflect deflections by using ELSYM5 or a similar layered-theory program, these discontinuities are significant in the case of a subgrade supported by a rigid foundation because the first sensor is 10 in away from the loading point and thus is above an irregular deflection as predicted by these programs. Therefore, if the deflection measurements are made near the loading point, BISAR should be used to compute fitted deflection basins.

These factors need to be considered when subgrade moduli are predicted from deflection measurements, and, to this end, Figure 5 has been prepared. This figure was produced from regression analysis of the results of layered-theory computations of the behavior of typical existing pavement structures. It shows the relationship between the thickness of the subgrade layer and the ratio of the subgrade modulus predicted from sensor-5 Dynaflect deflections for a semiinfinite subgrade depth and the subgrade modulus predicted from the same deflection measurement if a rigid foundation exists at some depth.

The figure was obtained as follows:

1. Numerous layered-theory computations of the deflections at sensor 5 under the Dynaflect load were made.
2. A regression equation describing the subgrade modulus as a function of the sensor-5 deflection and the depth to the rigid foundation was obtained. This equation is as follows:

$$E_R = 10 \exp(-1.3832 - 0.0016\ 584 \cdot D_3 + 0.6394 \cdot \log D_3 - 0.7582 \cdot \log W5 - 0.2034 \cdot \log D_3 \cdot \log W5) \quad (1)$$

where

E_R = subgrade modulus as predicted by layered theory from deflections when a soft subgrade is supported by a rigid foundation,
W_5 = sensor-5 Dynaflect deflection, and
D_3 = thickness of the soft subgrade layer (in).

3. Equation 1 was the ratio divided by the equations presented in Figure 2 for the same pavement structure and an infinitely thick subgrade and then reduced to the following by fixing W_5 = 0.004 in:

$$E_R/E = 0.0011 \times 10 \exp(-0.001\ 66D_3 + 1.33 \cdot \log D_3) \quad (2)$$

From Figure 5, it is apparent that this type of analysis may result in substantial reductions to the subgrade modulus, depending on the thickness of the soft subgrade layer. The accuracy of Equation 2 is reflected by the results presented in Figure 6. This graph was developed by making a number of random calculations by using layered theory within the ranges of layered thicknesses and moduli shown in Figure 5. Although some substantial errors may occur in the moduli predicted by using these equations, they are not significant when compared with the uncertainty regarding the actual change of subgrade modulus with depth. Figure 5 can thus be used to provide an approximate estimate of the reduction to the subgrade modulus calculated from deflections only if a rigid foundation exists. Seismic testing and engineering judgment (provided by test borings for bridge foundations, etc.) should be used to estimate whether any reduction to the subgrade modulus calculated by using deflections is required for a particular area.

Seasonal Effects

Deflections measured along the road change due to seasonal changes of moisture and temperature. With continuously reinforced concrete (CRC) pavements, changes in the environment affect the deflection measurements in two ways. Cold temperatures caused the concrete surface layer to shrink, causing an increase of the transverse crack widths. Periods of increased rainfall result in slightly higher moisture contents in the subgrade and a corresponding lower subgrade modulus. The effects of these factors on deflections have been illustrated by McCullough and Treybig (7).

First, let us consider the effect of these environmental factors on the sensor-1 Dynaflect de-

Figure 6. Comparison of subgrade modulus used in layered-theory analysis and subgrade modulus estimated by using graphs from layered-theory deflections.

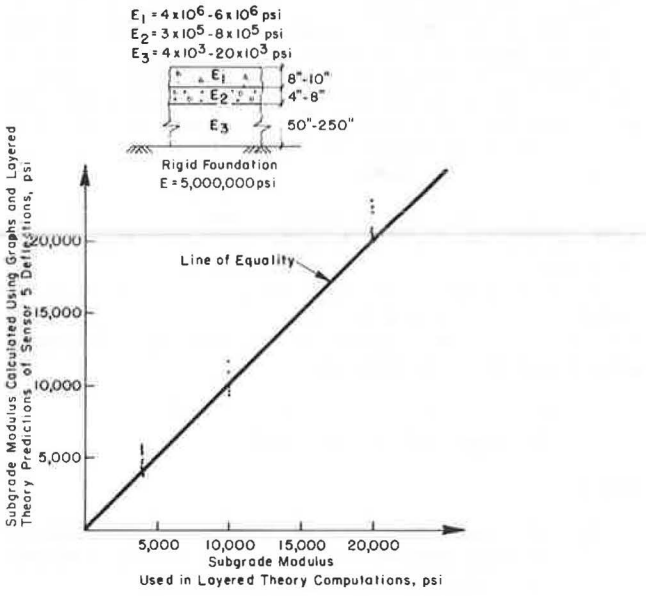

flections or, in other words, on deflections near the center of the deflection basin. A wet winter will result in an increase in deflections compared with those from other seasons. This will be due to the wet, soft subgrade and the low effective modulus of the surface layer caused by shrinkage and the resulting relatively wide transverse cracks. A dry summer will result in a decrease in this deflection due to the dry stiff subgrade and the high effective surface modulus caused by expansion and the resulting narrowing of the transverse cracks in the CRC pavement. Wet summers or dry winters may not appreciably change this deflection relative to other seasons, due to the counterbalancing effects of the environment on the different layer moduli.

If, on the other hand, the sensor-5 Dynaflect deflection and the slope of the deflection basin are considered, environmental factors that affect the subgrade and surface may be distinguishable. Moisture effects on the subgrade should affect the sensor-5 deflection, and temperature effects on the surface should affect the basin slopes.

Therefore, if laboratory testing can be done to determine the moduli of the surface and subbase layers, deflection measurements should be made during the wettest season of the year to obtain the most critical subgrade modulus from these measurements.

Discontinuities in Pavement Structure

Cracks in the rigid pavement layer may have an effect on deflections if some loss of load transfer is caused by the cracks. With CRC pavements, the cracks are tightly closed, which results in very little loss of load transfer. As explained, a drop in temperature can cause these cracks to open; thus some loss of load transfer may result. This will cause an increase in the sensor-1 deflection with a corresponding change in basin slope and the moduli predicted from this deflection parameter. The effect of these cracks on stresses in the concrete layer has been discussed in more detail (1).

VARIATION IN PAVEMENT LAYER STIFFNESSES

Stresses in the upper pavement layers resulting from heavy axle loads will be affected by variation of the pavement layer stiffnesses. The layer stiffnesses are in turn affected by variations in layer thickness and modulus. These material stiffnesses may vary in both the horizontal and vertical planes. Different pavement layers will have different amounts of variation associated with them.

Effect of Varying Layer Stiffnesses on Stresses in Pavement

Before the variations associated with each layer's stiffness are discussed, it is useful to know what effect a change in a specific layer stiffness will have on the tensile stresses in the design layers of the pavement. (The design layers of a pavement are defined as those layers calculated to last the design life of the pavement, based on fatigue.) This is shown in a study made by using a typical three-layered pavement structure by varying the layer moduli. From the study, it is apparent that decreasing subbase and subgrade moduli results in an increase of the tensile stresses in the surface layer under load. Increasing surface modulus also increases this critical stress. The effect of changing layer thickness on the critical tensile stress in the pavement is difficult to quantify. For example, very thin pavement layers may have no tensile stresses in them under load. It is sufficient to say that, within the range of thicknesses typical of CRC pavements, an increase in layer thickness will decrease the tensile stresses in the rigid pavement layer.

Methods of Accounting for Variations in Layer Stiffnesses

One of the best methods for obtaining an idea of the amount of variation in the layer stiffnesses along the length of a road is with deflection measurements taken at fixed intervals along the road. The measurements are then plotted to provide a visual indication of the variation. This method has the advantages of economy and speed over material sampling and laboratory testing. If stage construction is used, the method can be applied equally well to the compacted subgrade of the pavement under construction and to the surface of an existing pavement in need of rehabilitation.

The variation in layer stiffnesses can be divided into two groups: random variation and stratified variation. Random variation is present in all pavement materials and structures. It is normal and due to the heterogeneous nature of the pavement layers. This variation is often reflected in the deflection measurements by some scatter among the results for a section of roadway. Stratified or assignable variation occurs due to a significant change in factors such as layer stiffnesses or thicknesses. For example, the subgrade stiffness in a cut or fill area may be slightly different. If possible, the stratified variations should be accounted for by separating design sections with assignable differences. This is not always practical; for example, if an area of a certain weak subgrade type is small, it may be included within a larger adjacent section and its variation added to the random variation of the larger section. The random variation may, for example, be accounted for by designing for a deflection based on a certain statistical confidence limit (8,9).

AREAL VARIATIONS

A major consideration in selecting material properties for pavement analysis is the variation of prop-

erties along the road. Thus, one must select the design sectors considering this variation, but the length must be responsible and practical.

Selection of Design Sections

A visual indication of the deflection and layer stiffness variation is provided when deflection measurements are plotted to scale as a function of distance. The PLOT program, documented by Schnitter, Hudson, and McCullough (9), provides a plot of deflections by means of a computer line printer. This plot facilitates dividing the roadway into sections based on stratified variation of deflection data. Previously, deflection sections have been selected based only on sensor-1 deflections. Now that layer stiffnesses may be predicted from deflection measurements, as described previously, sections may be selected based on the sensor-5 deflections and the slopes of the deflection basins. The sensor-5 deflection is used to select sections with different subgrade stiffnesses and the basin slopes are used to select sections with different effective surface stiffnesses. Sections are selected subjectively based on a plotted profile of these deflection parameters.

When design sections are selected, each section that represents a change in sensor-5 deflection should also represent a change in the sensor-1 minus sensor-5 deflection parameter, but not vice versa. This is because the subgrade modulus does have a significant effect on the basin slope, but the surface stiffness does not have a significant effect on the sensor-5 deflection.

Furthermore, implementation of the overlay design procedure (RPOD2) has shown that changes in deflection variance are as important as the changes in the mean deflection in the selection of design sections. Areas with similar mean sensor-5 deflections but with significantly different variation thereof should be separated into different design sections.

Because sections are selected by considering two deflection parameters and their variances, this process may result in many small sections. In order to keep the number of short sections to a minimum, limits of sections selected from different deflection parameters should be made to coincide wherever possible.

After selection of different design sections, RPOD2 recommends the use of the Student's t-test to determine whether the section means are significantly different at specific confidence levels. However, one of the shortcomings of this test is that it assumes that the sections (or data) being tested have similar variances.

As indicated earlier, different sections may have different variances, and, if so, these differences are important factors in the selection of sections. This shortcoming could be overcome by using a statistical test designed for testing differences between sample variances. Before embarking on such a course, the consequences of incorrectly selecting or not selecting a section should be examined.

Section Size

As recommended above, contiguous design sections are selected based on the mean and variance of the Dynaflect sensor-5 deflections and the slope of the deflection basins. The shortest section selected should be long enough so that it is practical and important to construct a distinct set of pavement thicknesses and materials over the length of the section. Implementation of the RPOD2 design procedure has indicated that this length is approximately 1000 ft. The section should also be long enough to contain sufficient deflection measurements for the designer to make fairly accurate inferences about the section's overall behavior from this sample of deflections. If the deflection measurements are normally distributed, a statistical formula can be used to determine the sample size. If, for example, the sample mean should only have a probability α of differing from the population mean by more than d percent, then the formula is as follows (10):

$$N = (tS)^2/D^2 \quad (3)$$

where

N = sample size,
t = abscissa of normal curve that cuts off area α at tails,
S = standard deviation of the population, and
D = dy where y is sample mean.

Implementation of the RPOD2 design procedure has shown that a typical value for S of the sensor-5 deflection is 0.10 mil. The sensor-5 deflection depends on the subgrade modulus and typically varies from 0.2 mil to 0.5 mil. A value of 0.3 mil can be used as representative of a fairly good subgrade. Therefore, if α = 5 percent and d = 10 percent, then

$$N = (1.96 \times 0.1)^2/(0.1 \times 0.3)^2 = 24 \quad (4)$$

This indicates that if a section length of 1000 ft is the shortest practical construction unit length, then, for these constraints on inference accuracy, deflection measurements are required at 50-ft intervals within that section. This inference accuracy becomes important when confidence limits of deflections for the different design sections are predicted.

SUMMARY

The procedure for characterizing the material properties of a pavement may be summarized as follows:

1. For a new pavement, material tests should be used to obtain an indication of the mean and variance of the layer moduli. If stage construction is used, take deflection measurements every 50 ft along the length of the prepared roadbed. Similar measurements should be taken in the event that an existing pavement needs rehabilitation. The measurements should be taken approximately 3 ft in from the outside shoulder.
2. Run the PLOT4 program by using the deflection data as input. This program will plot the profile of the W5 and W1 minus W5 deflections along the length of the road, as illustrated by Schnitter, Hudson, and McCullough (9).
3. Select contiguous sections from this plot by using the means and variances of both the plotted deflection parameters as selection criteria with a minimum length of approximately 1000 ft. To prevent having a number of short sections during the selection process, the limits of sections selected based on W5 deflection and on the basin slope measurements should be made to coincide where possible.
4. A design value should be selected based on the statistical variability and desired level of confidence.
5. The output from steps 3 and 4 may be used as a guideline for selecting sections that have similar sensor-5 deflections for obtaining core samples.
6. Obtain cores from the bound pavement layers and push-barrel samples of the subgrade layer. In

the event of a granular subgrade, in situ densities and moisture contents should be obtained and the specimens recompacted in the laboratory to simulate field conditions.

7. Conduct indirect tensile tests on the bound layers and resilient modulus tests on the unbound layers. The moduli obtained from these tests should be used as first estimates of the layer material properties. The slope of the M_R principal stress difference line should provide a reasonable estimate of the subgrade stress sensitivity.

8. Deflection basin-fitting techniques are then used to obtain the surface and subbase layer moduli. The design W5 deflection of a section is used in Figure 2 to obtain the modal subgrade modulus for the section. This modulus should be used in conjunction with the modulus estimates for the bound layers obtained from indirect tensile tests as initial input to a layered-theory program. The deflection basin slope of this structure under the Dynaflect load as predicted by layered theory is then compared with the measured basin slope of the section. The input moduli for the bound pavement layers may require adjustment, and this process is repeated until the basin slope predicted by layered theory corresponds to the basin slope. Should a computer not be readily available, Figure 3 can be used to provide estimates of these moduli.

9. This process will provide a set of effective layer moduli that occur most frequently in the section under the Dynaflect load. In order to obtain a reasonably conservative design, a subgrade modulus representative of the weaker spots within a section should be used. The cumulative distribution curve of the sensor-5 Dynaflect deflection for the section may be used for this purpose. Depending on the design reliability required, the W5 deflection corresponding to a required percentile can be selected from the distribution curve to represent the weaker subgrade. This design deflection is now used in Figure 2 to obtain the design subgrade modulus under the Dynaflect load.

10. Should the designer have some idea of the nature of the change of subgrade modulus with depth, the design subgrade modulus should be reduced as indicated in Figure 5.

11. The final step in the materials characterization process is to take the stress sensitivity of subgrade into account. One method is to use the slope of the log resilient modulus log deviator stress line obtained from the resilient-modulus test as an indicator of the stress sensitivity. The method has been described in detail.

12. The materials characterization for the pavement structure used in layered-theory analysis is now complete.

This materials characterization is one of the most important steps of a pavement design procedure. The tensile stress in the bound pavement layers, and consequently the fatigue life of the pavement, will depend on the moduli of the layers used as inputs in layered-theory analysis.

CONCLUSIONS

The procedures described in this report provide guidelines for a designer to use Dynaflect deflections as input for developing elastic properties, i.e., layer moduli, for use with elastic-layer analysis procedures. The guidelines permit consideration of statistical variation along a roadway, variations in depth of subgrade, stress sensitivity of materials, etc. Without accounting for these conditions, a designer may arrive at properties that are erroneous, thus destroying the credibility of the design analyses.

Although the charts provided herein are applicable to Dynaflect loading, the concepts may be applied to any deflection-measuring equipment. Furthermore, stress sensitivity procedures must be accounted for with any type of measuring equipment since the load may not be the same as those using the roadway.

ACKNOWLEDGMENT

The research and development work discussed in this paper was conducted under a cooperative agreement between the Center for Transportation Research at the University of Texas at Austin, the Texas State Department of Highways and Public Transportation, and the Federal Highway Administration. The purpose of the project is to develop an overlay design procedure for concrete pavements.

REFERENCES

1. A. Taute, B.F. McCullough, and W.R. Hudson. Improvements to the Materials Characterization and Fatigue Life Prediction Methods of the Texas Rigid Pavement Overlay Design Procedure. Center for Transportation Research, Univ. of Texas at Austin, Res. Rept. 249-1, March 1981.
2. F.H. Scrivner and C.H. Michalak. Linear Elastic Layer Theory as a Model of Displacement Measured Within and Beneath Flexible Pavement Structures Loaded by the Dynaflect. Texas State Department of Highways and Public Transportation, Austin; Center for Highway Research, Univ. of Texas at Austin, College Station, Res. Rept. 123-25, Aug. 1974.
3. The AASHO Road Test. HRB, Special Rept. 73, 1962.
4. W.R. Hudson and T.W. Kennedy. An Indirect Tensile Test for Stabilized Materials. Center for Highway Research, Univ. of Texas at Austin, Res. Rept. 98-1, Jan. 1968.
5. K. Nair and C.Y. Chang. Flexible Pavement Design and Management--Materials Characterization. NCHRP, Rept. 140, 1973.
6. B.F. McCullough. A Pavement Overlay Design System Considering Wheel Loads, Temperature Changes, and Performance. Univ. of California, Berkeley, Institute of Transportation and Traffic Engineering Graduate Rept., July 1969.
7. B.F. McCullough and H.J. Treybig. A Statewide Deflection Study of Continuously Reinforced Concrete Pavement in Texas. Texas Highway Department, Austin, Tech. Rept. 46-5, Aug. 1966.
8. H. Treybig, B.F. McCullough, P. Smith, and H. von Quintus. Overlay Design and Reflection Cracking Analysis for Rigid Pavements, Volume 1: Development of New Design Criteria. Federal Highway Administration, Res. Rept. FHWA-RD-77-66, Aug. 1977.
9. O. Schnitter, W.R. Hudson, and B.F. McCullough. A Rigid Pavement Overlay Design Procedure for Texas SDHPT. Center for Highway Research, Univ. of Texas at Austin, Res. Rept. 177-13, May 1978.
10. W.G. Cochran. Sampling Techniques. Wiley, New York, 1963.

Publication of this paper sponsored by Committee on Strength and Deformation Characteristics of Pavement Sections.

Material Layer Coefficients of Unbound Granular Materials from Resilient Modulus

GONZALO RADA AND MATTHEW W. WITCZAK

The overall objective of this study was to determine and evaluate AASHO-based material design parameters for unbound granular base/subbase materials from laboratory nonlinear resilient-modulus tests. A total of 101 nonlinear M_r-relationships were developed on six typical Maryland State Highway materials. Various levels of saturation and compactive effort were evaluated with each material. By using the M_r-θ (bulk-stress) relationships developed, a nonlinear elastic-layered analysis was undertaken on 40 different pavement cross sections to establish typical bulk-stress and resilient-modulus values. The correlations between modulus and layer coefficients (a_i) and composite modulus of subgrade reaction (k_c) given in National Cooperative Highway Research Program (NCHRP) Report 128 were used to evaluate the influence of subgrade support, material type, thickness of asphalt surfacing, compactive effort in the granular layer, and degree of saturation on the a_i- and k_c-values. Substitution ratios were also developed for flexible pavement design concepts by using a dense-graded aggregate base-course material as the reference. For each material investigated, predictive equations for the layer coefficient values (a_i) were determined as functions of the subgrade California bearing ratio, compaction, saturation, and thickness of asphalt. All these variables were found to be significant from a design viewpoint. Average reductions in the a_i-value of 0.065, 0.044, 0.041, and 0.029 were found for the range in subgrade support, saturation level, compactive effort, and asphalt thickness, respectively. In the study of the composite modulus of subgrade reaction k_c used in rigid pavement analysis, it was found that the greatest influence was exerted by the subgrade support and thickness of the granular subbase layer. The maximum influence of material type, compactive effort, and/or degree of saturation on the k_c-value was less than ±10 percent for all cases considered. Reliable predictive equations for k_c were developed in terms of the primary variables evaluated.

It is current Maryland State Highway Administration (MSHA) design practice to use modified forms of the Interim Guide of the American Association of State Highway Officials (AASHO) for design of rigid and flexible pavements within the state highway system (1). For flexible pavement design, the current MSHA practice is based on the AASHO analysis, combining the use of selected substitution ratios for various subbase and base materials (2).

One significant shortcoming of the rigid and flexible pavement design procedure pertains to the general characterization of the subbase and base materials from the performance of the AASHO Road Test. For rigid pavement design practice, Westergaard's modulus of subgrade reaction (k) is used in the MSHA analysis as a typical property of foundation substrata. The AASHO Interim Guide has one major advantage to this procedure in that it provides for the estimate of the composite modulus of subgrade reaction (k_c) based on subbase (base) thickness and the resilient modulus in stiffness of the subbase type used. This characterization is shown in Figure 1. As a method of using this plot, general ranges of stiffnesses are recommended for several subbase types. For granular materials, the recommended range, from the AASHO Interim Guide, is from 8000 to 28 000 psi.

For current flexible pavement design practice, the use of substitution ratios (SR) or layer equivalents is advocated by the MSHA design procedure (2). Values for the various MSHA granular material categories are SR = 1.0 for dense-graded aggregate (DGA), SR = 1.0 for sand aggregates, and SR = 0.75 for bank-run gravel.

Even though SRs have been (and are) used in flexible pavement design procedures, it should be emphasized that the basis for determining the magnitude of the ratio can also be explained and derived in terms of a_i-values (structural layer coefficients) directly used in the AASHO flexible design equation for the structural number (SN):

$$SN = a_1 D_1 + a_2 D_2 + \ldots + a_i D_i \quad (1)$$

where a_i are layer coefficients representative of each layer and D_i are layer thicknesses.

A general interpretation of the SRs used in the MSHA procedure (2) is as follows:

$$SR = (a_2/a_i)\,DGA \quad (2)$$

where a_2 is the layer coefficient for the MSHA DGA base course and a_i is the layer coefficient for any other material in the ith layer.

In Report 128 of the National Cooperative Highway Research Program (NCHRP), additional guidance concerning the selection of the specific a_i-value for a wider selection of material types and properties is presented (3). It is of special importance to note that among the correlative material properties suggested to determine the a_i-value of granular layers, the stiffness or resilient modulus of the material is recommended. The specific nomographs suggested for granular base and subbase materials are shown in Figure 2.

STUDY OBJECTIVES

Based on the general background information provided in the introduction, it is important to note that the resilient modulus or stiffness characterization of materials can be directly used in both rigid and flexible pavement design procedures used by MSHA as well as for pavement rehabilitation studies. However, one major limitation of the use of the modulus is that at present only suggested ranges of stiffnesses for a limited number of subbase and base types have been made. Thus, the design process for MSHA conditions must still allow for considerable engineering judgment for estimation of a design modulus of subgrade reaction (k_c) or SRs determined from an analysis of the structural layer coefficients (a_i). In view of this, an extensive laboratory study was initiated at the University of Maryland for MSHA to characterize the specific major types of base and subbase materials that are currently used in the state and to provide much-needed and important design input for both rigid and flexible pavement design systems.

From the relatively large data base that was generated from the study, the following specific objectives were studied in the project:

1. To determine from laboratory resilient-modulus test results, typical resilient-modulus relationships of granular base and subbase materials used by MSHA,
2. To determine typical structural layer coefficient (a_i) and SR-values for flexible pavement design based on an analysis of these modulus relationships by using Figure 2, and
3. To determine typical composite modulus of subgrade reaction values for rigid pavement design based on an analysis of the typical modulus relationships and Figure 1.

Figure 1. Modified AASHO chart for estimating k_c-values.

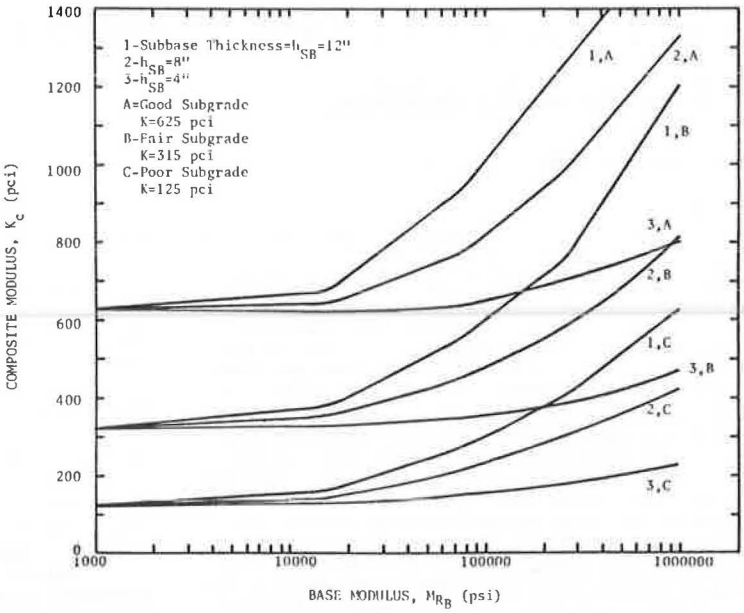

Figure 2. AASHO layer coefficient and modulus correlations for granular material.

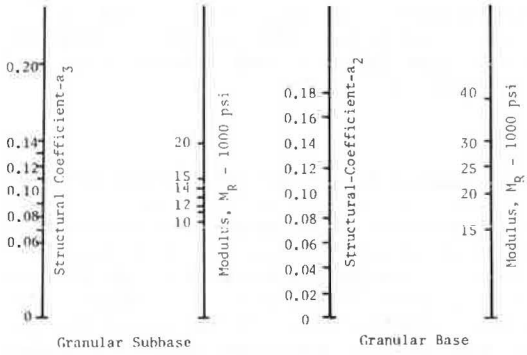

SOURCE OF DATA

For the laboratory modulus study, 101 test results obtained at the University of Maryland were used as the data base. However, it should be noted that 170 other modulus results found in the literature were used as an aid in determining the effect of different factors (discussed in the next section) on M_r. The agencies, number of tests, material types studied, and references from which these results were obtained have been presented in a previous publication (4).

The University of Maryland study involved testing six different aggregate types (two limestones that met MSHA DGA specifications, a crushed stone and slag that met MSHA CR-6 specifications, a bank-run gravel that met MSHA GP specifications, and a sand-aggregate subbase blend). For each aggregate type investigated, three hand-blended gradations were used. On each aggregate-gradation combination, three compaction energies (low, standard, and modified) were used to develop moisture-density relationships.

The resilient-modulus phase of the test program involved testing 18 specimens per aggregate type. In general, for each aggregate-gradation combination, three M_r-tests were conducted at modified compaction effort (MCE) (optimum and ±2 percent optimum moisture), two tests at standard compaction effort (SCE) (optimum and +2 percent optimum), and one at optimum for a low compaction effort (LCE) (2200 ft·lb/ft^3). The above test program should have yielded 108 data points, but seven specimens were unable to be tested.

RESULTS

Typical Mr-Values for MSHA Granular Materials

The initial objective of the overall study was to develop typical M_r-values for the MSHA unbound granular base and subbase materials. In order to do this, an investigation of the factors affecting M_r was undertaken. The details and results of this specific portion of the study have been the subject of a previous technical paper (4) and only a brief summary is presented here. The results of this effort indicated that the factors that most significantly affect M_r are the stress state, degree of saturation, and compactive effort. The amount of fines (percent passing the No. 200 sieve) and gradation were also found to affect M_r; however, their influence was very small when compared with the effect of the factors previously stated.

With these factors in mind, typical $M_r = f(\theta)$ relationships for the six aggregate types studied were developed and are summarized in Table 1. As can be seen in this table, instead of a single M_r-relationship for each aggregate type, several relationships that reflected the relative influence of the significant variables--stress state, saturation, and compaction (density)--on the k_1- and k_2-constants in the equation $M_r = k_1\theta^{k_2}$ were developed.

A more comprehensive discussion of factors influencing M_r and typical M_r-values for the MSHA unbound granular materials shown in Table 1 is presented in papers by Rada and Witczak (4) and by Rada (5).

Layer Coefficients and SRs

The second objective of this study was to develop typical values for the structural layer coefficient (a_i) and the SR for the MSHA unbound granular materials under investigation based on the M_r (or k_1-k_2-relationships) results of the previous

Table 1. Typical M_r-relationships for MSHA unbound granular aggregates.

	Dry (S_r < 60 percent)				Wet (S_r > 85 percent)			
	SCE		MCE		SCE		MCE	
Aggregate	K_1	K_2	K_1	K_2	K_1	K_2	K_1	K_2
DGA-limestone-1[a]	8 500	0.5	10 500	0.5	7000	0.4	9000	0.4
DGA-limestone-2[a]	11 500	0.3	15 000	0.3	6000	0.5	7500	0.5
CR-6-crushed stone[a]	6 000	0.5	9 000	0.5	3500	0.7	5000	0.7
CR-6-slag[a]	12 500	0.35	20 000	0.35	5600	0.35	9000	0.35
Sand-aggregate blend[b]	3 800	0.5	6 000	0.5	1900	0.7	3000	0.7
Bank-run gravel[b]	5 000	0.4	8 000	0.4	1250	0.7	2000	0.7

[a] K_1- to K_2-values typical for fines percentage (No. 200) less than 15-18 percent.
[b] K_1-value should be decreased and K_2-value increased if fines percentage is greater than 10 percent.

section. In this study, layer coefficients (a_i) were calculated by using the NCHRP Report 128 (a_i-M_r) correlations presented in Figure 2 (3). SRs were also computed by using Equation 2. It is important for the reader to understand that new correlations were not developed in this study, but rather, the existing correlation found in NCHRP Report 128 was used to develop the typical a_i- and SR-values.

Base and Subbase Bulk-Stress Values

Before any investigation of the a_i- and SR-values could be undertaken, typical modulus M_r-values had to be calculated for the different material-property combinations investigated. Obviously, these modulus values should approximate those encountered in actual pavement systems and conditions.

Recalling the typical k_1-k_2 relationships previously developed for the six MSHA unbound granular materials (Table 1), which account for the physical properties influencing the resilient response of these materials (degree of saturation and compaction), the only remaining variable necessary to predict typical M_r-values for the unbound granular materials is the typical states of stress (θ) in the granular materials under different pavement conditions.

The different conditions used to estimate the θ-values for the different base course and subbase course materials were developed from a matrix of typical pavement structures designed in accordance with the MSHA flexible pavement design procedure.

The various pavement structure components were used in a multilayer elastic analysis to determine bulk-stress values. Elastic-layered input used in the study was as follows:

h_1 (AC thickness): 3, 4.5, 6, and 8 in;
h_2 (granular base): 6 in;
h_3 (subbase): varied by h_1- and E_4-value; five values per h_1; 0-27 in;
E_1 (AC modulus): 1.5×10^5 psi and 1×10^6 psi;
E_4 (subgrade modulus): California bearing ratio (CBR) = 3, 5, 10, 20, and 30 (E_4 = 1500 CBR);

$E_2 = M_{R_b} = 9100\theta^{0.45}$ psi; and

$E_3 = M_{R_{sb}} = 3870\theta^{0.58}$ psi.

This input represented pavement structures capable of handling critical lane traffic levels varying from 50 to 2600 equivalent 18-kip single-axle loads (ESALs) per day. In order to minimize the number of elastic-layered computer program solutions necessary, typical k_1-k_2-relationships for a base material and subbase material were used to estimate the bulk stress. Altogether, 40 different pavement structures were analyzed in this phase of the study.

Finally, for all pavement conditions evaluated, the bulk-stress values were computed by using the nonlinear resilient modulus (NLRM) computer program (5) developed at the University of Maryland. Because the program yields as output the modulus (M_r) value from nonlinear characterizations and not θ, the bulk-stress values were backcalculated for each solution by using the following equation:

$$\theta = (M_r/k_1)^{(1/k_2)} \quad (3)$$

where M_r, k_1, and k_2 are known values for both the base and subbase layers.

The resulting bulk-stress values ranged between 4 and 60 psi for the base layer and from 4 to 25 psi for the subbase materials. These values have been presented in detail by Rada (5).

Layer Coefficient Values (a_i)

By using the k_1-k_2 relationships shown in Table 1 and the bulk-stress values previously developed, resilient moduli were calculated for the six MSHA unbound granular materials prior to computing the a_i-values. Since for each of the six MSHA base and subbase materials investigated, four k_1-k_2-relationships were developed (combinations of saturation and compactive effort) as well as 40 different pavement systems (combinations of E_i or M_{r_i}, h_i, and CBR_{s_g}), a total of 960 (640 for base, 320 for subbase) M_r-values were computed. These values have been summarized by Rada (5, Chap. 4).

In Figure 2, the NCHRP nomographs relating the a_i-value for granular base and subbase material to the resilient modulus were presented. Mathematically, these relationships can be defined as follows:

Base layer:

$$a_{2b} = 0.249 \log M_r - 0.977 \quad (4)$$

Subbase layer:

$$a_{2sb} = 0.227 \log M_r - 0.839 \quad (5)$$

By using these relationships and the M_r-values computed by the previous bulk-stress (k_1-k_2) study, a_{2i}-values were determined for all 960 combinations investigated.

Table 2 represents a condensed summary of the a_{2i}-values as a function of material types, asphalt-layer thickness, subgrade support, saturation level, and compactive effort. In this table, it can be observed that the values shown are based on an average temperature value (average or typical AC modulus). For the range of AC modulus studied, the influence of this factor, especially for levels of asphalt thickness used in practice, was not very sensitive to a_{2i}-changes. In addition, average layer coefficient values for the two DGA aggregates are shown along with average values for the two

Table 2. Typical layer coefficient values.

Material	Asphalt Thickness (in)	Subgrade CBR	Dry (S_r < 60 percent) SCE	Dry (S_r < 60 percent) MCE	Wet (S_r > 85 percent) SCE	Wet (S_r > 85 percent) MCE
Base						
DGA	<5	3	0.124	0.150	0.092	0.117
		5	0.130	0.157	0.098	0.125
		10	0.144	0.170	0.113	0.139
		25	0.171	0.197	0.145	0.171
	≥5	3	0.100	0.126	0.065	0.090
		5	0.104	0.130	0.069	0.095
		10	0.110	0.137	0.076	0.102
		25	0.139	0.165	0.108	0.134
Crusher run	<5	3	0.096	0.140	0.091	0.129
		5	0.103	0.147	0.100	0.138
		10	0.120	0.164	0.124	0.163
		25	0.155	0.199	0.174	0.212
	≥5	3	0.066	0.110	0.048	0.087
		5	0.071	0.115	0.055	0.093
		10	0.079	0.123	0.067	0.105
		25	0.115	0.159	0.116	0.155
Slag	<5	3	0.137	0.187	0.050	0.101
		5	0.141	0.192	0.054	0.105
		10	0.154	0 204	0.067	0.118
		25	0.178	0.229	0.091	0.142
	≥5	3	0.115	0.166	0.028	0.080
		5	0.119	0.170	0.032	0.083
		10	0.124	0.175	0.037	0.089
		25	0.149	0.200	0.062	0.114
Subbase						
Sand/gravel	<5	3	0.060	0.100	0.024	0.042
		5	0.071	0.117	0.035	0.060
		10	0.100	0.145	0.054	0.102
		25	-	-	-	-
	≥5	3	0.060	0.100	0.024	0.042
		5	0.068	0.113	0.029	0.054
		10	0.082	0.128	0.033	0.078
		25	0.103	0.148	0.064	0.110

Table 3. Layer coefficient equations.

Layer	Material	Equation
Base	DGA	$a_i = (0.140 + 0.0029CBR_{sg}) + f_c + f_s + f_t$
	Crusher run	$a_i = (0.130 + 0.0035CBR_{sg}) + f_c + f_s + f_t$
	Slag	$a_i = (0.180 + 0.0024CBR_{sg}) + f_c + f_s + f_t$
Subbase	Sand/gravel	
	Thin AC	$a_i = (0.080 + 0.0064CBR_{sg}) + f_c + f_s$
	Thick AC	$a_i = (0.100 + 0.0021CBR_{sg}) + f_c + f_s$

Notes: Above equations based on following conditions: dry (S_r <60 percent), modified compactive effort, and thin asphalt surface (h_1 < 5 in). Equations valid for CBR_{sg} < 15 - 20.

subbase materials investigated (bank-run gravel and sand-aggregate blends).

From Table 2, it can be observed that the a_{2i}-values increase with an increase in subgrade support and decrease as compactive effort is reduced from modified to standard; the materials become more saturated and the thickness of the asphalt layer is increased. For one well-versed in pavement stress-distribution effects and nonlinear modulus characterization, these results are all very logical.

Relative to the influence of subgrade support, as stronger foundation soils are encountered, the stress state (θ) in the granular layer is increased. This increase in the bulk stress with increasing support will tend to increase the granular modulus and hence structural layer coefficients. Previous studies have shown that a reduced level of compactive effort tends to decrease the k_1-term in the expression $M_r = f(\theta)$. As such, this change in reduced compactive effort results in a lower

Table 4. Correction factors.

Layer	Material	f_c[a] (compactive effort)	f_s[b] (saturation)	f_t[c] (AC thickness)
Base	DGA	-0.026	-0.033	-0.035
	Crusher run	-0.040	-0.010	-0.045
	Slag	-0.051	-0.087	-0.025
Subbase	Sand/gravel	-0.045	-0.046	NA

Note: f-values vary ±0.005 with subgrade CBR_{sg}; average values shown.

[a] Used when going from MCE to SCE.
[b] Used when going from dry (S_R < 60 percent) to wet (S_R > 85 percent).
[c] Used when going from thin AC surface (<5 in) to thick AC surface (≥5 in).

modulus and hence decreased a_{2i}-value. It is also known that the influence of moisture in granular materials is a significant factor (especially for S_r-values greater than 85 percent). When high levels of degree of saturation occur, a reduction in the k_1-value and increase in k_2 occur, which have the net effect of a reduced modulus and a_{2i}-value. Finally, the thickness of asphalt is an important factor because it directly interfaces with the stress distribution within the granular layers. From basic slab rigidity concepts, stress attenuation is directly proportioned to the third power of layer thickness. As a result, when the thickness of the asphalt layer is increased, stress levels (i.e., θ) in the underlying layers are reduced. This results in a reduction in the M_r (a_{2i})-value as the thickness is increased. In Table 2, it can be observed that two levels of asphalt thickness have been selected. An analysis of the results indicated that for asphalt thicknesses of 5 in or more, there are only minor changes in the a_i-coefficient.

Although each of the four materials shown in Table 2 has its own unique relative ranking of factors regarding their sensitivity toward changing the a_{2i}-magnitude, the asphalt thickness had the least effect, whereas the subgrade support (over a range in CBR from 2 to 20) exhibited the greatest. The other two factors (compactive effort and degree of saturation) were intermediate and generally of the same order of magnitude. The average change in the a_{2i}-coefficient values over the range of parameters investigated in the study was found to be $\Delta a_{2i} = 0.029$ (asphalt thickness); $\Delta a_{2i} = 0.041$ (compactive effort); $\Delta a_{2i} = 0.044$ (saturation); and $\Delta a_{2i} = 0.065$ (subgrade support).

In analyzing the a_{2i}-values, it was found that for a given material, all the Δa_{2i}-values for a given parameter were independent (noninteracting) of the other factors. This was true for all cases except the thickness effect of the subbase (sand/gravel) material. This important conclusion allowed for the development of very simple and practical predictive equations (by material type). Table 3 summarizes these equations. In general, they are considered very accurate and applicable for subgrade CBR values less then 15-20.

The equations shown are all based on granular material at a modified compaction effort; dry (S_r <60 percent), and a thin asphalt (<5-in) pavement layer. For conditions other than these, simple correction factors (f_c, f_s, f_t) must be applied to the a_i-values. These factors are shown in Table 4. As a simple example, consider the a_{2b}-value for a slag base course used with a 3-in asphalt layer on a CBR = 10 subgrade. If the slag is assumed to exist in an in situ condition of 90 percent saturation at 100 percent standard compaction, the a_i-value would be, from Table 2,

$$a_{2b} = (0.180 + 0.0024CBR_{sg}) + f_c + f_s + f_t \quad (6)$$

Figure 3. Influence of parameters investigated on layer coefficients (base course, DGA).

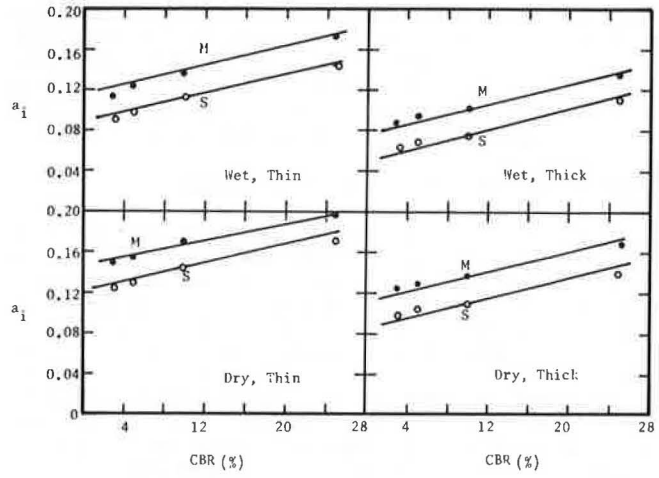

Figure 4. Influence of parameters investigated on layer coefficients (base course, crusher run).

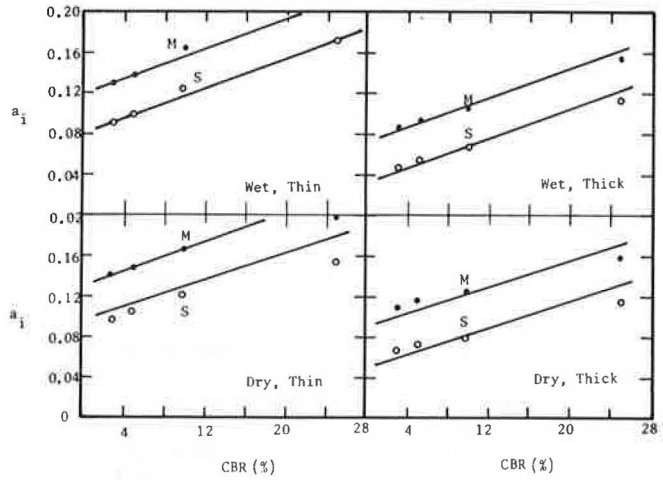

Figure 5. Influence of parameters investigated on layer coefficients (base course, slag).

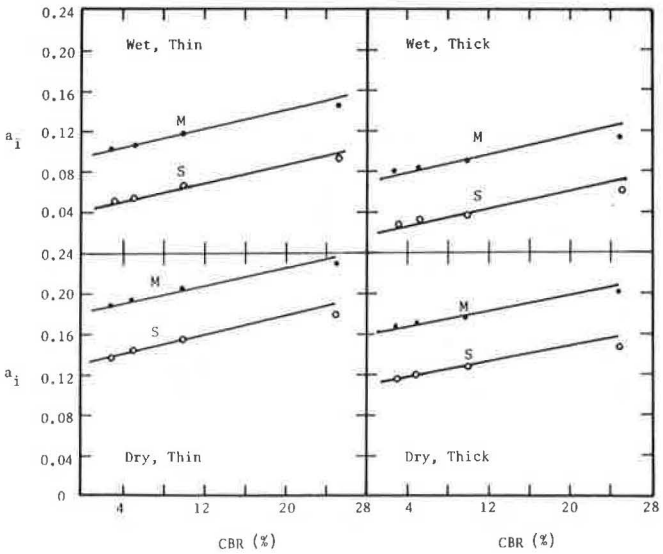

Figure 6. Influence of parameters investigated on layer coefficients (subbase course, sand gravel).

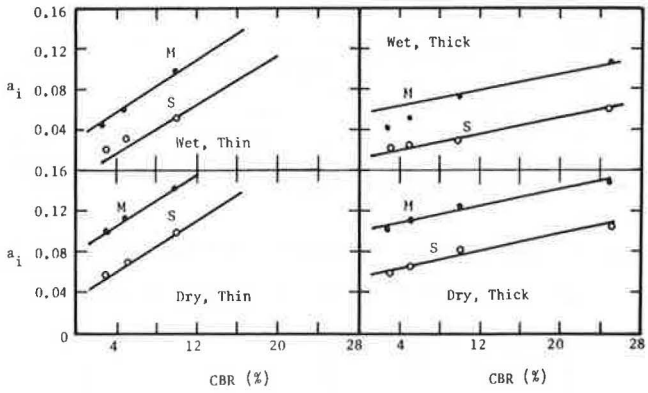

where

f_c = -0.051,
f_s = -0.087, and
f_t = 0 (no thickness correction necessary since thin category is present);

or

$$a_{2b} = 0.180 + 0.024 - 0.051 - 0.087 = 0.066 \quad (7)$$

(a_2 is 0.067 from Table 2.)

Although the a_{2b}-value of 0.066 may at first appear to be low, the influence of saturation on this material (as reflected by f_s = -0.087) was quite large in the laboratory M_r test program. This can be observed by viewing the reduction in the k_1-values in Table 1 for the CR-6-slag material between the dry and the wet conditions.

In order to help visualize the accuracy of the predictive equations noted in Table 3, Figures 3 through 6 show the predicted relationships compared with the individual data points noted in Table 2.

SR-Values

The development of typical SRs for unbound granular base and subbase materials was simply a continuation of the a_i-calculations and predictive equations developed. SR-values were developed by using Equation 1 and the predictive a_i-equations summarized in Table 3. The basic a_2-value selected for the computations was the DGA base material, compacted at modified compaction, dry (S_r < 60 percent), and with a thin asphalt layer (<5 in).

Because the a_i-values are functions of the subgrade CBR, the SR-values calculated were all evaluated at the same CBR value for the DGA and ith material-property combination. Figures 7 and 8 summarize the results of this analysis for the base and subbase materials, respectively. In these figures, only the extreme combinations are plotted (dry, modified to wet, standard). The range between these two combinations reflects the general variation in the SR-value due to variable compaction-moisture conditions that would probably be expected to occur in the field.

As can be noted, each combination (of compaction and saturation) is a function of the subgrade CBR. From a practical viewpoint, the SR-value decreases with an increase in subgrade support. However, with the exception of several wet-standard plots, the practical effect of subgrade is not significant,

especially as the compactive effort is increased and low saturation levels are encountered.

Table 5 is a general summary of typical SR-values (at a subgrade CBR = 10) for the factors evaluated in the study. Obviously, with the exception of subgrade support (normalized in the SR-computations), the same parameters and their relative ranking influencing the a_i-value affect the SR-values. The table clearly indicates the influence of compactive effort, moisture, and thickness of asphalt on the resultant values.

Figure 7. Influence of parameters investigated on base material SR-values.

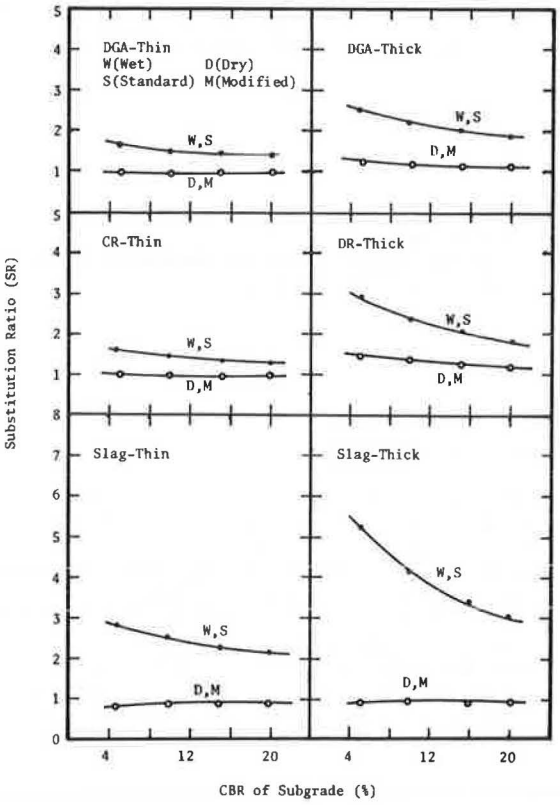

Figure 8. Influence of parameters investigated on subbase material SR-values.

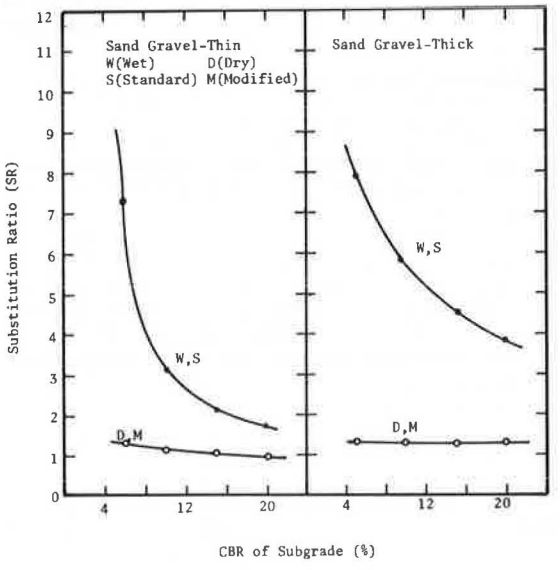

Composite Modulus of Subgrade Reaction

The other major objective of this study was to develop composite modulus of subgrade reaction values k_c for the six MSHA materials investigated, based on the resilient-modulus (k_1-k_2) relationships previously developed. As stated in this report, these k_c-values were to be based on the relationships presented in NCHRP Report 128 (3).

Bulk-Stress Values of Subbase Materials

Like the layer coefficient and SR study for flexible pavements, the only unknown parameter needed to predict the resilient moduli for granular subbase layers beneath the rigid pavement is the bulk-stress value. In this analysis, a value of 4.2×10^6 psi for the modulus of the concrete layer and a linear relationship between log E_1 (modulus of surface layer) and θ (bulk-stress value) were assumed. Bulk-stress values were then found for the subbase materials under rigid pavement (8-10 in thick) by extrapolating the NLRM computer program results.

Based on this study, an average bulk-stress value of θ = 4 psi was selected as the value that defined the typical state of stress in the subbase layer for all subbase conditions.

Composite Modulus (k_c) Results

Once the typical bulk-stress value of 4 psi was selected, the M_r-values for the six aggregate types in this study were computed by using the following equation:

$$M_r = k_1 \theta^{k_2} = k_1 (4)^{k_2} \text{ psi} \quad (8)$$

where k_1 and k_2 are the values (for combinations of saturation and compaction) found in the first part of the study. The M_r-values calculated for the different combinations of saturation and compaction are presented in Table 6.

By using these M_r-values for each of the aggregates and in situ conditions previously described, the existing NCHRP nomograph for the composite modulus of subgrade reaction value was used to determine k_c-values at three levels of subbase thickness (h_{sb} = 4, 8, and 12 in) and three levels of native subgrade support as follows:

Support	k (pci)	CBR (%)	Mr (psi)
Poor	125	2	3 000
Fair	315	5	7 500
Good	625	10	15 000

This study resulted in k_c-values for all possi-

Table 5. Summary of typical material SRs.

Material	Asphalt Thickness (in)	Dry (S_r < 60 percent) SCE	Dry (S_r < 60 percent) MCE	Wet (S_r > 85 percent) SCE	Wet (S_r > 85 percent) MCE
Base					
DGA	Thin (<5)	1.20	1.00	1.55	1.25
	Thick (≥5)	1.60	1.25	2.25	1.65
Crusher run	Thin (<5)	1.35	1.00	1.50	1.10
	Thick (≥5)	2.10	1.40	2.40	1.55
Slag	Thin (<5)	1.10	0.85	2.55	1.45
	Thick (≥5)	1.30	0.95	4.10	1.85
Subbase					
Sand/gravel	Thin (<5)	1.70	1.15	3.20	1.70
	Thick (≥5)	2.20	1.40	5.60	2.25

Notes: Values shown reflect SR at CBR_{sg} = 10 percent. Some material-physical condition combinations may vary significantly with CBR value.

Table 6. Typical M_r-values for subbase layer of rigid pavements.

Material	Dry (S_r < 60 percent)		Wet (S_r > 85 percent)	
	SCE	MCE	SCE	MCE
DGA-limestone	17 000	21 000	12 188	15 670
DGA-limestone-2	17 430	22 736	12 000	15 000
CR-6-crushed stone	12 000	18 000	9 237	13 195
CR-6-slag	20 306	32 490	9 097	14 621
Sand-aggregate blend	7 600	12 000	5 014	7 917
Bank-run gravel	8 705	13 930	3 300	5 778

ble combinations of material type (six), degree of saturation (two), percentage of compaction (two), subbase thickness (three), and subgrade support (three). These values have been summarized in both tabular and graphical form elsewhere (5).

Discussion of Results

By referring to Figure 1 and Table 6, it can be observed that the sensitivity of the subbase modulus for unbound granular materials is very slight on the final composite k_c-value (on the type of subbase layer). This fact was obviously reflected by the results obtained in this study. From a practical design viewpoint, a simple but reliable predictive equation of the k_c-value for unbound granular subbase materials was found to be as follows:

$$k_c \text{ (pci)} = f_o (k_{sg} + 7.5h_{sb} - 20) \quad \text{for } h_{sb} \geq 4.0 \text{ in} \tag{9}$$

where

k_{sg} = modulus of subgrade reaction (pci),
k_c = composite granular subbase-subgrade reaction value (pci),
h_{sb} = thickness of granular subbase (in), and
f_o = adjustment factor reflecting material type and in situ conditions.

In this equation, the typical f_o-values are shown below:

Subbase Material	fo-Value Dry-Modified	Wet-Standard
Crushed stone	1.00	0.95
Sand/gravel	0.95	0.90
Slag	1.08	0.92

In essence, the greatest influence on k_c is reflected by the foundation support value and thickness of the subbase layer. The maximum influence of material type, compactive effort, and/or degree of saturation on the k_c-value appears to be less than 10 percent for all cases considered.

SUMMARY AND CONCLUSIONS

The study presented in this report was based on resilient-modulus test results of granular materials obtained from an extensive laboratory study. Based on this analysis, the following conclusions were obtained.

1. An analysis of the University of Maryland M_r-test results indicated that the primary variables influencing the M_r-response of granular materials are the stress state, degree of saturation, and degree of compaction. The amount of fines (percent passing the No. 200 sieve) or gradation was also found to have an effect on M_r; however, it was relatively small and not considered as a primary variable in the study.

2. Several relationships (instead of a single M_r-relationship for each aggregate) that reflected the relative influence of the significant variables--stress state, saturation, and compaction--on the k_1 and k_2 (constants in $M_r = k_1\theta^{k_2}$) values were developed for six MSHA unbound granular materials investigated. These relationships were presented in Table 1.

3. The study of the factors influencing the structural layer coefficients a_i and SRs showed that degree of saturation (S_r), percent compaction (PC), subgrade CBR, and asphalt layer thickness were important parameters affecting their magnitude.

4. By using the $M_r = f(\theta)$ relationships and bulk-stress (θ) values developed in this study and the a_i and M_r correlations from NCHRP Report 128, typical layer coefficients (a_i) and SRs were developed for the MSHA granular materials investigated. Predictive equations for the structural layer coefficient values of these materials were developed in terms of the primary variables studied.

5. The final study phase dealt with determining composite modulus of subgrade reaction values (k_c) for the MSHA materials studied. A typical bulk-stress value of θ = 4 psi was found to be applicable based on elastic-layered studies for rigid pavement subbase layers. By using this, typical M_r-values were determined and the relationship between k_c and M_r found in NCHRP Report 128 was used to investigate the influence of variables on the composite modulus of subgrade reaction. It was found that the effect of material type and subbase modulus (for all combinations of saturation and compaction) on k_c is small when compared with the influence of the subgrade modulus and subbase layer thickness. As in the a_i study, simple predictive equations were developed in terms of the variables considered.

REFERENCES

1. AASHO Interim Guide for Design of Pavement Structures 1972. American Association of State Highway Officials, Washington, DC, 1972.
2. Flexible Pavement Design Procedure. Materials and Research, Maryland State Highway Administration, Brooklandville, Nov. 1969.
3. C.J. Van Til, B.F. McCullough, B.A. Vallerga, and R.G. Hicks. Evaluation of AASHO Interim Guides for Design of Pavement Structures. NCHRP, Rept. 128, 1972.
4. G. Rada and M.W. Witczak. Comprehensive Evaluation of Laboratory Resilient Moduli Results for Granular Material. TRB, Transportation Research Record 810, 1981, pp. 23-33.
5. G. Rada. Evaluation of Design Parameters for MSHA Unbound Granular Materials. University of Maryland, College Park, Master's thesis, 1981.

Publication of this paper sponsored by Committee on Strength and Deformation Characteristics of Pavement Sections.

Moduli of Pavement Systems from Spectral Analysis of Surface Waves

J.S. HEISEY, K.H. STOKOE II, AND A.H. MEYER

A nondestructive technique for pavement evaluation is necessary to determine moduli of the various materials in existing pavement systems. Dynamic field testing can be used to calculate moduli from velocities of surface waves propagating through the different layers of the pavement system. A new, efficient technique incorporating an impulsive source has been developed to replace the slower, steady-state vibration technique. Frequency and phase content of the surface waves generated by the source are collected with portable spectral-analysis instrumentation. Results for field tests conducted at two flexible pavement sections yielded wave velocities measured by the spectral-analysis technique that were within 10 percent of velocities determined from cross-hole tests performed at both sites. This comparison confirms that an accurate profile of velocity versus depth (hence modulus versus depth) can be obtained by using this rapid, nondestructive spectral-analysis technique.

Pavement life is usually defined as the length of service of the pavement system before maintenance or rehabilitation is required. Estimates of remaining life as well as appropriate remedial measures are based on the elastic moduli of the various pavement materials. Elastic moduli are used to characterize the stress-strain behavior of the pavement system, which in turn is used to indicate the potential for deterioration and tensile cracking in the surface layer. Numerous methods have been developed to determine elastic moduli in pavement systems in the field. This paper presents an advance in the state of the art in the application of one of these field methods, the wave-propagation method.

There are four general methods used to evaluate elastic moduli of pavement systems (1): static deflections, steady-state dynamic deflections, impact-load response, and wave propagation. The first three methods measure deflections or displacement response of the entire pavement system caused by a static or dynamic load. Moduli are then calculated indirectly by using some form of elastic-layer theory. The major drawback of these methods is that the overall stiffness of the pavement system is measured, and it is generally difficult to separate properties of the individual layers.

Wave-propagation methods measure the velocities of elastic waves traveling through the pavement system rather than the deflections caused by the vibration source. Elastic waves can be generated by steady-state vibrations or transient impulses, and they can propagate through individual layers or the entire pavement system. Wave-propagation methods offer the most direct approach to determining elastic moduli of pavement systems since each layer is uniquely identified by the wave propagation velocity of the material within the layer.

MEASUREMENT OF ELASTIC PROPERTIES BY WAVE PROPAGATION

Since the stress-strain properties of a material govern wave-propagation velocities in that material, dynamic (or seismic) testing can be used to determine wave-propagation velocities from which moduli of elastic materials can be calculated. Furthermore, most field techniques include methods to determine thicknesses or depths of different layers on the basis of wave-propagation velocities.

Wave Propagation in Elastic Half-Space

Wave motion created by a disturbance within an infinite, homogeneous, isotropic, elastic medium ("whole space") can be described by two kinds of waves: compression waves and shear waves. These waves are called body waves because they propagate within the body of the medium. When the elastic medium forms a half-space with a surface of infinite extent on the top, a third type of wave motion occurs. This third type of wave occurs in a zone near the surface of the half-space. The surface wave is called a Rayleigh wave, after its first investigator. Each of these three waves displays a different type of motion and travels at a different velocity.

The compression wave exhibits a push-pull motion and hence is referred to as a dilatational wave. This dilatational motion occurs in the same direction as the direction of wave propagation. The compression wave travels with a faster velocity than either the shear wave or the Rayleigh wave. Since the compression wave appears first in a travel-time record of wave motions, it is commonly called the primary wave, or P-wave. The velocity of the P-wave is given by the following equation:

$$v_p = [(\lambda + 2G)/\rho]^{1/2} \quad (1)$$

where

$$\lambda \text{ (Lame's constant)} = \nu E/[(1 + \nu)(1 - 2\nu)] \quad (2)$$

$$G \text{ (shear modulus)} = E/2(1 + \nu) \quad (3)$$

and E, ν, and ρ are Young's modulus, Poisson's ratio, and mass density, respectively, of the elastic material.

The shear wave, also called a distortional wave, exhibits shearing motion perpendicular to the direction of wave propagation. The shear wave travels significantly slower than the P-wave and, as a result, appears later in a travel-time record. It is commonly called the secondary wave, or S-wave, because it arrives after the P-wave. The velocity of the S-wave is given by the following equation:

$$v_s = (G/\rho)^{1/2} \quad (4)$$

Unlike P-waves, the velocity of which can vary with the degree of saturation of a porous medium (such as soil), S-waves have the same velocity in a saturated medium as in an unsaturated medium because the fluid cannot transmit shearing motion.

The Rayleigh wave, or R-wave, does not propagate into the body of the elastic medium but travels along the surface of the half-space. The wave motion causes both horizontal and vertical particle displacements, which describe a retrograde ellipse at the surface. The amplitude of the wave decays quickly with depth so that at a depth of one wavelength, the amplitude of particle motion is only about 30 percent of the original amplitude of the surface. The velocity of the R-wave is nearly equal to the S-wave velocity, particularly for values of Poisson's ratio above about 0.25. In addition, R-wave velocity is independent of frequency in a homogeneous half-space. Since an ideal elastic half-space has a unique R-wave velocity, each frequency has a corresponding wavelength according to the following relationship:

Figure 1. Types of waves in elastic half-space.

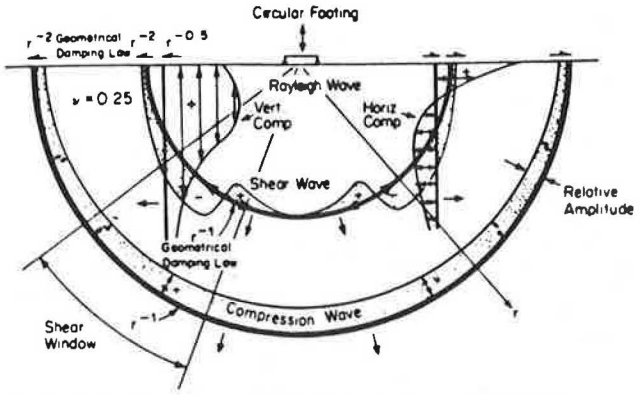

(a) Distribution of waves from a vertically vibrating footing on a homogeneous, isotropic, elastic half-space (3).

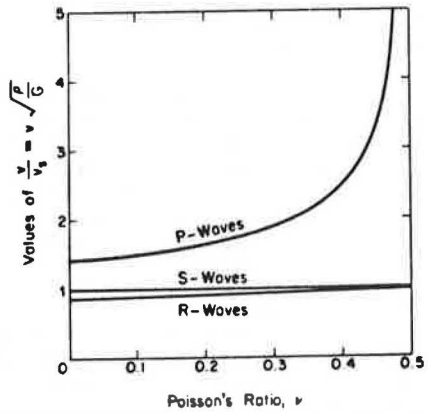

(b) Relationship between Poisson's ratio and wave velocities in an elastic half-space (3).

Figure 2. Steady-state Rayleigh-wave testing in layered systems.

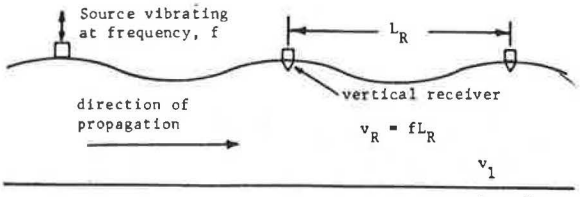

(a) Measurement of steady-state, Rayleigh-wave motion.

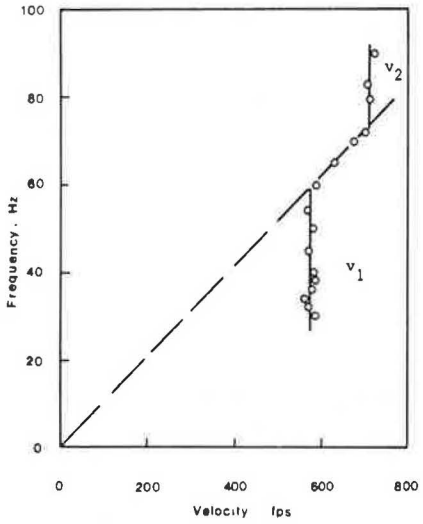

(b) Typical results.

$$v_R = f \cdot L_R \quad (5)$$

where f is the input frequency of excitation that generates a Rayleigh wave of wavelength L_R. The frequency-independent nature of the R-wave is the basis for certain types of dynamic testing.

The propagation of wave energy away from a vertically vibrating circular footing at the surface of an elastic half-space is shown in Figure 1a, which illustrates the three types of waves just discussed. Miller and Pursey (2) found that 67 percent of the input energy from a vertically oscillating circular source propagated away in the form of Rayleigh wave energy, whereas 26 percent was carried by the shear wave and 7 percent was carried by the compression wave. Body waves, P- and S-waves, propagate radially outward along a cylindrical wave front at the surface. The relationships governing the geometrical damping of the wave energy as a function of radial distance from the source (r) are also shown in Figure 1a. At the surface, the P-wave and S-wave decrease in amplitude by $1/r^2$, whereas the R-wave decreases by $1/\sqrt{r}$.

The propagation velocities of all these waves relative to the shear-wave velocity are shown as a function of Poisson's ratio in Figure 1b. Note that the velocities v_p, v_s, and v_R are the propagation velocities of the respective wave fronts and not the particle velocities of the medium itself due to the wave energy.

Body Waves in Layered System

In the case of a pavement system, seismic waves propagate through a layered system, which complicates the problem, especially for body waves. When body waves reach an interface between two layers, some of the body-wave energy is reflected back into the first layer and some is transmitted by refraction into the second layer. The combination of reflected and refracted body waves from a layered system greatly increases the complexity in analyzing wave arrivals, especially for measurements made at the pavement surface. In addition, pavement systems include the complication of having higher-velocity material overlying lower-velocity material (3).

Field Techniques for Determining Wave Velocities

Various techniques are used for in situ measurement of wave velocities. The type of wave that is generated and recorded depends on the source of vibration as well as the location of receivers. Site conditions may also govern which technique is most effective.

Steady-state techniques generally use a vertically oscillating mass placed on the surface to excite the system with primarily Rayleigh waves. Vertical motion transducers are then moved along the surface until the distance between successive troughs or peaks of wave motion is established. This distance is the wavelength of the Rayleigh wave L_R, and if the frequency of vibration of the source is known, the velocity is readily determined from $v_R = f \cdot L_R$. This technique is illustrated in Figure 2. It should be noted that a range of frequencies must be excited to develop a site profile adequately.

When the steady-state technique shown in Figure 2 is used at a given site, low frequencies generate long wavelengths corresponding to deep sampling of the site. Conversely, high frequencies generate

Figure 3. Representation of complex time signal by its frequency spectrum.

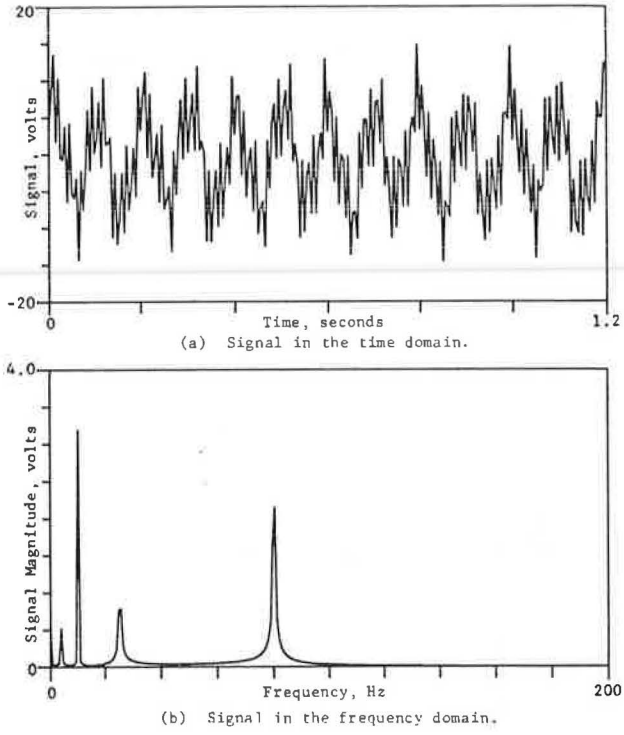

(a) Signal in the time domain.

(b) Signal in the frequency domain.

short wavelengths corresponding to shallow sampling. In multilayered systems, the Rayleigh wave propagates at a velocity that reflects the material properties of the layer(s) that the wavelength samples. Short wavelengths within the surface layer will measure properties in that layer only. Long wavelengths (relative to the depth of the surface and base courses) will travel predominantly through the subgrade. Intermediate wavelengths will sample the base course or average the properties of all three materials: surface, base, and subgrade. Each wavelength will then have a corresponding phase velocity, depending on how much of each layer the wave samples.

The mathematical analysis required to interpret the relationship between phase velocity and wavelength for several typical pavement sections was studied by Jones (4). Jones assumed homogeneous elastic layers while treating the subgrade as a semiinfinite medium and showed that at infinitely long wavelengths, the phase velocity approached the R-wave velocity of the semiinfinite medium. Similarly, at very short wavelengths, the phase velocity approached the R-wave velocity of the surface layer. Theoretical solutions for an intermediate layer required more assumptions.

Although earth materials are neither perfectly homogeneous or elastic, field investigations indicate that such assumptions are reasonable. Heukelom and Foster (5) reported a profile of velocity versus depth that showed good correlation with the pavement profile when the effective sampling depth was taken as one-half of the Rayleigh wavelength. Szendrei and Freeme (6) found a similar correlation by using an effective sampling depth of approximately one-third of the Rayleigh wavelength.

Other surface measurement techniques utilize an impulsive source. Usually, velocities of P-waves are determined in these surveys. Travel times and travel distances to the received may be determined from the direct arrival or for an initial reflection in the upper layer. However, refracted waves are normally encountered and care must be taken not to identify refracted waves as direct waves. To overcome this problem, refraction surveys are performed that take advantage of the faster-traveling refracted waves to develop the profile and corresponding velocities for a layered system. Such an analysis is greatly complicated for a site with many layers or dipping strata. Refraction surveys are also hindered when a higher-velocity layer overlies a lower-velocity layer, as in the case of a pavement surface that overlies a base course or subgrade.

An alternative to surface measurement techniques is crosshole testing (7). The source and receivers are placed in drilled holes so that direct arrivals of waves can be determined. Both P- and S-wave velocities can be measured in this type of test. Layering and velocities are accurately determined. Proper spacing of the boreholes eliminates or minimizes problems caused by refracted waves. The constraint of a quick, nondestructive test precludes this method from application in pavement evaluation. However, crosshole testing was used in this research as a tool to verify the accuracy of the proposed procedure.

Of the various wave-propagation methods, the steady-state technique appears to be most feasible for pavement testing. Unfortunately, the time required to develop the velocity profile at a given location is prohibitive. Data acquisition at just one test location may take up to several hours depending on the type of equipment used, the degree of resolution required, and the experience of the field personnel. However, if a wide range of frequencies (or wavelengths) could be excited and measured with a single excitation, the testing time could be greatly reduced. Such a procedure requires the spectral analysis of a wave pulse generated by an impact at the pavement surface.

FREQUENCY DOMAIN MEASUREMENTS

In the past 10-15 years, the development of microprocessors and the fast-Fourier-transform (FFT) algorithm has greatly extended the capability to measure and analyze dynamic systems in the frequency domain. Instrumentation now exists that rapidly filters and converts an analog signal to a digitized signal, transforms the signal from its representation in the time domain into its frequency components, and analyzes the data in various formats. Consequently, frequency spectrum analysis provides a quick and feasible approach to evaluate the propagation of elastic waves through layered systems.

Advantages of Spectral Analysis

The primary reason for utilizing spectral analysis is that information can be extracted from the data that was not apparent from the time domain representation of the signal. For example, the components of the signal in Figure 3a are indistinguishable in the time record, but each wave and its relative contribution to the overall waveform are easily observed in the frequency spectrum shown in Figure 3b. The amplitude and phase of each frequency component in the waveform can be determined. In addition, relationships between two signals can be easily identified.

Measurements in Frequency Domain

Several types of measurements can be made directly with most of the spectral analyzers that are currently available. The basic requirement is the linear spectrum, generally of both an "input" signal and an "output" signal. Other functions are defined

by using these two spectra or their complex conjugates.

The linear spectrum, denoted by $S_x(f)$, is simply the Fourier transform of the signal. The linear spectrum provides both magnitude and absolute phase information for all frequencies within the bandwidth for which the measurement was taken. Since the absolute phase is measured, a trigger is required to synchronize the signal for averaging. Linear spectrum averaging is useful for determining predominant frequencies of excitation, identifying fundamental modes and harmonics of a dynamic system, or extracting a true signal out of background noise.

The autospectral density function $G_{xx}(f)$, commonly called the autospectrum, is defined as the linear spectrum $S_x(f)$ multiplied by its own complex conjugate $S_x^*(f)$. The magnitude of the autospectrum is the magnitude squared of the linear spectrum. This magnitude can be thought of as the power (or energy of a transient impulse signal) at each frequency in the measurement bandwidth. However, multiplication by the complex conjugate eliminates the imaginary components of the spectrum, so no phase information is provided by the autospectrum. The advantage of the autospectrum is that it provides information similar to that of the linear spectrum but does not require a trigger to synchronize the averaging of signals.

The cross spectral density function $G_{yx}(f)$, or cross spectrum, is the Fourier transform of the cross-correlation function between two different signals x(t) and y(t). The cross spectrum is defined by the following equation:

$$G_{yx}(f) = S_y(f) \cdot S_x^*(f) \quad (6)$$

where $S_y(f)$ is the linear spectrum of the output and $S_x^*(f)$ is the complex conjugate of the linear spectrum of the input. The magnitude of $G_{yx}(f)$ is a measure of the mutual power between the two signals, making the cross spectrum an excellent means of identifying predominant frequencies that are present in both the input and output signals. The phase of $G_{yx}(f)$ is the relative phase between the signals at each frequency in the measurement bandwidth. Since the phase is a relative phase, the cross-spectrum measurement can be made without a synchronizing trigger. The cross spectrum is used primarily to determine the phase relationships between two signals that may be caused by time delays, propagation delays, or varying wave paths between receivers.

The transfer function H(f), or frequency response function, characterizes the input-output relationship of a dynamic system. The frequency response function is the ratio of the spectrum of the system's response (output) to the spectrum of the system's excitation (input). Thus, the transfer function is similar to the cross spectrum. Both provide the same phase information; the magnitude of the transfer function is normalized by the autospectrum of the input $G_{xx}(f)$ relative to the magnitude of the cross spectrum. Consequently, the transfer function of a given system should be constant regardless of the input (if the system does not undergo nonlinear behavior). Generally, the input is a force measurement derived from the signal of a load cell mounted on the source of excitation. Depending on the quantity measured as output, the transfer function may provide a measurement of impedance, dynamic stiffness, or one of several other system properties. The transfer function is frequently used to identify natural frequencies and damping coefficients of a dynamic system.

The coherence function $\gamma^2(f)$ is a measurement made in conjunction with the transfer function. The coherence is a real-valued function that is the ratio of the response (output) power caused by the measured input to the total measured response power. Therefore, if $\gamma^2(f) = 1$, all the output at the particular frequency of interest is due to the measured inputs. Reasons why the coherence function may be less than unity are as follows:

1. There are multiple input signals in the system that are not being measured;
2. Background noise is present in the measurement;
3. The frequency response function is nonlinear for the system;
4. There are closely spaced resonant peaks that cannot be detected with the given frequency resolution inherent in the digitization of the signal; or
5. Waves in the frequency range of poor coherence are not adequately excited.

EXPERIMENTAL PROCEDURE

Equipment

Two different sources were used to propagate waves through the pavement system. Each source generated an impulsive load on the surface of the pavement. Therefore, all signals were transient events. To develop a quick and efficient technique to determine the velocity profile, a wide range of frequencies (and corresponding wavelengths) must be excited by the source. An impulsive source is quicker and more efficient than a steady-state oscillator with regard to this requirement. An impact hammer is a satisfactory source if it adequately excites the bandwidth of frequencies needed to sample the pavement profile properly.

The larger source was a falling-weight deflectometer (FWD) similar to the Phoenix falling-weight deflectometer manufactured in Denmark (8). This device was mounted on a two-wheel trailer that could be towed on the highway by a passenger vehicle. The hammer was a falling mass that weighed 331 lb and could be dropped from various heights. Measurements were triggered internally by using the signal from the receiver closest to the source.

A second source, called simply a drop hammer, consisted of a cylindrical steel mass weighing approximately 6 lb. The cylinder had a hole through the center so that it could fall from any height along the 24-in rod that guided the hammer to hit the base plate, which was 2.5 in in diameter. Measurements were triggered with a resistance-capacitance (RC) trigger (7). The RC trigger permits accurate determination of the direct arrival time of the wave from the source to the receiver.

Velocity transducers, commonly called geophones, were used to detect wave propagation through the pavement system. Both vertical and horizontal geophones were employed to allow sensitivity for several different types of waves and directions of motion. The geophones were mounted on steel blocks (with a largest dimension of 2.75 in), which were then epoxied to the asphalt surface to ensure adequate coupling. The geophones had natural frequencies of 8 and 14 Hz (1 Hz = 1 cycle/s) with an approximately linear response over the range of 20-1600 Hz. Since only wave-propagation velocities (and not particle velocities) were desired, no calibration factor was determined to relate voltage to absolute particle velocity.

The instrument used to record the signals was the Hewlett-Packard Model 5420A digital signal analyzer. The instrument includes a set of signal filters, an analog-to-digital converter (ADC), a dual-channel digital oscilloscope, and a magnetic cassette tape

for storage and recall of permanent records. The analyzer can directly measure the frequency domain measurements previously discussed. In addition, the type of signal, type and number of averages, bandwidth (or time length), and trigger conditions can all be specified by the operator. The analyzer can be easily interfaced with an x-y plotter to provide a hard copy of the data.

Setup

The general configuration of the source, geophones, and recording equipment used in these tests is shown in Figure 4. The geophones were placed in a linear array to minimize anisotropic effects that might influence wave propagation. The line of geophones extended parallel to the direction of the roadway. Vertical geophones (subsequently identified by the symbol V) were located approximately 1, 2, 5, and 10 ft from the source. Horizontal geophones (subsequently identified by the symbol H) were located at the same positions and were aligned radially from the source so as to detect wave motion occurring in the direction of wave propagation. Hereafter, measurements are identified by the type of geophone used (V or H) and the location of the geophone(s) from the source (1, 2, 5, or 10 ft). For example, measurement V2-V5 used vertical geophones located 2 ft and 5 ft from the source.

Measurements were made by using only two geophones for any one impulse, since the recording instrument was a dual-channel device. Comparative records were taken for responses of both vertical and horizontal geophones. Both time-domain and frequency-domain measurements were recorded, although the thrust of the data acquisition was toward spectral analysis. Frequency-domain measurements included the linear spectrum, autospectrum, cross spectrum, transfer function, and coherence function. Records with one average and with five averages were used to compare the advantages of averaging.

Figure 4. Experimental setup.

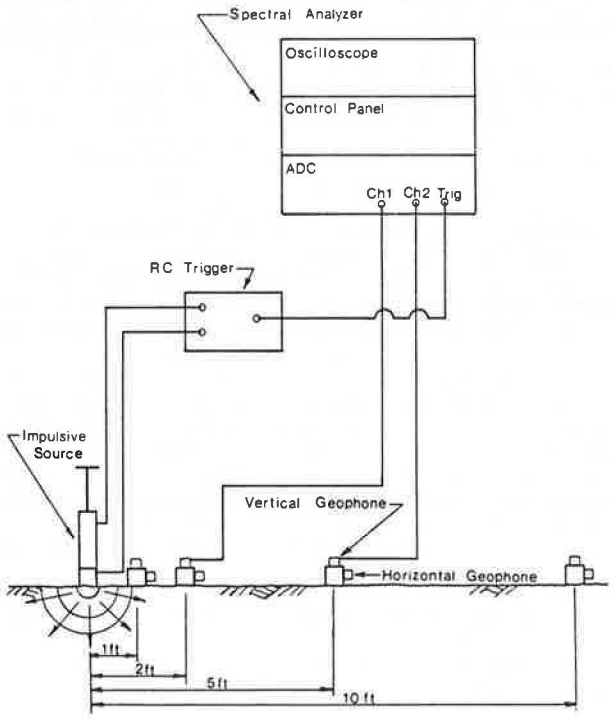

Method of Analysis

Since more than two-thirds of the energy generated by a vertical force propagates away from the source in the form of a Rayleigh wave, it was assumed that the recorded responses of the geophones represented primarily R-wave motion. Analysis by using the R-wave is desirable since it is not significantly affected by reflections that complicate P-wave and S-wave analyses. Furthermore, due to the relationship between frequency and wavelength of the R-wave, the entire profile (to a depth of interest for a pavement system) can be investigated without borings being required.

By using the phase information provided by the cross spectrum, travel times can be calculated for each frequency that is excited. The phase difference θ between the signals of the input and output geophones represents the time lag or travel time Δt for an R-wave (of frequency f and velocity v_R) to propagate over the distance between the two geophones. The phase difference is 360 degrees for a travel time equal to the period of the wave T. With T/360 degrees as a proportionality factor, the relationship for travel time is as follows:

$$t = (T/360^\circ) \cdot \theta \tag{7}$$

Because the frequency is the inverse of the period, travel time can be written as follows:

$$t = [(\theta/360^\circ)] \cdot [(1/f)] \tag{8}$$

The distance between the geophones is a known parameter, and therefore the velocity is readily calculated by the following equation:

$$v_R = (\text{distance}/\Delta t) \tag{9}$$

Now both frequency and velocity are known, so the wavelength of the R-wave can be calculated from Equation 5. The profile of velocity versus depth is based on an appropriate fraction of the wavelengths corresponding on the effective sampling depth of the wave.

A typical set of calculations is shown in Table 1. Further details regarding the reduction and analysis of the data may be found in the report for this study (9).

Test Sites

Field tests were conducted at two sites; both profiles consisted of a subgrade, base course, and flexible pavement. Crosshole test data were available for comparison purposes at both sites.

The first site was an asphalt section of Interstate 35 in Austin, Texas (referred to here as the Austin site). The longitudinal section profile is shown in Figure 5a. The thickness of the asphalt is approximately 6.5 in. The flexible base is compacted in three layers, each approximately 5 in thick, and is underlain by a sandy subbase approximately 1 ft thick. The subgrade is primarily a stiff silty clay extending to a depth of about 13 ft. Average unit weights of the materials are 145, 140, 135, and 115 pcf for the pavement, base, subbase, and subgrade, respectively. Poisson's ratios were assumed to be 0.35 for the pavement and 0.40 for the base, subbase, and subgrade.

The second site was a section of Texas Route FM 971 near Granger (referred to here as the Granger site). The section is located on a constructed fill embankment. The subgrade is a compacted clay to a depth of approximately 20 ft. The base course is approximately 11 in thick and consists of two layers

Figure 5. Longitudinal section profiles and material properties at test sites.

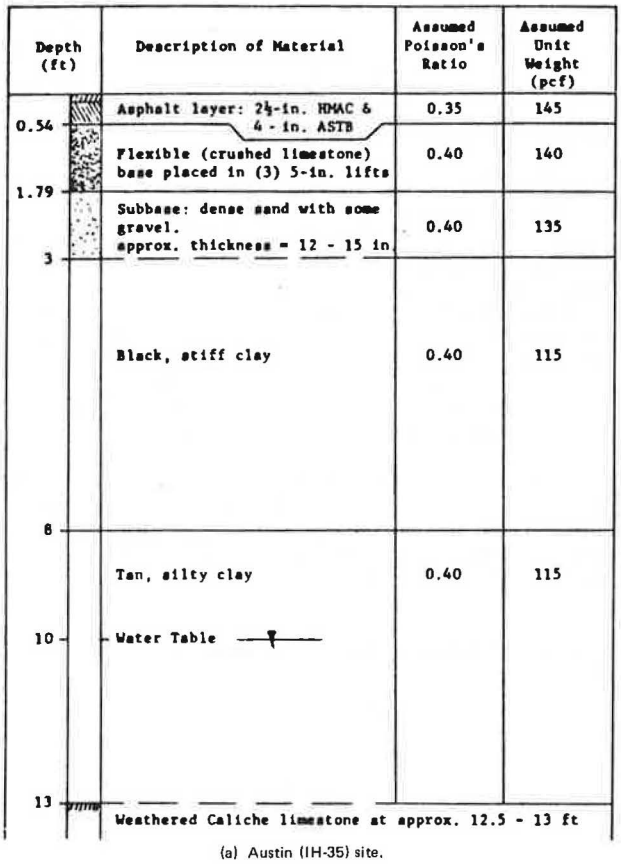

(a) Austin (IH-35) site.

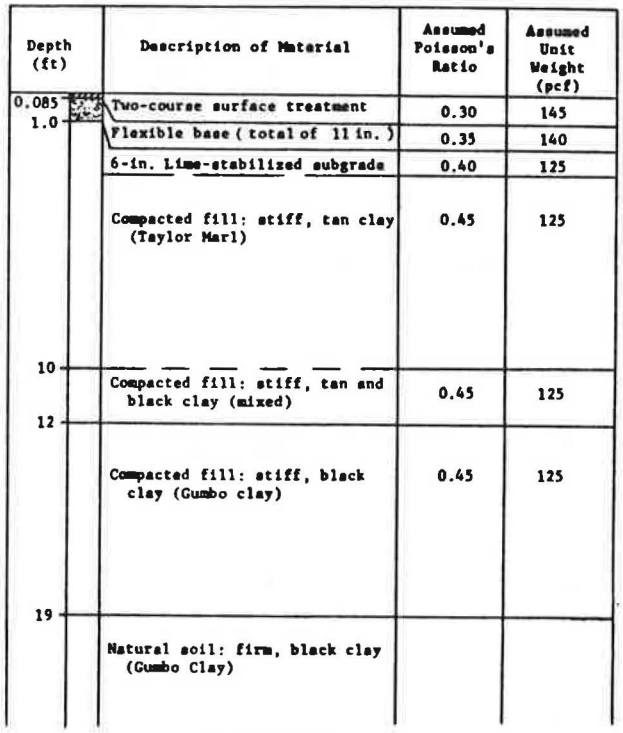

(b) Granger (FM 971) site.

Table 1. Calculations from phase of cross spectrum for determining profile of velocity versus depth.

Frequency (Hz 000s)	Phase (deg)	Travel Time (ms)	Velocity (ft/s)	Wavelength (ft)	Depth L/3 (ft)
12	18.35	4.248	1907.9	158 992	52 997
14	16.57	3.288	2465.0	176 071	58 690
16	17.17	2.981	2718.7	169 919	56 640
18	24.98	3.855	2102.3	116 793	38 931
20	34.31	4.765	1700.7	85 034	28 345
22	50.11	6.327	1280.9	58 222	19 407
24	81.28	9.407	861.5	35 894	11 965
26	109.30	11.677	694.0	26 693	8 898
28	130.89	12.985	624.1	22 290	7 430
30	149.44	13.837	585.7	19 523	6 508
32	164.78	14.304	566.6	17 705	5 902
34	175.84	14.366	564.1	16 592	5 531
36	179.80	13.873	584.1	16 226	5 409
38	187.92	13.737	590.0	15 525	5 175
40	198.78	13.804	587.1	14 677	4 892
45	228.95	14.133	573.4	12 743	4 248
50	248.71	13.817	586.5	11 731	3 910
54	275.96	14.195	570.9	10 572	3 524
59	293.72	13.655	593.5	9 933	3 311
65	300.91	12.859	630.2	9 696	3 232
69	300.18	11.998	675.5	9 719	3 240
75	310.71	11.508	704.2	9 390	3 130
79	323.33	11.369	712.8	9 023	3 008
83	343.29	11.489	705.4	8 499	2 833
90	361.33	11.152	726.7	8 074	2 691
95	374.94	10.963	739.2	7 781	2 594
100	388.62	10.795	750.7	7 507	2 502

Note: Distance between geophones = 8.104 ft.

of crushed limestone. The pavement is a two-course oil and stone surface treatment, approximately 0.5-1 in thick. The section profile is shown in Figure 5b. Unit weights of the materials were assumed to be 145, 140, and 125 pcf for the pavement, base, and subgrade, respectively. Poisson's ratios were assumed to be 0.30, 0.35, and 0.45 for the pavement, base, and subgrade, respectively.

TEST RESULTS

Austin Site

Testing was first performed by using the FWD as the source. The complete time history of the FWD is shown in Figure 6a. The signal was recorded with a geophone attached to the base of the FWD. The signal was triggered (t = 0) with the initial downward hit of the weight. A pretrigger delay was used to capture the negative-time part of the signal. The small upward displacement at approximately t = -0.25 s is due to the slight rebound of the base plate when the weight is released to undergo free fall. Multiple impacts occur for about eight or nine rebounds of the weight. These additional impacts do not interfere with the initial pavement response because all data are collected from the first impulse before the subsequent impulses occur. The time interval for a wave traveling from 2 to 10 ft is of the order of 10 ms, whereas the time interval between the first and second impacts of the weight is approximately 450 ms.

The Fourier transform of the time signal, the linear spectrum, is shown in Figure 6b. The major frequency component excited by the falling weight is approximately 21 Hz. This corresponds quite closely to the pulse created by the first trough of the signal in the time domain. This pulse width is approximately 25 ms, yielding a predominant period T = 50 ms or a predominant frequency of 20 Hz. The level of excitation greatly decreases with increasing frequencies.

Figure 6. Impulsive loading created by FWD.

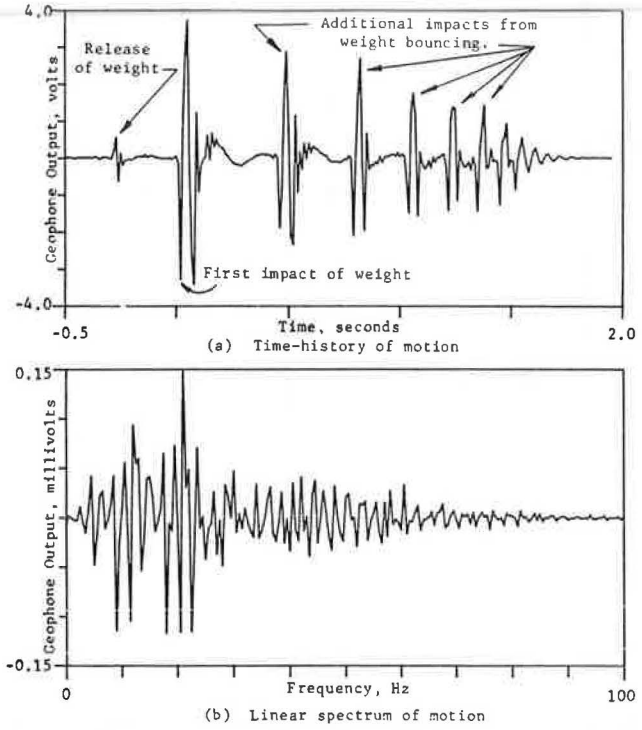

Comparisons for both time- and frequency-domain measurements indicate that there are no significant differences between one-average records and five-average records. This is probably a result of the high reproducibility of the impulse. Occasionally, one-average records exhibited apparent anomalies. To avoid anomalies, all analyses were performed by using five-average records.

A comparison of responses from vertical geophones and horizontal geophones indicates that responses are similar, although the magnitude of the vertical response is approximately 100 times the magnitude of the horizontal response since the source is designed to input energy in the vertical direction. However, velocities obtained from measurements by using horizontal geophones were somewhat higher than those obtained from measurements by using vertical geophones. One possible explanation of this difference in velocities may be the greater sensitivity of the horizontal geophones to higher-velocity P-wave energy.

The velocity profile was determined from three records by using phase information of the cross spectrum obtained from plots such as the one in Figure 7. The three records include V1-V2 with bandwidth (BW) = 200 Hz; V2-V5 with BW = 1600 Hz

Figure 7. Plot of cross-spectrum phase versus frequency used to determine Rayleigh wave velocity.

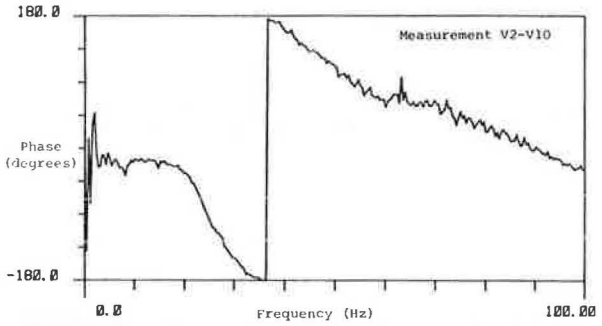

Figure 8. Rayleigh wave velocity profile: Austin site.

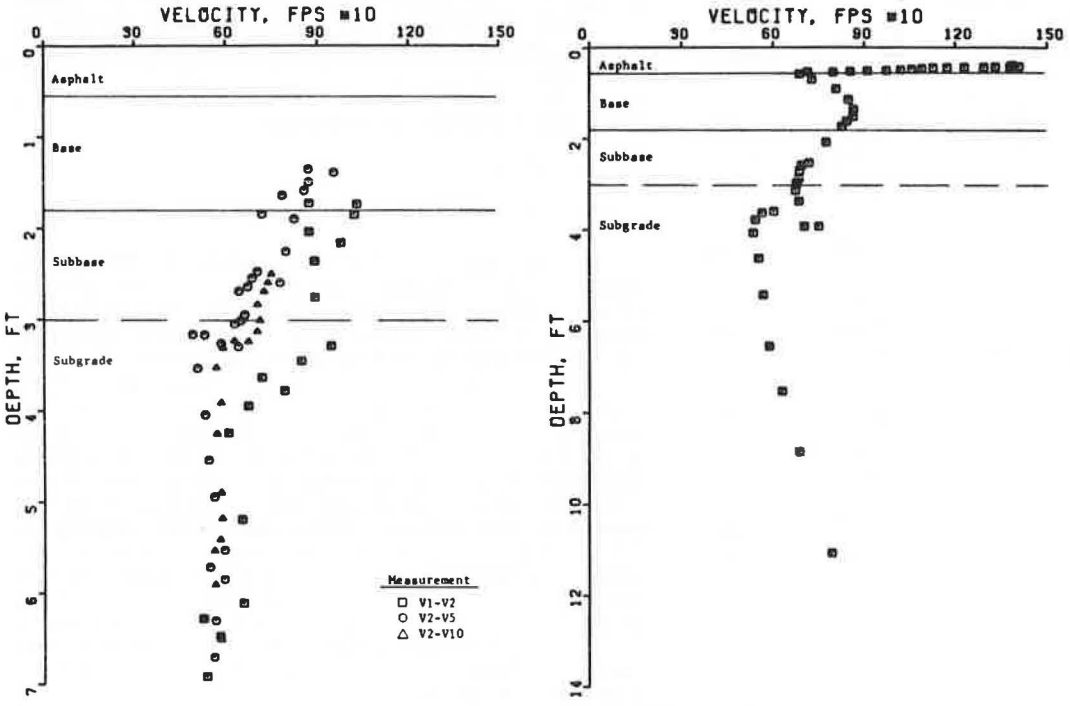

(a) FWD as source.

(b) Drop hammer as source.

(although useful data did not exist beyond about 250 Hz); and V2-V10 with BW = 100 Hz. A typical set of calculations is shown in Table 1. Depths given in the table were calculated by using the one-third wavelength criterion. The resulting profile is shown in Figure 8a.

Velocities could not be determined with the FWD as the source for the upper 15 in of the profile. For typical velocities of pavement materials, the FWD cannot excite high enough frequencies to generate the short wavelengths needed to sample the upper layers. Previously, it had been shown that the level of excitation of the FWD decreased with increasing frequency. Nearly all the energy of excitation is contained within 100 Hz, and essentially no frequencies are excited above 250 Hz. Above 250 Hz, the phase of the cross spectrum becomes erratic, as illustrated in Figure 9a. Similarly, the coherence displays irregularities above 250 Hz. These results indicate that the FWD does not sufficiently excite the necessary frequencies to evaluate the entire pavement system by the spectral analysis of propagated waves.

Measurements for the drop hammer source were made by using one set of vertical receivers, V2-V5. The phase of the cross spectrum, shown in Figure 9b, provides useful data up to about 1400 Hz. Concurrently, the measurement exhibits high coherence up to approximately 1300-1400 Hz.

The profile of velocity versus depth is shown in Figure 8b. The layering in the velocity profile (which used one-third of the Rayleigh wavelength as the depth) correlates well with the actual profile. By using the profile, Rayleigh wave velocities were estimated as 1400, 860, 690, and 560 ft/s for the asphalt, base, subbase, and subgrade, respectively.

Velocities obtained from cross-spectrum measurements by using both the FWD and the drop hammer are compared in Figure 10. The profiles from the two sources agree quite closely. The R-wave velocities for each layer are summarized in Table 2. The close agreement of velocities from the relatively light load (drop hammer) with those from the relatively heavy load (FWD) suggests that the moduli of the pavement materials are not stress (strain) sensitive over the range of stresses up to and including those generated by the FWD. Consequently, a lighter and sharper impulse is more desirable to sample all materials in the pavement since the heavier FWD could not generate high enough frequencies to sample the surface layer.

Velocities from cross-spectrum (surface) measurements were also compared with velocities from crosshole tests performed at the Austin site. Two borings were made and crosshole data were obtained for shear waves traveling directly in each layer. The S-wave velocity profile from crosshole testing,

Figure 9. Comparison of phase of cross spectrum for measurement V2-V5 by using different sources.

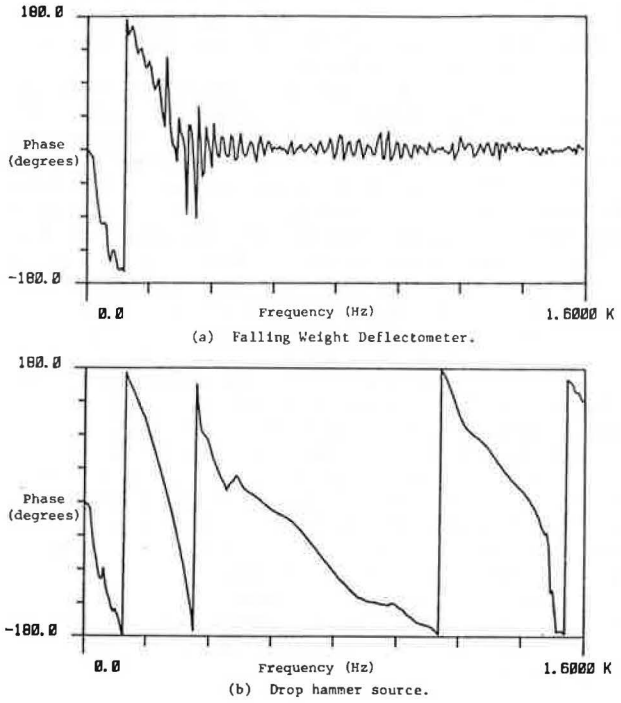

Figure 10. Comparison of crosshole velocities with shear-wave velocity profile obtained by using cross-spectrum (surface) measurements.

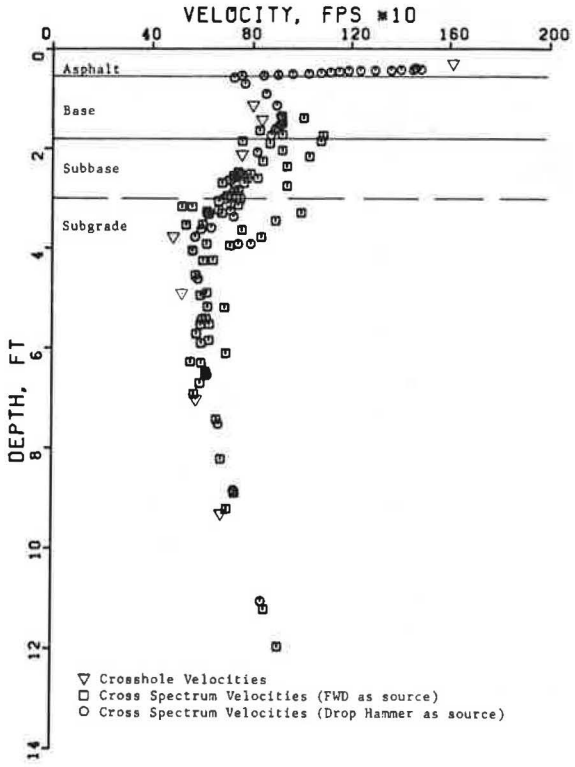

Table 2. Summary of R-wave velocities determined from cross-spectrum measurements at Austin site.

Material	Approximate Thickness (in)	Unit Weight (pcf)	Poisson's Ratio	Velocity (ft/s)			
				R-Wave			
				FWD	Drop Hammer	Avg	S-Wave
Asphalt	6.5	145	0.35	-	1400	1400	1500
Base	15	140	0.40	880	860	870	925
Subbase	12-15	135	0.40	700	690	695	740
Subgrade	120	115	0.40	580	560	570	605

shown in Figure 10, compares very closely with the S-wave velocity profiles obtained by cross-spectrum measurements. The comparison for each layer is summarized below. The close agreement in velocities with an independent technique such as crosshole testing indicates the validity and accuracy of determining velocities (moduli) from spectral analysis of surface waves by the cross-spectrum method.

	S-Wave Velocity (ft/s)		
Material	Cross-Spectrum Measurements	Crosshole Tests	Percentage of Difference
Asphalt	1500	1610	6.8
Base	925	823	12.4
Subbase	740	743	0.4
Subgrade	605	565	7.1

By using the S-wave velocities determined from cross-spectrum measurements (Table 2), a shear modulus and Young's modulus were calculated for each layer. In addition, Young's moduli for the various layers were backcalculated from deflection basins measured during Dynaflect testing conducted at the Austin site. The Young's moduli by wave propagation (cross spectrum) and those by deflection methods (Dynaflect basin) are summarized below. For the most part, the moduli determined from the two methods are comparable, which suggests again that the cross-spectrum method is a valid and accurate approach. Slight differences in each layer may be a result of the uncertainty and variability in determining moduli by backfitting a deflection basin by using elastic theory (ELSYM5):

	Shear Modulus	Young's Modulus E (psi 000s)	
Material	(psi 000s)	Wave Propagation	Deflection Method
Asphalt	70	190	250
Base	26	72	108
Subbase	16	45	40
Subgrade	9	25	17

Figure 11. Rayleigh wave velocity profile: Granger site.

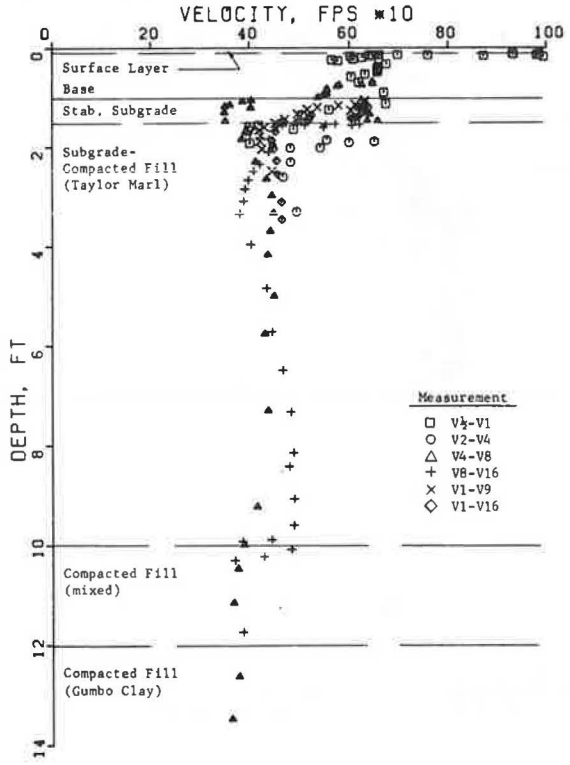

Granger Site

Cross-spectrum measurements at the Granger section were obtained by using only the drop hammer as the source. Measurements were made along the centerline of the road and along a wheel path for various spacings of geophone pairs, ranging from 0.5 and 1 ft to 8 and 15 ft. The frequency bandwidth of the measurements was varied from 50 to 3200 Hz to obtain data for wavelengths sampling each layer.

The profile of velocity versus depth is plotted in Figure 11 by using a depth criterion of $L_R/3$. The velocity profile shows distinct layering, which correlates well with the actual section profile. By using the profile, Rayleigh wave velocities were estimated as 980, 670, and 430 ft/s for the pavement, base, and subgrade, respectively. By using the unit weights and Poisson's ratios previously listed for these materials, the Rayleigh wave velocities were converted to shear-wave velocities, and values of Young's modulus were calculated to be 91 000, 42 000, and 16 000 psi for the pavement, base, and subgrade, respectively.

Young's moduli were also backcalculated from deflection basins measured during Dynaflect testing at the Granger site. These moduli are summarized in Table 3 along with those determined from wave-propagation velocities (cross-spectrum method). The best agreement between the two methods occurs in the subgrade layer, although the overall agreement is not so good as that exhibited at the Austin site. It is not clear which method is more "accurate" nor is it clear whether the use of elastic-layer theory and deflection measurements is reasonable for a thin-layered, surface-treated pavement such as the test section at the Granger site. However, the cross-spectrum method did provide a velocity profile that correlated closely with the profile layering.

Shear-wave velocities in the subgrade determined from crosshole tests ranged from 490 to 530 ft/s compared with 420-480 ft/s for velocities determined from the spectral analysis of surface waves. The lower velocities from cross-spectrum measurements may have been a result of greater moisture in the soil following a period of heavy rainfall at the site. In any case, the difference between velocities is only about 10 percent, which is quite acceptable for engineering purposes.

Table 3. Summary of wave velocities and elastic moduli determined at Granger site.

Material	Unit Weight (pcf)	Poisson's Ratio	Velocity (ft/s)		Shear Modulus (psi)	Young's Modulus E (psi 000s)	
			R-Wave	S-Wave		Wave Propagation	Deflection Method[a]
Surface	145	0.30	980	1060	35 000	91	50
Base	140	0.35	670	720	15 700	42	13
Stabilized subgrade	125	0.40	520	550	8 100	23	12.5
Subgrade	125	0.45	430	450	5 500	16	12

[a]Moduli were backcalculated from fitted deflection basin by using elastic-layer theory (ELSYM5).

SUMMARY AND CONCLUSIONS

A method to determine elastic moduli at soil and pavement sites was proposed and tested. Criteria that guided the development of this method included the restraint of nondestructive testing, accuracy of moduli for all layers regardless of thicknesses, and quickness and efficiency for rapid, extensive testing. To meet these criteria, surface receivers were utilized to evaluate the Rayleigh wave motion created by a vertical, impulsive source that could excite a wide range of frequencies with a single impact. Analysis was facilitated by using a portable spectral analyzer to study the magnitude and phase of the frequency content of the recorded wave pulse. Phase information from the cross-spectrum function was used to calculate Rayleigh wave velocities, which were converted to shear-wave velocities. Elastic moduli (shear moduli and Young's moduli) were then calculated from the shear-wave velocities.

For pavement sites consisting of a flexible (asphalt concrete) surface, frequencies up to 2-5 kHz should be excited. This upper bound will vary depending on the thickness and stiffness of the surface layer. Higher frequencies are necessary for thinner, stiffer pavements. Based on tests at two pavement sites, it appears that geophones provide good response up to at least 3 kHz. For higher frequencies, it may be necessary to use accelerometers.

Comparisons between moduli calculated from wave-propagation velocities and moduli backcalculated from measured Dynaflect deflection basins indicate that the wave-propagation method is a valid method to determine Young's modulus for each layer in a pavement system. Agreement between the two methods was quite good at the Austin site where the pavement was newly constructed but was not so good at the Granger site where the pavement was several years old and showed signs of deterioration. The poorer comparison at the Granger site may result from assumptions in the elastic-layer theory that are not reasonable for a thin, surface-treated pavement.

Shear-wave velocities in the subgrade obtained from surface measurements correlated well (typically within 10 percent) with those obtained from crosshole testing, which suggests that the cross-spectrum (surface) method is not hindered by the relatively stiff asphalt layer at the surface. However, both of the pavement systems investigated in this study consisted of flexible surface layers, with stiffnesses about 5-10 times those for the subgrade. For rigid pavements, the stiffness of the surface layer is considerably greater and may complicate the analysis of subgrade velocities and moduli. Further research is necessary to determine whether the cross-spectrum method is applicable for rigid pavements.

Based on comparisons with shear-wave velocities from crosshole testing and Young's moduli calculated from Dynaflect deflection basins, the cross-spectrum analysis of surface waves was found to be a valid and accurate method to determine moduli of pavement systems. Furthermore, the cross-spectrum method can be used to test a given location in only a few minutes, whereas the previous steady-state method might require several hours at a given location. As a result, the cross-spectrum method allows more data acquisition (and at lower costs) to evaluate pavement condition.

ACKNOWLEDGMENT

This research was conducted under the Cooperative Highway Research Program, Project HPR-0010(5). We are grateful for the funding support and technical services provided by the Texas State Department of Highways and Public Transportation under Research Project 3-8-80-256.

REFERENCES

1. R.L. Lytton, W.M. Moore, and J.P. Mahoney. Pavement Evaluation, Phase 1: Pavement Evaluation Equipment. FHWA, Rept. FHWA-RD-75-78, 1975
2. G.G. Miller and H. Pursey. On the Partition of Energy Between Elastic Waves in a Semi-Infinite Solid. Proceedings of the Royal Society, London, Part A, Vol. 223, 1955, pp. 251-541.
3. R.F. Richart, Jr., J.R. Hall, Jr., and R.D. Woods. Vibrations of Soils and Foundations. Prentice-Hall, Englewood Cliffs, NJ, 1970.
4. R. Jones. Surface Wave Technique for Measuring the Elastic Properties and Thicknesses of Roads: Theoretical Development. British Journal of Applied Physics, Vol. 13, 1962, pp. 21-29.
5. W. Heukelom and C.R. Foster. Dynamic Testing of Pavements. Journal of the Soil Mechanics and Foundation Division of ASCE, Vol. 86, No. SM1, Feb. 1960
6. M.E. Szendrei and C.R. Freeme. Road Responses to Vibration Tests. Journal of the Soil Mechanics and Foundation Division of ASCE, Vol. 96, No. SM6, Nov. 1970, pp. 2099-2124.
7. R.J. Hoar and K.H. Stokoe II. Generation and Measurement of Shear Waves In Situ. In Dynamic Geotechnical Testing, American Society for Testing and Materials, Philadelphia, PA, Special Tech. Publ. 634, 1978.
8. A. Bohn, P. Ullidtz, R. Stubstad, and A. Sorenson. Danish Experiments with the French Falling Weight Deflectometer. Proc., 3rd International Conference on the Structural Design of Asphalt Pavements, Univ. of Michigan, Ann Arbor, Vol. 1, 1972, pp. 1119-1128.
9. J.S. Heisey. Determination of In Situ Shear Wave Velocities from Spectral Analysis of Surface Waves. Univ. of Texas at Austin, Master's thesis, 1981.

Publication of this paper sponsored by Committee on Strength and Deformation Characteristics of Pavement Sections.

Comparative Study of Selected Nondestructive Testing Devices

MARIO S. HOFFMAN AND MARSHALL R. THOMPSON

An extensive program of flexible-pavement nondestructive testing (NDT) was conducted by the Illinois Department of Transportation (IDOT) in cooperation with the University of Illinois. Different (mostly in-service) pavements were tested. Conventional granular base and stabilized base material sections were studied. NDT devices used were the IDOT road rater model 2008, the Benkelman beam, and the falling-weight deflectometer. An accelerometer was used to measure surface pavement deflections under moving trucks. The main findings of the comparative NDT program are reported. Deflection-basin parameters for structural pavement evaluation are defined. Correlations and comparisons between the different devices are presented. Overall, the falling-weight deflectometer is the best NDT device for simulating pavement response under moving wheel loads. The road rater, because of its harmonic loading without rest periods and the static preload, induces pavement deflections lower than those achieved with the falling-weight deflectometer and moving wheel loads. Finally, the quasistatic loading in Benkelman beam measurements induces the highest pavement deflections.

There is general agreement among pavement engineers and researchers that pavement surface deflection-basin measurements provide valuable information for structural evaluation. Pavement deflections, however, are highly dependent on loading mode (vibratory, impulse, vehicular) and magnitude. The ideal responses for structural pavement evaluation are thus surface deflections under moving design loads. One of the main goals of this study was to determine the nondestructive testing (NDT) equipment and procedure that best simulate pavement response under moving loads.

With that goal in mind, the Illinois Department of Transportation (IDOT) in cooperation with the University of Illinois has developed an extensive flexible-pavement evaluation method based on the interpretation of measured surface deflections (1,2). The first stage of the program included the collection of 11 000 deflection measurements over a period of three years on different (mostly in-service) pavements.

Throughout the deflection data collection, different selected NDT devices and methods were used. These included the Benkelman beam (BB), IDOT road rater (RR), falling-weight deflectometer (FWD), and an accelerometer implanted in the pavement's surface to measure deflections under different moving trucks at varying speeds.

The different types of pavements tested in the program (see Table 1) included the following:

1. Conventional flexible pavements: asphalt-concrete (AC) surface over granular bases and subbases;
2. Stabilized pavements: AC surface over a stabilized base including cement aggregate mixture (CAM), pozzolanic aggregate mixture (PAM), and bitumen aggregate mixture (BAM);
3. Surface treatments: a nominal asphalt and chips covering over a granular base; and
4. Test sections: selected flexible sections in Loop 1 of the American Association of State Highway Officials (AASHO) Test Road in Ottawa, Illinois.

Except for the sections on Loop 1 of the AASHO Test Road, all the sections are in-service pavements. The effects of the following factors on surface deflections were investigated: RR load and driving frequency, FWD load, seasonal effects, vehicle weight and speed, and loading mode--quasi-static (BB), steady-state (RR), impulse (FWD), and vehicular (moving trucks). In addition to the deflection data collection, most pavement sections in the program were sampled for subsequent laboratory testing.

This paper presents the main findings of the comparative study of selected NDT devices. A detailed description of this study and a full summary of the results have been presented elsewhere (1). An extensive literature review of other deflection studies has also been given elsewhere (1,2).

NDT EQUIPMENT AND PROCEDURES

To facilitate the direct comparison of the different NDT devices, soil type and existing pavement conditions were kept uniform. Measurements were made on 20 points in each 100-ft-long section of pavement. The same 20 points (10 on each traffic lane, 10 ft apart) were tested at different times during a three-year period.

Benkelman Beam

A truck that had an 18-kip rear axle with dual tires (70-80 psi tire pressure) was used in the BB rebound method. The rebound deflection of the pavement was measured when the truck moved away from the testing point at creep speed.

Road Rater

The RR (model 2008) used in the study is an electrohydraulic vibrator capable of generating harmonic loads of up to 8 kips (peak to peak) at driving frequencies between 6 and 60 Hz. When the vibrator is set over the testing point, a static preload of 5 kips is applied through the 12-in-diameter circular loading plate. The desired peak-to-peak load is then generated at the preselected driving frequency, and peak-to-peak deflections are recorded with velocity transducers (geophones). The IDOT RR has four deflection sensors, located at the center of

Table 1. Description of pavement sections.

Section	Cross Section	Subgrade Classification (AASHTO)
Bement	Asphalt concrete, 4 in; field-mixed soil cement, 6 in	A-7-6(24)
Coffeen	Asphalt concrete, 3 in; lime-fly ash, 10 in	A-4(5)
Deland	Surface treatment; granular base B, 8 in	A-7-6(21)
Hillsboro	Asphalt concrete, 6.3 in; seal treatment, 2 in; crushed gravel, 6 in	A-7-6(18)
Midlothian "A"	Asphalt concrete, 5 in; lime-fly ash, 6 in; gravel, 10 in	A-6(14)
Midlothian "B"	Asphalt concrete, 7 in; gravel, 7 in; lime-fly ash, 6 in	A-6(10)
Monticello	Asphalt concrete, 3.5 in; plant-mixed CAM, 8 in	A-6(8)
Neoga North	Asphalt concrete, 5.5 in; BAM, 7 in	A-7-6(18)
Neoga South	Asphalt concrete, 2.5 in; BAM, 7 in	A-6(8)
Pana	Asphalt concrete, 5.5 in; BAM (MC-800), 10 in	A-7-6(16)
Sherrard	Asphalt concrete, 4 in; crushed stone, 14 in	A-4(6)
Viola	BAM (HFE-300), 9 in	A-6(9)
AASHO-845	Asphalt concrete, 3 in; crushed stone, 6 in; sandy gravel, 8 in	A-6(6)
AASHO-872	Asphalt concrete, 5 in; crushed stone, 6 in	A-6(6)
AASHO-874	Asphalt concrete, 5 in; crushed stone, 6 in; sandy gravel, 16 in	A-6(6)

the loading plate and 1, 2, and 3 ft away from the center.

Falling-Weight Deflectometer

The FWD is a deflection-testing device operating on the impulse-loading principle. A mass is dropped from a preselected height onto a footplate that is connected to a baseplate by a set of springs. The baseplate (12 in in diameter) is placed in contact with the pavement surface over the testing point. By varying the drop height, the impulse load was varied from 2 to 11 kips. The duration of the impulse loading ranges from 30 to 40 ms.

FWD deflections are measured with velocity transducers (geophones). One of these sensors is located at the center of the loading plate. Two additional sensors are movable and can be placed at any desired distance away from the center of the plate. During this testing program, the FWD sensors were placed 1, 2, and 3 ft away from the center of the loading plate, the same spacing used for the RR.

Figure 1. Deflection-basin characterization.

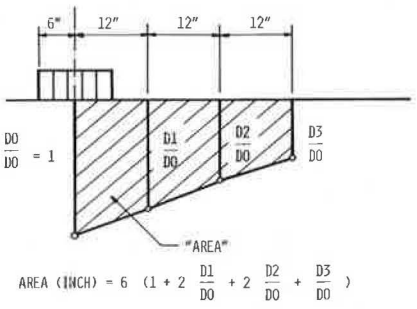

Figure 2. BB versus RR coefficients of variability.

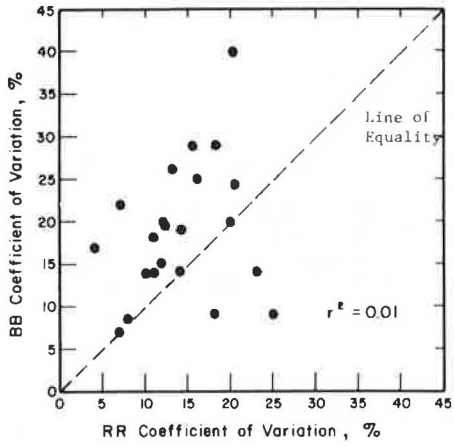

Table 2. Variables in stepwise multiple-regression analysis of BB and RR deflections.

Variable Considered	Range of Values Max	Min
BB: Benkelman-beam deflection (mils)	194.0	8.0
RR: road rater deflection[a] (mils)	99.0	5.8
F1: RR shape factor 1	1.68	0.15
F2: RR shape factor 2	1.83	0.20
Area: RR deflection-basin area (in)	31.4	15.7
T: surface pavement temperature (°F)	115	64
Tac: thickness of AC layer (in)	8.0	0.0
Tgr: thickness of granular layer (in)	14.0	0.0
Tsta: thickness of stabilized layer (in)	10.0	0.0
Sta: Flag = 1 if stabilized layer in section; 0 if not		
Seas: Flag = 1 if spring measurement; 0 if other		

[a] 8-kip peak-to-peak load; 15-Hz driving frequency.

Accelerometer Measurements

An accelerometer was implanted in the surface of selected AASHO Test Road (Loop 1) sections (sections 845, 872, and 874) to measure deflections under moving trucks and under the FWD's loading plate. The accelerometer was placed in a hole 2 in in diameter by 2 in deep in the outer wheelpath. The single wire coming off the accelerometer was buried in a slot 1 in deep and 3/8 in wide sawed perpendicular to the direction of travel.

The following trucks were used in the testing:

Truck	Rear-Axle Weight (lb)
Light	5 100
Medium	9 000
Heavy	18 000

The trucks distributed the rear-axle weight shown through a single-axle, dual-wheel configuration. Truck speeds ranged from 8 to 30 mph.

DEFLECTION-BASIN CHARACTERIZATION

The deflection basin, measured with the RR and FWD, is characterized as follows:

1. D0, centerline plate deflection;
2. D1, D2, D3, surface deflections at 1, 2, and 3 ft, respectively;
3. Deflection-basin area, parameter combining all measured deflections in basin (see Figure 1), defined as Area (in) = 6 (1 + 2D1/D0 + 2D2/D0 + D3/D0); and
4. F1, F2, basin shape factors (dimensionless), F1 = (D0 - D2)/D1 and F2 = (D1 - D3)/D2.

The deflection-basin area ranges from a calculated practical minimum of 11 in (Boussinesq approximation) to a maximum of 36 in (maximum by definition). Also, the area increases with increasing pavement stiffness (2). The basin shape factors are analogous to a derivative of the deflection-basin curves, representing the variation of surface deflection with lateral distance from the centerline. In general, stiff pavements have lower shape factors (1).

RESULTS

Comparison of BB and RR Deflections

The comparative study between BB and RR deflections was performed on 12 different in-service pavement sections. Nine of the sections were tested twice at different times of the year for a total of 21 cases. The RR followed the BB at routine RR testing conditions of 8-kip peak-to-peak load and 15-Hz driving frequency. The same 20 points per section were evaluated at each testing date. The following results were obtained:

1. Without exception, mean BB deflections were higher than mean RR deflections; the ratio of mean BB and mean RR deflections ranged from 1.1 to 5.8.
2. The variability of the BB deflections was generally larger than that of the RR (18 of 21 cases). The mean coefficient of variation with the BB data was 19 percent and that of the RR data was 14 percent (Figure 2). There is no linear correlation between the BB and RR coefficients of variation

Table 3. Analyses of BB and RR deflections: stepwise regressions.

Group	N	Dependent Variable	R^{2a}	SEE (mils)	CV (%)	Constant a_0	Other Variables RR a_1	F1 a_2	F2 a_3	Area a_4	T a_5	Tac a_6	Tgr a_7	Tsta a_8	Sta a_9	Seas a_{10}
All data	418	BB	0.78	20.2	39	153	-0.47	-	84.2	-	0.43	-	-5.6	-3.2	-42.7	-20.2
Stabilized sections	200	BB	0.72	3.3	17	113	0.90	-36.5	-	-2.9	-	-	-	-1.29	-	-
Remainder of data	218	BB	0.66	23.5	29	680	-0.44	-156.4	66.3	-22.9	0.53	4.15	-7.15	-	-	-15.4

Note: Equation of the following form: $BB = a_0 + a_1 RR + a_2 F1 + \ldots + a_{10}$ Seas.

[a]Significant at 1 percent level.

Table 4. BB versus RR deflections.

Group	N	R^{2a}	SEE (mils)	CV (%)	Regression Equation
All data	418	0.38	33.7	65	BB = 14.3 + 1.53 RR
Stabilized sections	200	0.66	3.7	19	BB = 2.6 + 1.27 RR
Remainder of data	218	0.07	38.5	47	BB = 61.7 + 0.58 RR

[a]Significant at 1 percent level.

for a given section (Figure 2).

3. If we assume that the inherent variability is constant for a given section, BB testing errors must be greater than RR testing errors.

Different correlations between BB and RR deflections were attempted in the study. A section-by-section linear correlation of BB versus RR deflections (20 points per section) resulted in coefficients of determination (R^2) ranging from 0.05 to 0.85. In 12 of 21 cases, the R^2-values were significant at the 1 percent level. In three cases, R^2-values were significant at the 5 percent level, and in the remaining six cases there was no significant linear correlation between BB and RR deflections.

The addition of other variables permitted the use of stepwise multiple-regression analyses (see Table 2). Deflection data were combined in different groups: (a) all data (418 pairs of observations), (b) stabilized section (200 pairs), and (c) remainder of data (218 pairs). Tables 3 and 4 summarize the regression equations developed in the study for the different groups. While the coefficients of determination (R^2) of all three groups are significant at the 1 percent level, only the stabilized-section group has a standard error of estimate (SEE) acceptable for predictive purposes.

Overall, it does not seem that BB deflections can be reliably predicted from RR deflections. The study (1) concluded that the loading-mode effects of the BB (quasistatic) and the RR (vibratory with static preload) deflections are not predictable based solely on statistical models. A treatment of loading-mode effects on pavement response, far beyond the scope of this paper, has been given elsewhere (2).

Comparison of RR and FWD Deflections

Two types of tests were performed in the comparative studies of RR and FWD deflections: (a) routine and (b) load and frequency sweeps. In the routine test, the RR was operated at an 8-kip peak-to-peak load and 15 Hz, and the FWD was operated at 8 kips. The FWD followed the RR over the preselected 19 stations per test section (one station had been eliminated for coring and sampling). In the load and frequency-sweep tests, the RR was operated at peak-to-peak loads of 2, 4, 6, and 8 kips and driving frequencies between 6 and 30 Hz at 2-Hz intervals for each load. Following the RR, the FWD was operated at loads ranging from 2 to about 11 kips.

Routine RR and FWD Test Results

Table 5 summarizes the results of the RR and FWD routine tests for the five sections in the study. The results show the following:

1. Mean RR and FWD centerplate deflections (D0) are different. The hypotheses that the mean deflections are equal are rejected in all five cases (95 percent confidence level).
2. The mean FWD deflection-basin areas are statistically different ($\alpha = 0.05$) and consistently lower than the RR areas.
3. The mean basin shape factors (F1 and F2) are statistically different ($\alpha = 0.05$) and consistently larger for the FWD.
4. The FWD variability, expressed by the coefficient of variation (CV), is larger than the RR variability of most values in Tables 3 and 4.

Considering that both devices applied an 8-kip load, both loading plates were 12 in in diameter, and deflections were measured with geophones at the same basin locations, then the differences in Table 4 can be mainly attributed to the loading-mode effects: vibratory with the RR and impulse loading with the FWD.

Correlations Between RR and FWD

Despite the difference in surface deflections between RR and FWD, they were highly correlated. Figure 3 shows the correlation between FWD and RR centerplate deflections (D0), and Figure 4 shows the correlation between FWD and RR deflection-basin areas.

The regression equation relating FWD and RR deflections is as follows:

$$\Delta_{FWD}\,(\text{mils}) = -3.40 + 1.21\,\Delta_{RR}\,(\text{mils}) \quad (1)$$

The coefficient of determination (R^2) is 0.94 (significant at the 1 percent level), and SEE is 3.23 mils. Note that up to a 15-mil deflection, RR deflections are larger than FWD deflections. Above the 15-mil RR deflections, the FWD induced larger deflections than the RR did (Figure 3).

The regression equation relating FWD and RR deflection-basin areas is as follows:

$$\text{Area}_{FWD}\,(\text{in}) = -7.59 + 1.19\text{area}_{RR}\,(\text{in}) \quad (2)$$

Table 5. Summary of FWD and RR deflections.

Section	Date	Pavement Temperature (°F)	Measurement Device	D0 Deflection (mils)	D0 SD (mils)	D0 CV (%)	D1 Deflection (mils)	D1 SD (mils)	D1 CV (%)	D2 Deflection (mils)	D2 SD (mils)	D2 CV (%)	D3 Deflection (mils)	D3 SD (mils)	D3 CV (%)
Bement	10/17/79	83	RR	14.92	2.59	17.40	11.91	1.66	13.90	9.51	0.91	9.60	7.61	0.70	9.20
			FWD	12.93	2.91	22.50	9.96	1.66	16.70	7.20	0.77	10.60	5.22	0.45	8.60
Deland	10/17/79	67	RR	40.50	3.53	8.70	24.08	2.25	9.30	14.45	0.76	5.30	11.16	0.50	4.50
			FWD	43.47	5.34	12.30	19.07	2.98	15.60	7.55	0.24	3.20	5.33	0.19	3.50
Monticello	10/17/79	60	RR	14.39	2.55	17.70	11.39	1.75	15.30	8.87	0.79	8.90	7.25	0.42	5.80
			FWD	12.04	3.00	24.90	8.74	1.52	17.40	6.16	0.72	11.70	4.29	0.31	7.30
Sherrard	10/19/79	83	RR	16.24	0.61	3.70	11.61	0.57	4.90	7.71	0.30	3.90	4.45	0.23	4.20
			FWD	17.85	0.77	4.30	10.69	0.53	5.00	6.20	0.38	6.20	4.18	0.15	3.70
Viola	10/19/79	65	RR	28.21	3.92	13.90	14.11	2.11	14.90	8.00	1.37	17.20	6.16	1.12	18.20
			FWD	34.64	4.37	12.60	13.18	2.03	15.40	5.72	0.92	16.00	3.77	0.80	21.10

Section	Date	Pavement Temperature (°F)	Measurement Device	Shape Factor F1 Value	F1 SD	F1 CV (%)	F2 Value	F2 SD	F2 CV (%)	Area Deflection Basin (in)	Area SD (in)	Area CV (%)
Bement	10/17/79	83	RR	0.44	0.10	22.10	0.45	0.12	26.30	26.53	1.58	5.90
			FWD	0.56	0.16	29.30	0.65	0.18	28.40	24.81	2.34	9.50
Deland	10/17/79	67	RR	1.08	0.05	4.90	0.89	0.13	14.80	19.10	0.46	2.40
			FWD	1.89	0.15	7.70	1.82	0.41	22.50	14.12	0.55	3.90
Monticello	10/17/79	60	RR	0.47	0.13	26.70	0.46	0.15	31.60	26.18	1.91	7.30
			FWD	0.65	0.17	26.10	0.71	0.14	19.70	23.46	2.15	9.20
Sherrard	10/19/79	83	RR	0.74	0.06	8.00	0.80	0.07	8.60	22.30	0.70	3.10
			FWD	1.09	0.12	11.10	1.05	0.07	7.00	18.78	0.88	4.70
Viola	10/19/79	65	RR	1.44	0.14	9.50	1.01	0.20	20.30	16.72	0.76	4.50
			FWD	2.23	0.36	16.30	1.64	0.16	9.80	13.22	0.95	7.20

Notes: RR at 8000-lb peak-to-peak load, 15 Hz, 19 stations per section.
FWD at 8000-lb ±5 percent, 19 stations per section.

Figure 3. Correlation between FWD and RR deflections.

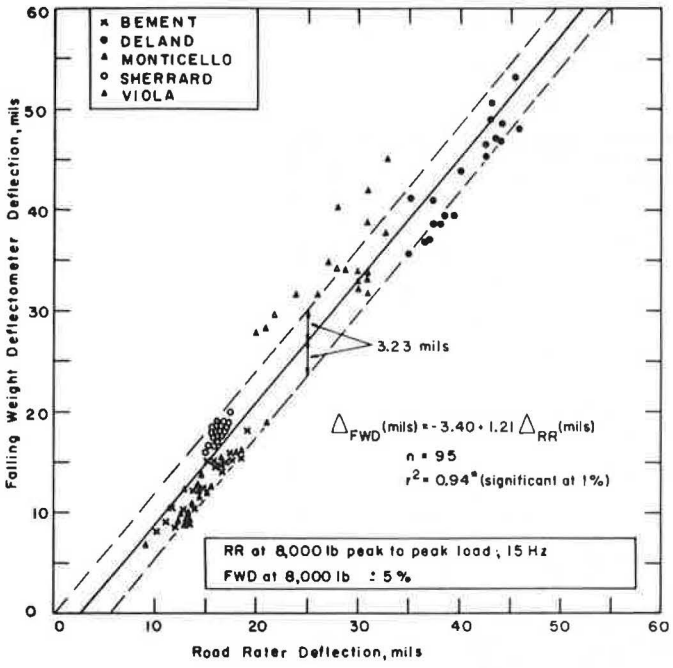

Figure 4. Correlation between FWD and RR areas.

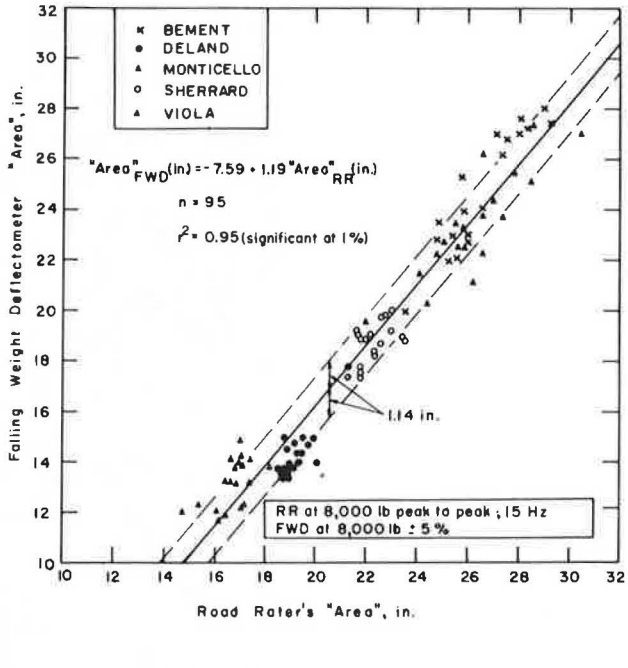

where the coefficient of determination is 0.95 and SEE is 1.14 in (Figure 4).

From the point of view of evaluation of structural pavement, pavements are stiffer when evaluated from RR data. The stiffening effect of the RR can be attributed to the static RR preload and the harmonic loading without rest periods (2). A summary of regression relations between FWD and RR deflection-basin parameters is given in Table 6.

RR and FWD Load and Frequency-Sweep Tests

Figure 5 shows results of typical RR and FWD load and frequency-sweep tests. The left-hand side of Figure 5 shows the variation of centerplate RR deflections with load and driving frequency. The right-hand side shows the variation of RR and FWD centerplate deflections with load. Numerous data similar to those in Figure 5 were gathered in the study; they are summarized elsewhere (1).

Figure 5 shows that

1. The different sections show a distinct RR peak deflection at different driving frequencies;
2. For a given section, the driving frequency corresponding to the peak RR deflection is the same for all peak-to-peak loads;
3. For the Monticello section, RR and FWD center-plate deflections agree at a driving frequency of 22-24 Hz for all load magnitudes; and
4. For the Sherrard and Deland sections, the FWD induces larger deflections than the RR at all loads and driving frequencies.

Table 6. Correlations between FWD and RR deflections.

Dependent FWD Variable	A	B	R^2[a]	SEE	Mean FWD Value	Mean RR Value
D0 (mils)	-3.40	1.21	0.94	3.23	24.19	22.85
D1 (mils)	1.68	0.72	0.92	1.13	12.24	14.62
D2 (mils)	3.98	0.27	0.54	0.64	6.57	9.71
D3 (mils)	2.69	0.25	0.48	0.55	4.56	7.52
Area (in)	-7.59	1.19	0.95	1.14	18.88	22.17
F1	-0.15	1.73	0.93	0.19	1.29	0.84
F2	0.03	1.57	0.72	0.26	1.16	0.72

Notes: FWD (variable) = A + B x RR (variable), Area = 6(D0 + 2D1/D0 + 2D2/D0 + D3), F1 = (D0 - D2)/D1, F2 = (D1 - D3)/D2.
RR at 8-kip peak-to-peak load and 15-Hz driving frequency; FWD at 8 kips ±5 percent; N = 95.

[a]Significant at 1 percent level.

To investigate the erratic response of different pavements to RR and FWD load and frequency tests, it is necessary to use pavement models capable of incorporating time or rate-of-loading variables. Hoffman used dynamic and viscous pavement models to that effect (3). That study concluded that it is theoretically difficult to predict pavement response under one loading mode based on the response measured under a different loading mode, i.e., impulse response (FWD) from vibratory response (RR). The main reason for that discrepancy is that the derived pavement parameters are dependent on loading mode and device (3).

Accelerometer Test Results

An accelerometer was used to check the FWD data-ac-

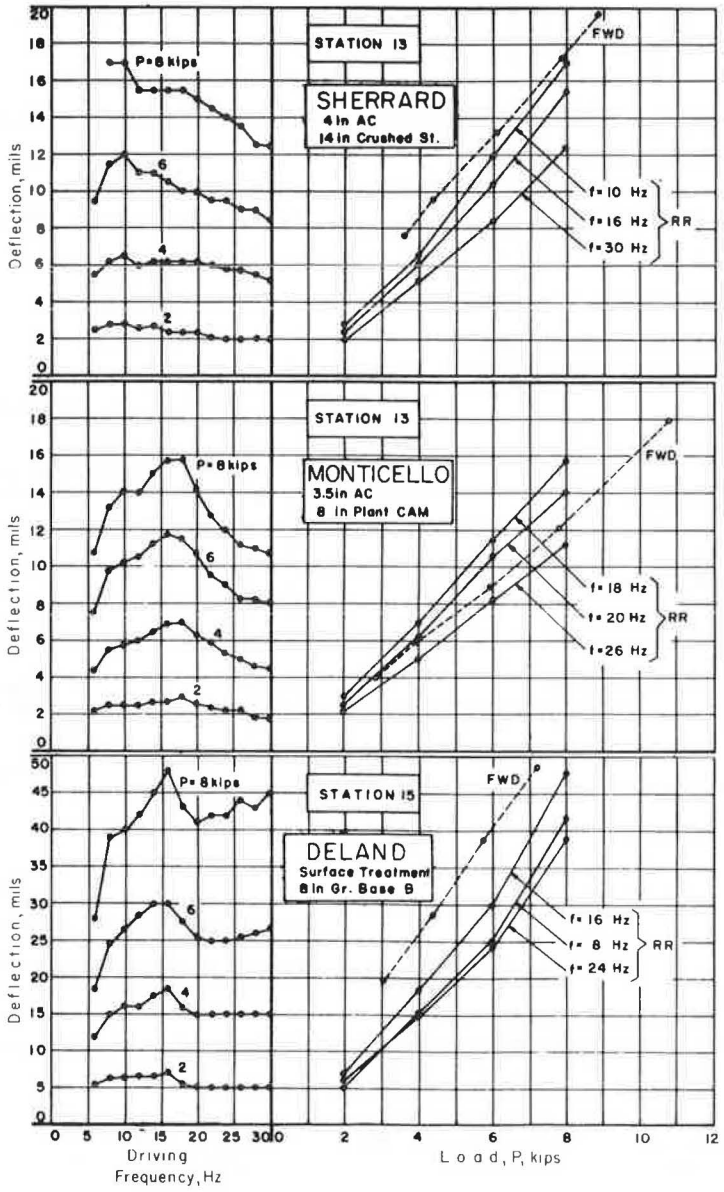

Figure 5. RR versus FWD deflections.

quisition system and generate deflection data under moving trucks at varying speeds. All tests were performed on selected AASHO Test Road sections (Loop 1).

The simultaneous measurement of FWD deflections with the accelerometer and the FWD centerplate sensor showed almost identical results (Figure 6). The agreement indicates that both measuring techniques provide reliable results.

Accelerometer outputs were used to generate acceleration, velocity, and deflection signals under moving trucks (Figure 7) and blows of the FWD (Figure 8). Note in Figures 7 and 8 the vertical and horizontal scales for signal amplitude and time duration, respectively. From additional data similar to Figures 7 and 8, the study (1) concluded that (a) truck signals have a longer duration than FWD signals; typical truck "pulse" durations at 50 mph were estimated at 120 ms whereas FWD pulses are of the order of 30 ms; and (b) as an approximation, truck signals start at the edge of the deflection basin zone of influence. Thus, the stiffer the pavement, the longer the equivalent truck pulse duration.

Pulse duration is relevant to the theoretical treatment of pavement response under different loading modes (3). Bohn and others (4) performed

Figure 6. FWD versus accelerometer deflections.

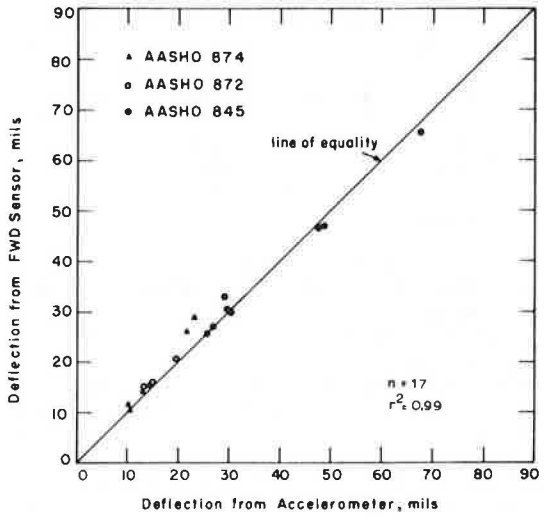

Figure 7. Acceleration, velocity, and deflection signals under moving trucks.

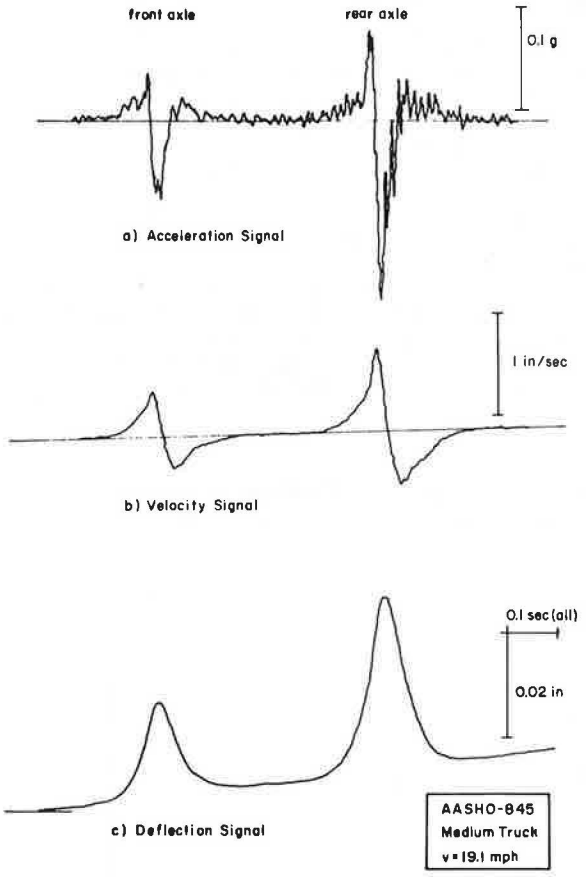

Figure 8. Typical FWD acceleration and deflection signals.

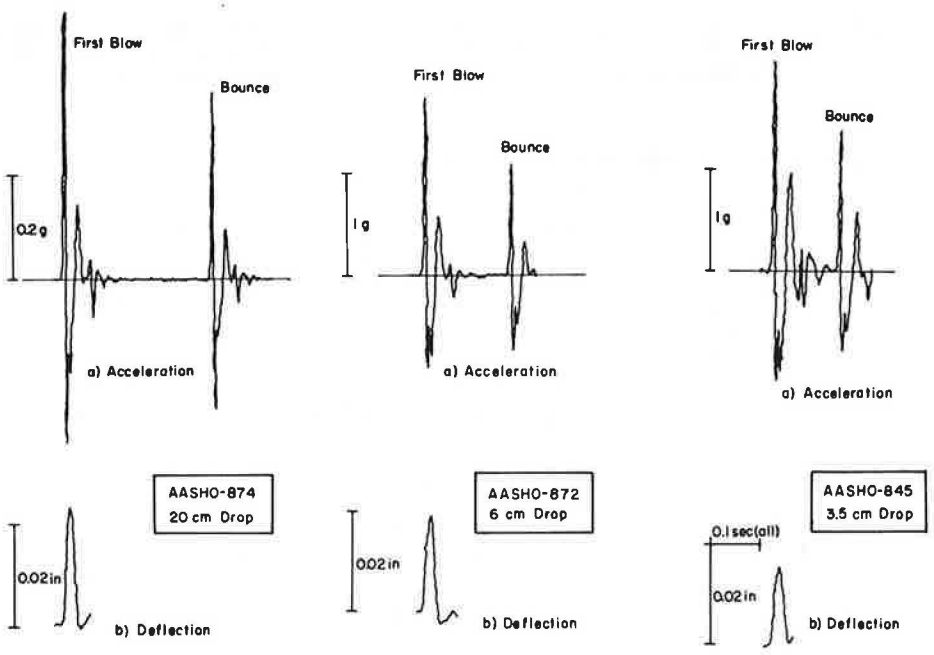

numerous moving-truck and FWD deflection measurements, and they also concluded that moving-truck signals were much longer than FWD deflection signals.

Figure 9 shows the relationship between the ground acceleration amplitude g and centerplate deflection caused by FWD blows determined from accelerometer measurements. From Figure 9 it is observed that (a) FWD-imposed ground accelerations can reach values of up to 4 times g and (b) there are different relationships between acceleration and deflection for different sections. The first observation suggests that inertia effects under FWD blows should be significant and may need to be included in theoretical analyses (3). The study also concluded that vehicle-imposed accelerations were approximately one-tenth of the FWD accelerations. The discrepancy between FWD and vehicle-imposed accelerations suggests that a fixed-in-place NDT device cannot simulate the loading effect of a moving load. However, FWD and moving-truck deflections in this study and those reported by Bohn and others (4) compared favorably.

One explanation for the different relationships between acceleration and deflection amplitudes (Figure 9) is that FWD pulse duration changes for different pavements. From accelerometer signals FWD pulse durations were estimated to range between 24 and 56 ms (2).

Figure 9. FWD acceleration versus FWD deflection.

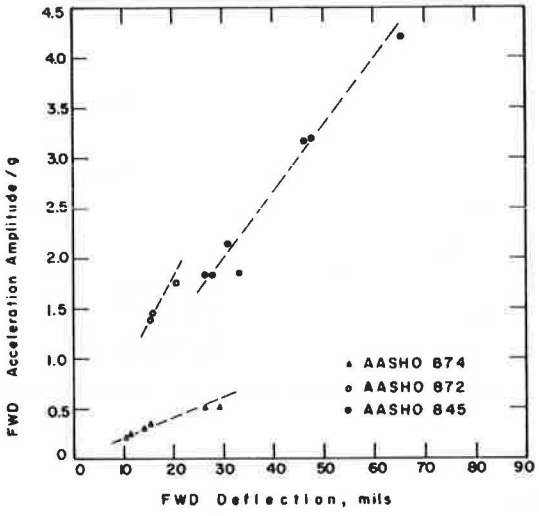

Deflections Under Moving Trucks

Figure 10 shows a typical relationship between deflection and vehicle speed for the AASHO Test Road sections tested in the study. Truck speed ranged from 8 to 30 mph.

Figure 10 shows no effect of vehicle speed on surface deflections. In fact, none of the nine deflection-speed relationships developed in the study (three per section per truck) showed a regression coefficient significantly different from zero. In other words, the mean deflection is indicative of the speed effect.

No generalizations are attempted based on the limited speed-effect data collected in the study. Bohn and others (4) performed speed-deflection studies at speeds between 6 and 38 mph (18-kip rear-axle truck) and reported no effect of speed on surface deflections. Other studies (5) reported a deflection decrease of 35 percent between creep and 40 mph. It is apparent that most of the deflection decrease with increasing speed takes place between creep speed and about 8-10 mph (1).

Comparison of Moving-Truck, RR, and FWD Deflections

Figure 11 shows the deflection-load relationship for moving trucks, the IDOT RR, and the FWD for the AASHO Test Road sections in the study. Average moving-truck deflections are shown since speed did not have a significant effect on deflections (see Figure 10). RR deflections are shown for the peak deflection frequency and the lowest deflection frequency. The following conclusions were drawn from these studies:

1. Peak RR deflections were consistently the lowest. At other frequencies RR deflections were even lower. At an 8-kip load level, RR deflections were about 25 percent lower than moving-truck deflections (average).
2. Moving-truck and FWD deflections were the closest. In two test sections, FWD deflections were slightly higher than moving-truck deflections. In the remaining section, moving-truck deflections were higher than FWD deflections. On the average, moving-truck and FWD deflections were in close agreement. Agreement between moving-truck and FWD deflections had been reported earlier (4).

The lower RR deflections can be attributed to the vibratory RR loading (without rest periods) and the RR's static preload. This loading mode produces a

Figure 10. Variation of moving-truck deflections with vehicle speed.

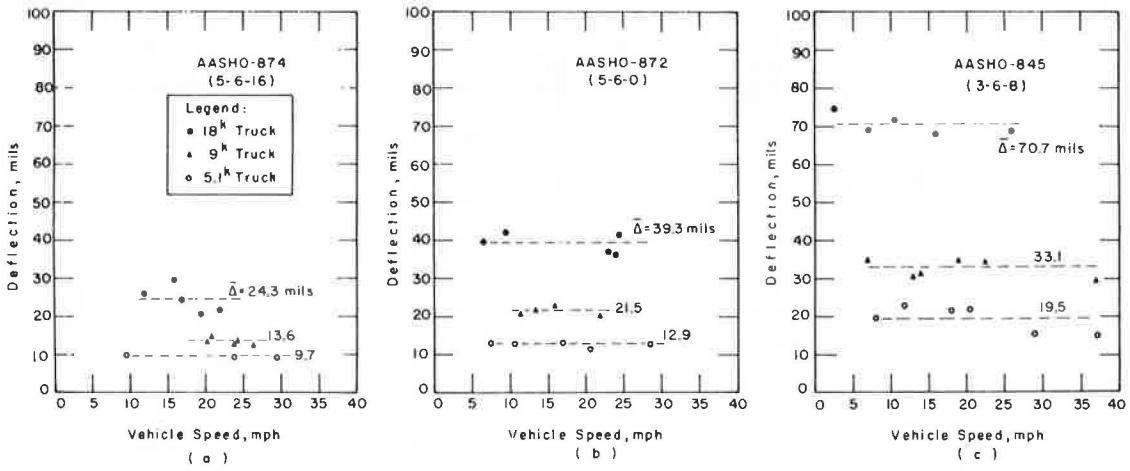

Figure 11. Variation of moving-truck, RR, and FWD deflections with load.

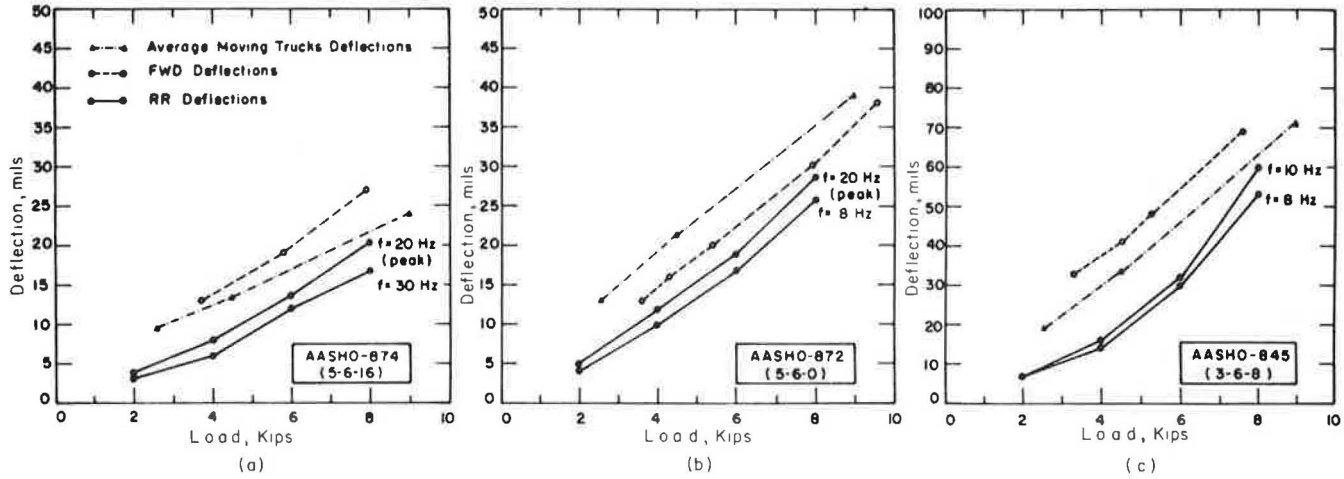

stiffening effect and thus lower pavement deflections. The study concluded that the FWD is the best NDT device to simulate pavement response (deflections) under moving loads.

Influence of Load on Surface Deflections

The influence of load on surface deflections was investigated with the RR and the FWD. RR loads ranged from 2 to 8 kips peak to peak and FWD loads varied from 2 to 11 kips. Load effects were analyzed by using the pavement-stiffness concept. Stiffness is defined as the load needed to cause a unit deflection (spring constant). The main findings of the study are as follows (Tables 7 and 8):

1. Most pavements showed a decrease in stiffness with increasing load (RR and FWD). A decrease in stiffness with increasing load means that the pavements soften (deflections increase faster than the load).
2. The ratio between the maximum and minimum pavement stiffness ranged from 1.0 to 2.5 (most values between 1.2 and 1.6) with the RR and from 1.03 to 1.26 (most values between 1.1 and 1.2) with the FWD. RR stiffness values were computed at the peak deflection frequency.
3. The deflection-basin area is less sensitive to load than centerplate deflections. RR (at a given driving frequency) and FWD areas varied within 10 percent for the range of loads considered. The deflection-basin area is thus a strong characterizing pavement parameter.

Influence of Driving Frequency on RR Deflections

The effect of driving frequency on RR deflections was investigated in frequency-sweep tests for driving frequencies varying from 6 to 30 Hz at 2-Hz intervals. The study indicated the following points:

1. Different sections show one distinct peak deflection at different driving frequencies (see Figure 5).
2. For a given section, the driving frequency at the peak deflection is roughly the same at different peak-to-peak loads.
3. The ratio between the peak deflection and the minimum deflection in the sweeps ranged from 1.3 to 3.9. Rigid pavements are more susceptible to driving frequency than are conventional flexible pavements.
4. The deflection-basin area reaches a peak at the same driving frequency as the peak deflections.

Table 7. Influence of load magnitude on RR deflections.

Section	Driving Frequency (Hz)	Stiffness at Peak-to-Peak Load Shown (kips/in)				Stiffness max / Stiffness min
		2 Kips	4 Kips	6 Kips	8 Kips	
Bement[a]	18	625	558	547	508	1.23
Deland[a]	16	296	245	224	197	1.50
Monticello[a]	18	723	597	549	522	1.39
Sherrard[a]	10	706	597	483	468	1.51
Viola[a]	8	400	343	281	267	1.50
AASHO-874	20	541	500	435	396	1.37
AASHO-872	20	400	333	275	275	1.45
AASHO-845	16[b]	250	200	182	100[c]	2.50

[a] Average of three stations.
[b] Not peak deflection frequency.
[c] Unstable readings at these conditions.

Table 8. Influence of load magnitude on FWD deflections.

Section	Stiffness at Load Shown (kips/in)				Stiffness max / Stiffness min
	3 Kips	6 Kips	8 Kips	>8 Kips	
Bement[a]	783	779	736	711	1.10
Deland[a]	175	172	170	-	1.03
Monticello[a]	677	647	639	617	1.10
Sherrard[a]	500	458	439	-	1.14
Viola[a]	316	276	261	261	1.21
AASHO-874	273	306	296	313	1.15[b]
AASHO-872	273	273	265	257	1.06
AASHO-845	100	110	110	-	1.10[b]

[a] Average of three stations.
[b] Increasing stiffness with increasing load.

5. The ratio between the maximum and minimum areas in a sweep never exceeded 1.36; most ratios were between 1.1 and 1.2.
6. The combined effects of load and frequency on pavement stiffness can be substantial. A typical flexible pavement with a stiffness of 1000 kips/in at a 2-kip peak-to-peak load and 8-Hz driving frequency can have a stiffness of only 500 kips/in or less at 8 kips and the peak deflection frequency. This illustrates the inconvenience of using low-load fixed-frequency NDT devices for structural pavement evaluation.

Seasonal Effects on Surface Deflections

Routine RR deflections (8-kip peak-to-peak load, 15-Hz driving frequency) were measured four to six

Table 9. Analysis of variance of RR deflections with testing date.

Section	N	F-ratio	Grand Total Mean Δ (mils)	Grand Total SD (mils)	Grand Total CV (%)	Duncan Multiple-Range Test						
Bement	120	2.02	15.34	2.84	18.5	Group	Oct. 78	June 78	Oct. 79	May 78	Apr. 79	Sept. 79
						Mean Δ	14.32	14.51	14.92	15.34	15.63	16.89
Coffeen	99	37.87[a]	9.93	1.98	20.0	Group	Oct. 78	Sept. 78	Apr. 79	May 78	Aug. 79	
						Mean Δ	7.21	9.46	10.52	10.67	11.74	
Deland	110	34.32[a]	43.55	7.76	17.8	Group	Oct. 78	Oct. 79	Sept. 79	May 78	Apr. 79	June 78
						Mean Δ	33.76	40.50	41.42	47.30	50.40	51.25
Hillsboro	99	106.48[a]	24.98	6.86	27.5	Group	Oct. 78	May 78	Sept. 78	Apr. 79	Aug. 79	
						Mean Δ	14.08	25.16	25.55	27.00	33.11	
Midlothian "A"	139	20.19[a]	7.95	1.90	23.9	Group	Nov. 78	May 79	Sept. 79	Aug. 78	Sept. 77	June 78
						Mean Δ	5.60	6.95	7.80	8.32	8.58	9.79
Midlothian "B"	139	20.95[a]	14.08	2.06	14.6	Group	Nov. 78	May 79	Aug. 78	Sept. 79	Sept. 77	June 78
						Mean Δ	11.08	13.76	14.11	14.44	14.80	15.63
Monticello	120	14.39[a]	17.13	3.78	22.0	Group	Oct. 79	Oct. 78	May 78	Sept. 79	June 78	Apr. 79
						Mean Δ	14.39	14.91	16.24	16.93	19.36	20.66
Neoga "N"	80	61.11[a]	28.67	12.66	44.2	Group	Oct. 78	Aug. 79	Apr. 79	Aug. 78		
						Mean Δ	11.84	28.08	34.97	39.83		
Neoga "S"	73	122.96[a]	21.87	6.33	29.0	Group	Oct. 78	Aug. 78	Aug. 79	Apr. 79		
						Mean Δ	12.61	24.28	25.29	27.15		
Pana	100	251.11[a]	20.71	8.69	42.0	Group	Oct. 78	May 78	Apr. 79	Sept. 78	Aug 79	
						Mean Δ	9.24	16.71	18.41	25.71	33.50	
Sherrard	116	134.76[a]	21.05	7.66	36.4	Group	Nov. 78	Oct. 79	Sept. 79	May 78	July 78	May 79
						Mean Δ	13.23	16.24	19.47	20.41	22.18	36.03
Viola	78	117.41[a]	39.11	23.04	59.0	Group	Nov. 78	Oct. 79	Sept. 79	May 79		
						Mean Δ	21.16	28.21	32.26	73.90		

[a]Significant at $\alpha = 0.05$.

Table 10. Analysis of variance of RR basin area with testing date.

Section	N	F-ratio[a]	Grand Total Mean Area (in)	Grand Total SD (in)	Grand Total CV (%)	Duncan Multiple-Range Test						
Bement	120	8.00	27.12	1.88	6.9	Group	Sept. 79	Oct. 78	Oct. 79	May 78	June 78	Apr. 79
						Mean area	25.95	26.25	26.50	27.41	28.07	28.52
Coffeen	99	4.89	29.24	1.75	6.0	Group	Aug. 79	Sept. 78	Oct. 78	May 78	Apr. 79	
						Mean area	28.59	28.78	28.85	29.44	30.78	
Deland	110	30.13	18.40	1.24	6.7	Group	May 78	June 78	Oct. 78	Oct. 79	Sept. 79	Apr. 79
						Mean area	17.21	17.43	18.12	19.10	19.52	19.65
Hillsboro	99	112.81	26.90	2.29	8.5	Group	Aug. 79	Sept. 78	May 78	Apr. 79	Oct. 78	
						Mean area	24.64	25.01	26.31	28.74	29.91	
Midlothian "A"	140	62.25	24.61	2.19	8.9	Group	June 78	Aug. 78	Sept. 77	Sept. 79	Nov. 78	May 79
						Mean area	22.71	23.17	23.80	24.83	25.43	28.56
Midlothian "B"	140	84.63	23.91	1.60	6.7	Group	Sept. 77	Aug. 78	June 78	Sept. 79	Nov. 78	May 79
						Mean area	22.85	23.00	23.17	23.96	24.75	26.91
Monticello	120	5.2	25.85	1.91	7.4	Group	Sept. 79	Oct. 78	June 78	Oct. 79	May 78	Apr. 79
						Mean area	24.82	24.89	25.62	26.18	26.54	27.04
Neoga "N"	80	106.90	22.75	2.42	10.6	Group	Aug. 78	Aug. 79	Apr. 79	Oct. 78		
						Mean area	19.49	22.32	23.91	25.30		
Neoga "S"	73	43.50	25.15	1.65	6.6	Group	Aug. 78	Aug. 79	Oct. 78	Apr. 79		
						Mean area	23.47	24.58	26.25	26.92		
Pana	100	254.62	23.74	2.47	10.4	Group	Sept. 78	Aug. 79	May 78	Apr. 79	Oct. 78	
						Mean area	20.80	21.58	23.62	25.86	26.86	
Sherrard	116	63.34	20.88	1.33	6.4	Group	July 78	Sept. 79	May 79	May 78	Nov. 78	Oct. 79
						Mean area	18.80	20.47	20.57	21.51	21.71	22.30
Viola	78	15.19	16.61	1.05	6.3	Group	Sept. 79	Oct. 79	Nov. 78	May 79		
						Mean area	15.55	16.72	16.81	17.31		

[a]Significant at $\alpha = 0.05$.

times in a two-year period on the 12 primary in-service sections of the program. Tables 9 and 10 show the analyses of variance of RR deflections and area with date of testing, respectively.

In addition to the F-ratio, which indicates whether the deflections and area changed with testing date, Tables 9 and 10 include the results of the Duncan multiple-range test. In this test, means that are statistically equal (95 percent confidence level) are grouped together and are underlined. Tables 9 and 10 indicate the following findings:

1. Except for the Bement section (deflections), mean RR deflections and area did change with testing date;
2. Within the testing period, mean RR deflections for a given section changed by factors of 1.4-3.6;
3. Within the testing period, mean RR area for a given section changed by factors of 1.07-1.30;
4. Without exception, the lowest mean RR deflection was measured in the fall (October or November);
5. The highest mean RR deflection was obtained either in the summer or the spring; and
6. There is no specific time of the year when the area is the highest or lowest in any given section.

SUMMARY AND CONCLUSIONS

This paper presented the main findings and conclusions of a comparative study of selected NDT devices for the structural evaluation of Illinois flexible pavements. The devices used were the Benkelman beam, the road rater (model 2008), the falling-weight deflectometer, and an accelerometer to measure surface deflections under moving trucks. The different (mostly in-service) pavements tested were selected to reflect typical flexible pavement constructions over a wide variety of subgrade soils throughout Illinois. Comparisons and correlations (where applicable) between different NDT devices were presented. The following conclusions were drawn:

1. Overall, BB deflections cannot be reliably predicted from RR deflections.
2. RR deflections (8-kip, 15-Hz) and FWD deflections (8-kip) are significantly different (statistically) for all pavements tested. However, RR and FWD deflections and areas are highly correlated.
3. Surface deflections are highly sensitive to the RR load and driving frequency. Low-load fixed-frequency vibrators can overestimate the pavement stiffness by factors of 2 or more.
4. Overall, the FWD is the best NDT device to simulate pavement response under moving loads. The RR, because of its harmonic loading without rest periods and static preload, induces pavement deflections lower than those achieved with the FWD and moving loads.
5. FWD deflections and deflection-basin areas at a 9-kip load level or converted RR deflections and area at 8 kips and 15 Hz (by using the FWD-RR correlations proposed) are recommended for structural flexible-pavement evaluation.

ACKNOWLEDGMENT

This paper is based on the results of Project IHR-508: Load Response Characteristics of Flexible Pavements. Project IHR-508 is a cooperative study. Project planning and development were joint efforts of IDOT and the University of Illinois. IDOT (P. Dierstein, J.S. Dhamrait, and K.W. Wicks) assumed responsibility for all NDT testing. Various IDOT districts aided in the field sampling. The Soils Laboratory of the Bureau of Materials and Physical Research under the supervision of T.S. Lewis conducted routine soil tests. Specialized soils and materials tests were conducted by the University of Illinois. V.J. McDonald, Research Engineer at the University of Illinois, and the IDOT Instrumentation Development Group of the Physical Research Section were responsible for accelerometer data acquisition and data processing. Data reduction, structural modeling analyses, and the development of procedures for analyzing NDT data were activities conducted by the University of Illinois.

Special thanks are extended to the various IDOT districts, County Superintendents of Highways, and Township Commissioners who willingly agreed to provide test pavement sites and general aid.

IHR-508 was sponsored by the Illinois Department of Transportation (Division of Highways) and the Federal Highway Administration, U.S. Department of Transportation.

REFERENCES

1. M.S. Hoffman and M.R. Thompson. Nondestructive Testing of Flexible Pavements--Field Testing Program Summary. Univ. of Illinois at Urbana-Champaign, Transportation Engineering Series 31, Illinois Cooperative Highway and Transportation Research Program Series 188, June 1981.
2. M.S. Hoffman and M.R. Thompson. Mechanistic Interpretation of Nondestructive Pavement Testing Deflections. Univ. of Illinois at Urbana-Champaign, Transportation Engineering Series 32, Illinois Cooperative Highway and Transportation Research Program Series 190, June 1981.
3. M.S. Hoffman. Mechanistic Interpretation of Nondestructive Pavement Testing Deflections. Department of Civil Engineering, Univ. of Illinois at Urbana-Champaign, Ph.D. thesis, Sept. 1980.
4. A. Bohn, P. Ullidtz, R. Stubstad, and A. Sorenson. Danish Experiments with the French Falling Weight Deflectometer. Proc., 3rd International Conference on the Structural Design of Asphalt Pavements, Univ. of Michigan, Ann Arbor, Vol. 1, 1972, pp. 1119-1128.
5. AASHO Road Test. HRB, Special Repts. 61 and 73, 1962.

Publication of this paper sponsored by Committee on Pavement Condition Evaluation.

Backcalculating Nonlinear Resilient Moduli from Deflection Data

MARIO S. HOFFMAN AND MARSHALL R. THOMPSON

A method (ILLI-CALC) is presented for backcalculating nonlinear resilient moduli based on the interpretation of measured surface deflection basins. ILLI-PAVE, a stress-dependent finite-element pavement model, was used to generate data for developing algorithms and nomographs for deflection-basin interpretation. Nonlinear stress-dependent material characterizations are directly incorporated into the ILLI-CALC procedure. Solutions presented are for conventional flexible pavements composed of an asphalt concrete layer, a typical crushed-stone base layer, and a fine-grained subgrade soil. ILLI-CALC is illustrated for two different flexible pavements by using deflection data collected on several testing dates. Agreement is achieved between backcalculated material properties and laboratory-determined properties. Agreement is also achieved between measured and predicted deflection basins. The backcalculated parameters by using ILLI-CALC can be used as input for overlay design. The change in the stress state in the pavement-subgrade system caused by a change in the pavement cross section (overlay layer) is accounted for by the nonlinear stress-dependent characterization of the granular base and subgrade soil materials in the ILLI-PAVE model.

Pavement engineers continually face the problem of characterizing material properties of existing in-service pavements. Material characterization is needed to (a) determine whether a pavement structure is adequate to accommodate an anticipated change in mission (traffic), (b) provide input for overlay design when the pavement is reaching its final serviceability, and (c) develop rehabilitative recommendations and optimal maintenance strategies based on routine structural evaluation.

There is general agreement among pavement engineers and researchers that the measured surface deflection basin provides valuable information for the structural evaluation of pavements. To interpret surface deflection measurements, the actual pavement structure and its subgrade must be replaced by a mechanistic pavement model.

The structural evaluation of a pavement is, to an extent, an inverted design process. If the cross section and properties of the paving materials and support system are known, it is possible to compute the pavement response (stresses, strains, and displacements) for given loading conditions (design process). In the evaluation process, the response of the pavement is measured, and the material properties are backcalculated. The same concern exercised in laboratory procedures to simulate the repetitive nature and magnitude of traffic loadings during sample testing applies to the full-scale testing of pavements.

Numerous flexible-pavement evaluation methods, based on the interpretation of measured deflection basins, have been developed in the last 15 years (1-5). These methods use two to five deflection-basin values to backcalculate two to five resilient moduli. All methods use a linear elastic pavement model and a computerized iterative solution, a graphical solution, or nomographs in the backcalculation analyses. All solutions are based on matching the measured deflection basin with the theoretical deflection basin to determine the corresponding E-values.

In recent years, several attempts have been made to consider nonlinear material properties (6;7, p. 123). Still, the analyses are made based on linear elasticity, and material nonlinearity is considered by indirect means.

This paper presents a method for backcalculating resilient moduli that directly incorporates nonlinear material characterizations. ILLI-PAVE, a stress-dependent finite-element pavement model, was used to generate data for developing algorithms and nomographs for deflection-basin interpretation. By using the proposed method, the backcalculated parameters can be used as input for overlay design. The change in the stress state in the pavement-subgrade system caused by a change in the pavement cross section (overlay) is accounted for by the nonlinear stress-dependent material characterization.

ILLI-CALC, the method presented and illustrated in this paper, is for conventional flexible pavements composed of an AC layer or surface treatment, a granular layer, and a fine-grained subgrade soil. A detailed description of the procedure and nomographs for full-depth asphalt pavements and flexible pavements with stabilized base layers have been published elsewhere (8).

DEFLECTION-BASIN CHARACTERIZATION

The first goal of the present study was the selection of an appropriate nondestructive testing (NDT) device for structural pavement evaluation. The basis for that selection was the capability of the NDT device to simulate pavement response under moving design traffic loads. The reason for that demand is that most mechanistic models used in pavement analysis and design are "static" models. Time of loading or loading mode are not included. Thus, undesirable extrapolations are minimized by analyzing pavement response under moving loads. Loading mode (vibratory, impulse, vehicular) significantly affects pavement response (9).

To accomplish that goal, the Illinois Department of Transportation (IDOT) and the University of Illinois engaged in an extensive deflection-testing program that included the Benkelman beam (BB), the IDOT road rater (RR), the falling-weight deflectometer (FWD), and an accelerometer to measure deflections under different moving trucks. A full description of the program and a summary of the results can be found elsewhere (9).

The deflection study concluded that the FWD is the best device to simulate pavement response under moving trucks. Highly significant correlations developed in the study between the IDOT RR and the FWD at the 8-kip level (Table 1) permit the use of RR deflection basins for structural evaluation. RR deflection basins, however, must be converted to equivalent FWD deflection basins prior to being used in the proposed procedure. Both the IDOT RR and the FWD have a loading plate 12 in in diameter, and deflections were measured at the centerplate and 1, 2, and 3 ft away from the centerplate.

The deflection basin is characterized as follows:

1. D0, centerplate maximum deflection;
2. D1, D2, D3, deflections at 1, 2, and 3 ft from the centerplate, respectively;
3. Deflection-basin "area" (see Figure 1), defined as follows: Area (in) = 6(1 + 2D1/D0 + 2D2/D0 + D3/D0); and
4. F1, F2, deflection-basin shape factors, defined as F1 = (D0 - D2)/D1 and F2 = (D1 - D3)/D2.

The deflection-basin area combines the four sensor deflections. It can vary from 11 in (Bous-

Table 1. Correlations between FWD and RR deflections.

Dependent FWD Variable	A	B	R^2[a]	SEE	Mean FWD Value	Mean RR Value
D0 (mils)	-3.40	1.21	0.94	3.23	24.19	22.85
D1 (mils)	1.68	0.72	0.92	1.13	12.24	14.62
D2 (mils)	3.98	0.27	0.54	0.64	6.57	9.71
D3 (mils)	2.69	0.25	0.48	0.55	4.56	7.52
Area (in)	-7.59	1.19	0.95	1.14	18.88	22.17
F1	-0.15	1.73	0.93	0.19	1.29	0.84
F2	0.03	1.57	0.72	0.26	1.16	0.72

Notes: FWD (variable) = A + B x RR (variable), Area = 6 (1 + 2D1/D0 + 2D2/D0 + D3/D0), F1 = (D0 - D2)/D1, F2 = (D1 - D3)/D2.
RR at 8-kip peak-to-peak load and 15-Hz driving frequency; FWD at 8 kips ±5 percent; N = 95.

[a]Significant at 1 percent level.

Figure 1. Deflection-basin characterization.

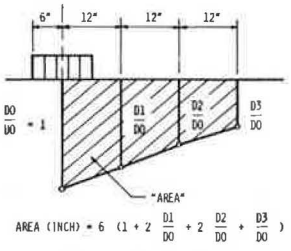

sinesq approximation) to 36 in (maximum by definition). Also, stiffer pavements have larger areas (9).

In the evaluation procedure, RR centerplate deflections (D0) at 8 kips and 15 Hz are converted to equivalent FWD deflection by using the correlations in Table 1. This equivalent D0 must then be multiplied by 1.125 for load adjustment (8-kip versus 9-kip in ILLI-PAVE solutions). RR basin area and shape factors must also be converted by using Table 1 but no load adjustment is required (8).

NONLINEARITY IN FLEXIBLE PAVEMENTS

Nonlinear stress-strain or load-deflection relations are exhibited in laboratory testing of soil and paving materials and in field testing of flexible pavements. Results of repeated-load tests on paving materials and subgrade soils show that the resilient modulus, and to some extent Poisson's ratio, depend on the stress state. Numerous research efforts have been devoted to defining nonlinear stress-strain relationships for repetitive laboratory testing conditions (10-13). Resilient modulus is defined as the ratio between the deviator stress and the recoverable strain.

The nonlinearity most frequently observed in flexible pavements is the relation between a load applied at the surface and the corresponding vertical deflection. Most flexible in-service pavements tested in the Illinois study showed softening (deflections increased more than the load) (9). For loads varying from 2 to 10 kips, pavement stiffness (load-deflection) decreases of 20-60 percent were noted.

The evidence of nonlinearity in flexible pavements justifies the inclusion of nonlinear material characterizations in the mechanistic pavement model. A stress-dependent material model is especially needed for overlay design since the added thickness will result in stress-state changes in the pavement layers and subgrade soil. These stress-state changes can be accounted for by stress-dependent material characterizations.

ILLI-PAVE MODEL

The ILLI-PAVE model is an axisymmetric solid of revolution based on the finite-element method (14). The model incorporates nonlinear stress-dependent material models and failure criteria for granular materials and fine-grained soils (15). The principal stresses in the granular and subgrade layers are modified at the end of each iteration so that they do not exceed the strength of the materials as defined by the Mohr-Coulomb theory of failure. Studies reported by Raad and Figueroa (15), Suddath and Thompson (16), and Traylor (17) comparing measured and ILLI-PAVE predicted load-deformation responses yielded favorable results.

Material Characterization

Table 2 (14) summarizes material properties and pavement cross sections of ILLI-PAVE solutions developed for conventional flexible pavements. The asphalt-concrete (AC) material was assumed to be linear elastic with E-moduli ranging from 100 to 1400 ksi. AC layer thicknesses ranged from 0 (surface treatment) to 8 in. Layer thicknesses were as follows:

AC Layer (in)	Granular Base (in)
0.0	4.0
1.5	6.0
3.0	9.0
5.0	12.0
8.0	18.0
	24.0

Two material models were used to characterize granular base materials. The general model was of the following form:

$$Er = k\theta^n \quad (1)$$

where

Er = resilient modulus (psi),
θ = first stress invariant or bulk stress (psi), and,
k,n = material constants determined in repetitive triaxial tests.

Note in Table 2 that the crushed-stone material has k- and n-values of 9000 and 0.33 and the gravel has k- and n-values of 6500 and 0.30, respectively. These granular material models were determined by Traylor (17) for base and subbase materials used for the American Association of State Highway Officials (AASHO) test road. Base layer thicknesses ranged from 4 to 24 in.

Four different fine-grained subgrade soil models (based on extensive previous research) (11) were used; they corresponded to typical stiff, medium, soft, and very soft conditions. These models are given in Table 2 and shown in Figure 2. Note in Figure 2 that the slopes of the curves for resilient modulus and deviator stress for the different subgrades are constant. The "breaking point" of the curves at a deviator stress of 6 psi (defined as σ_{di}) corresponds to a resilient modulus denoted Eri. For each of the four subgrade models chosen, Eri becomes the main parameter characterizing the nonlinear subgrade soil.

The crushed-stone material model in Table 2 was chosen in the first stage of the analyses and was kept constant. Thus, a typical three-layer conventional flexible pavement was characterized by four variables: (a) the thickness of the AC layer (Tac), (b) the modulus of elasticity of the AC layer (Eac),

Table 2. Material properties and cross-section geometries for ILLI-PAVE solutions.

Property	Asphalt Concrete			Crushed Stone	Gravel	Subgrade			
	40°F	70°F	100°F			Stiff	Medium	Soft	Very Soft
Unit weight (pcf)	145.00	145.00	145.00	135.00	135.00	125.00	120.00	115.00	110.00
Lateral pressure coefficient at rest	0.37	0.67	0.85	0.60	0.60	0.82	0.82	0.82	0.82
Poisson's ratio	0.27	0.40	0.46	0.38	0.38	0.45	0.45	0.45	0.45
Unconfined compressive strength (psi)	-	-	-	-	-	32.80	22.85	12.90	6.21
Deviator stress (psi)									
Upper limit	-	-	-	-	-	32.80	22.85	12.90	6.21
Lower limit	-	-	-	-	-	2.00	2.00	2.00	2.00
σ_{di} (psi)	-	-	-	-	-	6.20	6.20	6.20	6.20
Eri (ksi)	-	-	-	-	-	12.34	7.68	3.02	1.00
E-failure (ksi)	-	-	-	4.00	4.00	7.605	4.716	1.827	1.00
E-constant modulus (ksi)	400.00	500.00	100.00	-	-	-	-	-	-
Er model (psi)	-	-	-	$9000\theta^{0.33}$	$6500\theta^{0.30}$	-	-	-	-
Friction angle (°)	-	-	-	40.0	40.0	0.0	0.0	0.0	0.0
Cohesion (psi)	-	-	-	0.0	0.0	16.4	11.425	6.45	3.105

Figure 2. Subgrade soil material models for ILLI-PAVE analyses.

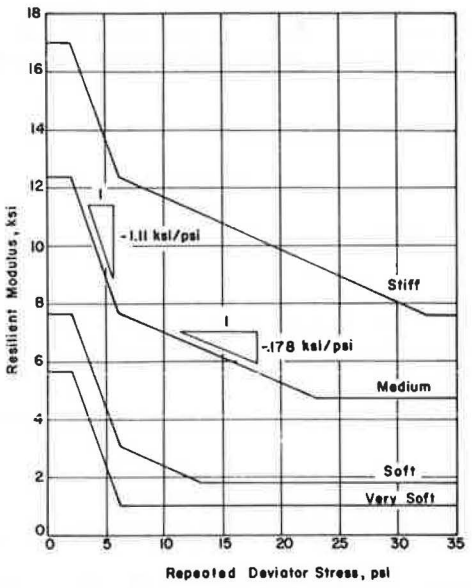

Figure 3. ILLI-PAVE and BISAR equivalent pavement cross sections.

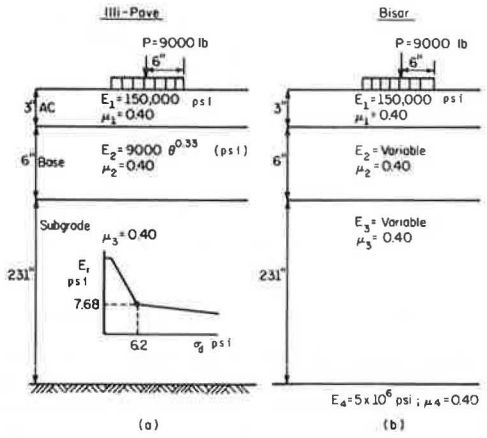

(c) the thickness of the granular base (Tgr), and (d) the modulus of the subgrade soil at the breaking point (Eri).

Linearity Versus Nonlinearity in Pavement Evaluation

To illustrate the effect of nonlinear material characterizations and the failure criteria in the ILLI-PAVE model, consider the typical flexible pavement cross section shown in Figure 3. The pavement is composed of a 3-in AC layer, a 6-in granular base, and a fine-grained subgrade soil. Figure 3a shows the ILLI-PAVE cross section and material properties, whereas Figure 3b shows the same cross section with linearly elastic materials. Note that Figure 3b includes a stiff material ($E = 5 \times 10^6$ psi) 231 in below the subgrade level to simulate the zero-displacement boundary of typical finite-element solutions.

The surface deflection basin was computed for the ILLI-PAVE pavement in Figure 3a. By using the BISAR multilayer elastic program (18), the values of E_2 and E_3 were determined for the pavement in Figure 3b so that both solutions yield identical deflection basins. Once E_2 and E_3 had been determined, the equivalent systems were compared for stresses and strains at selected locations.

Table 3. Comparison of ILLI-PAVE and BISAR solutions for identical deflection-basin systems.

Response Parameter	ILLI-PAVE	BISAR
D0, deflection at r = 0.0 in (mils)	37.86[a]	37.37
D1, deflection at r = 12.0 in (mils)	18.64	17.37
D2, deflection at r = 24.0 in (mils)	7.98	8.22
D3, deflection at r = 36.0 in (mils)	4.74	4.86
Deflection-basin area (in)	15.18[a]	15.00
Vertical stress, top of subgrade (psi)	15.80 (C)	20.90 (C)
Radial stress, bottom AC layer (psi)	40.00 (T)	112.40 (T)
Radial strain, bottom AC layer (0.0001 in/in)	4.90 (T)	5.90 (T)
Radial stress, bottom granular layer (psi)	3.80 (C)	14.10 (T)
Vertical strain, top of subgrade (0.001 in/in)	2.10 (C)	1.80 (C)
Deviator stress, top of subgrade (psi)	13.30	15.70
Deflection in AC layer (%)	1.00	1.50
Deflection in granular base (%)	20.00	25.50
Deflection in subgrade (%)	79.00	73.00

Note: (C) = compression; (T) = tension.

[a]Equal D0 and area are the basis of the "equivalent" pavement systems.

The E_2 and E_3 values in the BISAR system that yielded a surface deflection basin similar to that of the ILLI-PAVE system were 23 000 psi and 11 000 psi, respectively. Table 3 shows a summary of selected response parameters for the ILLI-PAVE and BISAR systems, which have identical deflection basins (D0 and area).

Table 3 shows that the BISAR and ILLI-PAVE systems, although they have identical deflection-basin

Table 4. ILLI-PAVE deflection-basin algorithms, group 3.

Dependent Variable	R^2[a] (%)	σ	CV (%)	Constant 0	Eri P	Eac q	Tac r	Tgr s	Standardized Regression Coefficient for Independent Variables: Eri	Eac	Tac	Tgr
log D0	95.5	0.04	3.0	1.900	-0.0197	-0.000 200	-0.0451	-0.007 07	-0.46	-0.58	-0.47	-0.18
Area	92.6	1.07	5.5	13.21	-0.359	0.004 09	0.946	0.127	-0.42	0.59	0.49	0.16
F1	90.9	0.13	12.1	1.72	0.0432	-0.000 458	-0.0804	-0.019 8	0.46	-0.60	-0.38	-0.23
F2	94.9	0.09	8.1	1.73	0.0453	-0.000 418	-0.0829	-0.017 5	0.51	-0.58	-0.41	-0.21

Note: Equation of the following form: Dependent variable = 0 + p x Eri + q x Eac + r x Tac + s x Tgr.
[a]Significant at 1 percent level.

Figure 4. Nomograph based on D0.

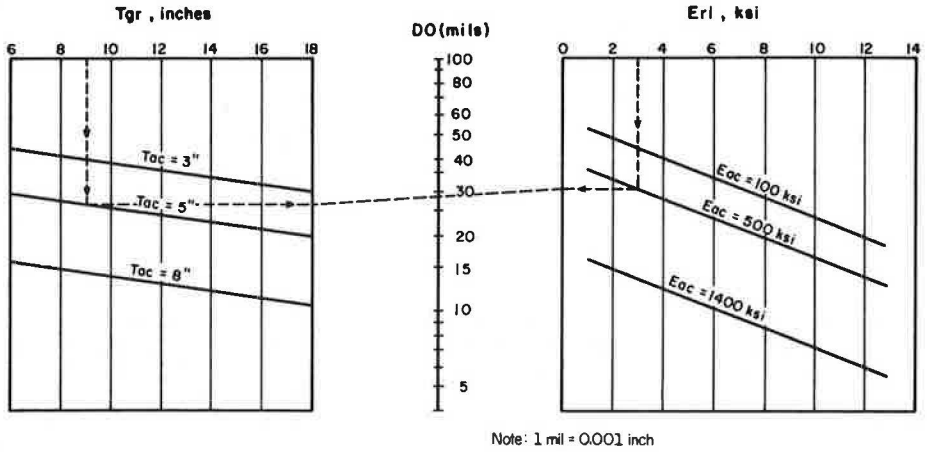

Figure 5. Nomograph based on area.

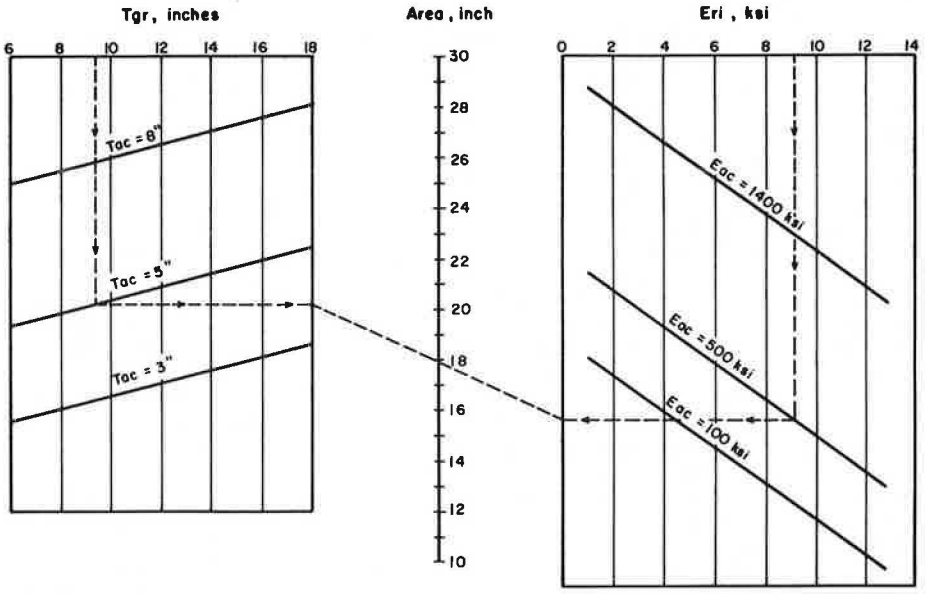

Table 5. Maximum and minimum values of ILLI-PAVE variables.

Variable	Maximum Value	Minimum Value
Eac (ksi), modulus of elasticity of AC layer	1400.0	100.0
Eri (ksi), subgrade modulus at intercept	12.34	1.0
Tac (in), thickness of AC layer	8.0	3.0
Tgr (in), thickness of granular base	18.0	6.0
log D0 (mils), deflection at R = 0	1.76	0.866
Area (in) = 6(1 + 2D1/D0 + 2D2/D0 + D3/D0)	29.64	13.29
F1 = (D0 - D2)/D1	2.08	0.27
F2 = (D1 - D3)/D2	2.00	0.31

Note: Valid cases, 60.

parameters, yield different stresses and strains at selected locations in the pavement structure. Note that the ILLI-PAVE radial stress at the bottom of the granular base layer is 3.8 psi (compression), and the corresponding BISAR stress is 14.1 psi (tension).

If it is accepted that the ILLI-PAVE solution is a more realistic simulation of the actual stresses and strains in the pavement structure, the equivalent linear elastic system, although adequate to simulate the deflection basin, is not adequate for computing certain stresses and strains. If it is further accepted that there are functional relationships between selected pavement response parameters

Table 6. Influence of granular material type on ILLI-PAVE deflection basins.

Tac (in)	Tgr (in)	Eac (ksi)	Eri (ksi)	D0 (G) (mils)	D0 (CS) (mils)	Change (%)	Area (G) (in)	Area (CS) (in)	Change (%)
Changing Eri									
1.5	6.0	500.0	12.34	35.03	30.40	15.2	12.31	13.05	-5.7
1.5	6.0	500.0	7.68	42.81	37.36	14.6	13.10	13.88	-5.6
1.5	6.0	500.0	3.02	58.06	50.62	14.7	14.22	15.22	-6.6
1.5	6.0	500.0	1.00	69.01	60.30	14.7	14.74	16.19	-9.0
Changing Tgr									
1.5	6.0	500.0	7.68	42.81	37.36	14.6	13.10	13.88	-5.6
1.5	9.0	500.0	7.68	40.05	33.62	19.1	13.51	14.50	-6.8
1.5	12.0	500.0	7.68	38.59	31.46	22.7	13.75	14.85	-7.4
Changing Eac									
1.5	6.0	100.0	12.34	40.35	33.83	19.3	11.33	12.30	-7.9
1.5	6.0	500.0	12.34	35.03	30.40	15.2	12.31	13.05	-5.7
1.5	6.0	1400.0	12.34	28.97	26.09	11.0	13.51	14.02	-3.6
Changing Tac									
0.0	6.0	0.0	7.68	61.86	51.96	19.1	10.90	11.92	-8.6
1.5	6.0	500.0	7.68	42.81	37.36	14.6	13.10	13.88	-5.6
3.0	6.0	500.0	7.68	28.46	26.24	8.5	16.13	16.57	-2.7

Notes: G = gravel; $Er = 6500\theta^{0.30}$ psi. CS = crushed stone; $Er = 9000\theta^{0.33}$ psi. Change (%) = (G - CS)/CS x 100.

(σ, ϵ, Δ) and pavement performance, the choice of a proper mechanistic model for pavement evaluation and design is of great significance.

Deflection Basins

By using the material properties and cross sections summarized in Table 2, ILLI-PAVE deflection-basin data were generated for a total of 144 combinations. A 9-kip load uniformly distributed over a circular area 12 in in diameter (the loading area of both RR and FWD) was used. A 9-kip load also corresponds to the rear-axle loading of an 18-kip single-axle design load.

Previous studies (19,20) have demonstrated the validity of the algorithm approach with the ILLI-PAVE model. By using multiple-regression techniques, deflection-basin predictive equations were developed as a function of the four ILLI-PAVE inputs (Eac, Eri, Tac, Tgr) for conventional flexible pavements. The crushed-stone material model in Table 2 was kept constant. Pavement cross-section combinations were grouped to yield optimum predictive equations. The solutions for one such group (AC layers between 3 and 8 in thick and granular bases between 6 and 18 in thick) are shown in Table 4. (Maximum and minimum values of the variables are given in Table 5.) Solutions similar to those in Table 4 were developed for a total of three groups.

The regression equations in Table 4 show that it is possible to predict ILLI-PAVE deflection-basin parameters with reasonable accuracy. The coefficients of determination (R^2) of the regression equations range from 90 to 95 percent (significant at the 1 percent level), and the coefficients of variation (CV) are less than 12 percent; most values are between 3 and 8 percent. The accuracy achieved is reasonable considering that

1. The deflection-basin predictive equations can be used in lieu of expensive and frequently unavailable computer runs,
2. The predictive equations are based on solutions of a complex and comprehensive stress-dependent pavement model, and
3. Predictive errors of the order of 10 percent are compatible with the variabilities commonly noted in field deflection-basin measurements.

To facilitate the use of ILLI-PAVE deflection-basin solutions, the regression equations were put in nomographical form. Figures 4 and 5 show the nomographs for centerplate deflection (D0) and deflection-basin area for the solutions in Table 4, respectively. Similar nomographs were developed for other conventional pavement groups, surface-treated full-depth asphalt, and stabilized pavements (8).

Influence of Granular Material Type

The advantage of using a constant material model for the granular base material (a typical dense-graded crushed stone) is obvious from the fact that the variables of the pavement model are reduced to four (Eac, Tac, Tgr, Eri). The effect of replacing the crushed stone by a gravel was determined for typical ILLI-PAVE solutions. The material model for the gravel is given in Table 2, and the results of the sensitivity analysis are summarized in Table 6. Results shown (D0 and area) are for a 9-kip load uniformly distributed over a 12-in-diameter circular area. Table 6 shows that

1. Gravel maximum deflections (D0) are consistently higher than crushed-stone deflections by 8.5-22 percent,
2. Gravel areas are lower than crushed-stone areas by 3-9 percent,
3. From the point of view of D0, the effect of granular material type is more pronounced for thicker granular layers, and
4. The influence of granular material type on D0 and area decreases for increasing AC stiffness and thickness.

From the point of view of pavement evaluation, neglecting the actual granular material type will result in minor errors in the backcalculated pavement parameters. This is not the case for stress and strain computations (14). The tensile strain at the bottom of the AC layer can be 40 percent higher for a gravel than for a crushed-stone base (14). Thus, although it is reasonable to use the algorithms in Table 4 for the interpretation of deflection-basin parameters for different granular material types (within limits), the prediction of additional pavement response parameters may require

Figure 6. Summary of laboratory data for Deland materials.

SECTION: DELAND

DATE OF SAMPLING: 6/19/1978
STATION SAMPLED : 10

TYPICAL CROSS SECTION

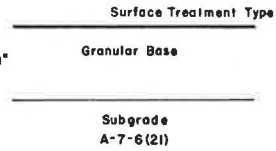

RESILIENT PROPERTIES OF SUBGRADE SOIL FROM SHELBY TUBE SAMPLES

Shelby Tube #	Depth (in)	γ_d (pcf)	ω (%)	S* (%)	q_u (psi)	E_R (ksi) σ_d = 6 psi	E_R (ksi) σ_d = 12 psi
1	0-4	100.5	18.8	73	-	5.0	-
2	1-5	93.2	25.6	84	-	3.3	2.9
1	4-8	94.0	26.2	87	15.6	-	-
2	6-10	91.8	27.0	85	10.5	-	-
1	12-16	90.1	24.6	75	-	4.1	-
2	12-16	90.2	27.0	82	-	3.0	2.9
2	21-25	89.5	27.1	81	8.9	-	-
1	28-32	101.9	18.6	75	-	4.0	-
2	27-31	-	20.6	-	-	5.1	3.9

*G_s = 2.75

SUBGRADE SOIL PROPERTIES (Upper 6 to 8 inches)

GRAIN SIZE			ATTERBERG LIMITS		CLASSIFICATION		G_s
%S	%Si	%C	LL	PL	TEXTURE	AASHTO	
3.3	62.2	34.5	45.3	24.3	SiCL	A-7-6(21)	2.75

NUCLEAR MOISTURE AND DENSITY

	γ_d(pcf)	ω (%)
Top of Base	134.8	5.3
Top of Subgrade	101.4	22.8

MOISTURE-DENSITY-CBR RELATIONSHIPS (AASHTO T-99)

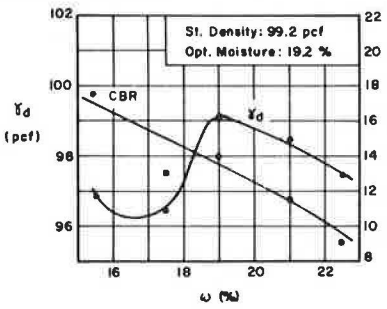

GRANULAR BASE MATERIAL

Washed Sieve Analysis

Sieve Size	1 1/4	5/8	3/8	No 4	No 10	No 50	No 200
% Passing	100	84	67	52	39	17	12

Limits of - No 40: NON-PLASTIC

Resilient Modulus of Recompacted Samples

Compaction Data: γ_d = 119.2 pcf; ω = 5.3 %

$$E_R = 3900\ \theta^{0.52} \quad (\theta = \sigma_1 + 2\sigma_3)$$

n= 7; r= 0.98

θ_{min}= 35 psi; $E_{R,min}$ = 25,000 psi

θ_{max}= 150 psi; $E_{R,max}$ = 57,000 psi

Figure 7. Evaluation nomograph for surface-treated pavements.

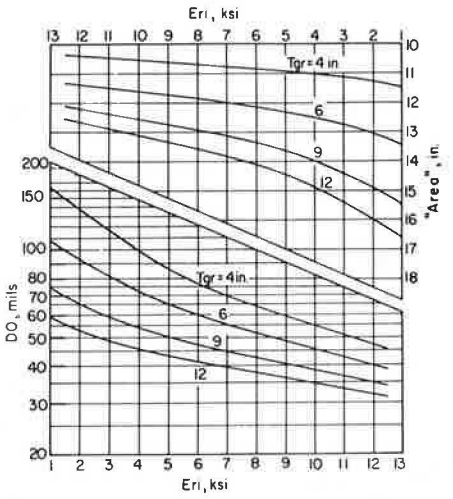

a closer identification of the granular material type (resilient behavior and shear strength).

ILLUSTRATION OF PROPOSED METHOD

Case 1: Deland Section

The Deland section is a surface treatment over a granular base layer 8 in thick. For evaluation purposes, Deland is a two-layer system with Tac and Eac equal to zero and Tgr equal to 8 in. RR deflections were measured at Deland on six different dates. On one testing date, one station was cored and sampled for laboratory testing (Figure 6).

Figure 7 shows a nomograph for the evaluation of surface-treated pavements by using the crushed-stone granular material model in Table 2. For given D0 and Tgr, the Eri value can be determined from Figure 7. The deflection-basin area can be used to check the validity of the solution.

Table 7 summarizes the step-by-step interpretation of measured RR deflections from the Deland section for the six testing dates. The table shows that (a) the backcalculated Eri value differs at different times of the year and ranges from 9 ksi (fall 1978) to 3 ksi (spring 1978) and (b) the ratios between the measured and predicted areas range from 0.93 to 1.18.

The laboratory-determined resilient modulus of the subgrade soil at a deviator stress of 6 psi (the stress level of Eri) ranges from 3 to 5.1 ksi (Figure 6). These values, which correspond to different samples obtained from two Shelby tubes that represent the top 30 in of the grade, compare reasonably with the backcalculated Eri value of 2.8 ksi (June 1978).

Figure 8 shows a nomograph for Deland deflection-basin interpretations that incorporates granular material models similar to the model determined at the laboratory (see Figure 6). Figure 8 shows an envelope of possible Deland solutions for two k-values in the $k\theta^n$-model and illustrates the influence of granular material type on surface-treated pavement deflections. The backcalculated Eri values and predicted areas by using the modified granular material models are shown in Table 8.

For practical purposes, it appears that the nomograph in Figure 7 (constant granular material model) is adequate for evaluating Eri for surface-treated pavements. The use of a particular granular material model, different from the one used in the nomograph, is justified only when there is disagreement between measured and predicted areas.

Case 2: Sherrard Section

The Sherrard section is a 4-in AC layer over a 14-in crushed-stone base. RR deflection basins were measured on five different dates (Table 9). In May 1979, one station was sampled for laboratory testing (Figure 9). Algorithms and nomographs for Sherrard deflection-basin interpretation are given in Table 4 and Figures 4 and 5, respectively.

Figure 10 illustrates the interpretation of Sherrard centerplate deflections (D0) and area for

the different testing dates. As noted, there are different combinations of Eac and Eri values that satisfy the D0 and area parameters individually on each testing date. The actual solution is the set of Eac and Eri values that satisfy D0 and area simultaneously.

The backcalculated parameters for different testing dates are summarized in Table 10, which shows that

1. The backcalculated Eri values range from 7.5 ksi to 13.1 ksi,
2. The backcalculated Eac values range from 40 ksi (surface pavement temperature of 98°F) to 1000 ksi (surface pavement temperature of 68°F), and
3. The measured deflection-basin shape factors (not used in the backcalculation process) and those predicted by using the backcalculated parameters and the algorithms in Table 4 are in good agreement.

While a direct comparison of backcalculated and

Table 7. ILLI-PAVE interpretation of Deland deflection basins.

Testing Date	(1) Mean RR Deflection (mils)	(2) Mean RR Area (in)	(3) Derived FWD Deflection (mils)	(4) Derived FWD Area (in)	(5) Derived D0	(6) Eri (ksi)	(7) Predicted Area (in)	(8) Measured Area / Predicted Area (in)
5/10/78	47.30	17.21	53.83	12.9	60.6	3.6	13.8	0.93
6/19/78[a]	51.25	17.43	58.61	13.2	65.9	2.8	13.9	0.95
10/24/78	33.76	18.12	37.45	14.0	42.1	9.0	12.5	1.12
4/19/79	50.40	19.65	57.58	15.8	64.8	3.2	14.0	1.13
9/7/79	41.42	19.52	46.72	15.6	52.6	5.0	13.3	1.18
10/17/79	40.50	19.10	45.61	15.1	51.3	5.2	13.4	1.13

Notes: (1) = Mean measured RR deflections at 8 kips, 15 hz.
(2) = Mean measured RR area at 8 kips, 15 Hz.
(3) = Predicted FWD deflections by using Table 1.
(4) = Predicted FWD area by using Table 1.
(5) = Column (3) times 1.125 for load adjustment in ILLI-PAVE solutions (9 kips).
(6) = Backcalculated Eri from nomograph in Figure 6.
(7) = Backcalculated area by using column (6) in nomograph in Figure 6.
(8) = Column (4) divided by column (7).

[a]Date of sampling for laboratory testing.

Figure 8. Influence of granular material type on Deland solutions.

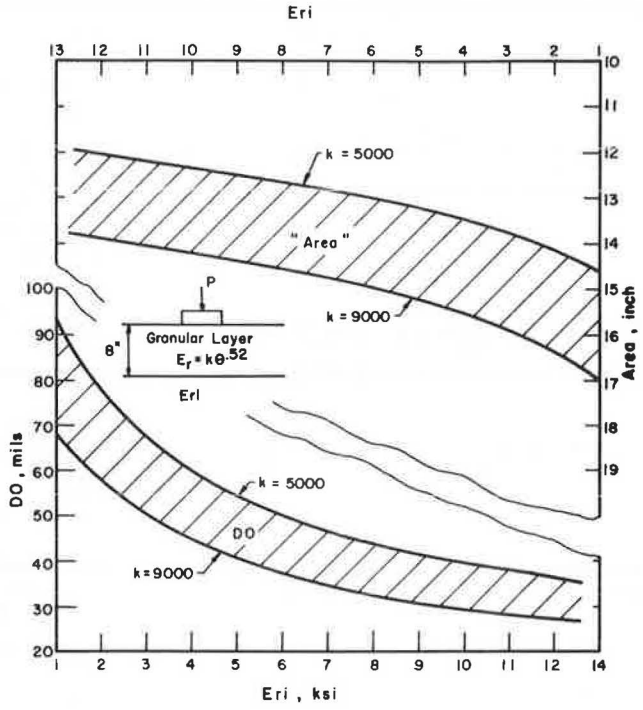

Table 8. Influence of granular material resilient response model on Deland backcalculated parameters.

Testing Date	Measured D0 (mils)	Backcalculated Eri[a] (ksi) k = 5000	Backcalculated Eri[a] (ksi) k = 9000	Area (in) Predicted for k = 5000	Area (in) Measured	Area (in) Predicted for k = 9000
5/10/78	60.6	4.0	1.7	13.4	12.9	16.5
6/19/78	65.9	3.2	1.2	13.7	13.2	16.8
10/24/78	42.1	8.8	4.6	12.5	14.0	15.4
4/19/79	64.8	3.3	1.3	13.6	15.8	16.7
9/7/79	52.6	5.5	2.7	13.2	15.6	16.0
10/17/79	51.3	5.7	2.9	13.1	15.1	15.9

Note: Granular base Tgr = 8 in, $Er = k\theta^{0.52}$.

[a]By using Figure 7.

laboratory-determined Eri values is not possible due to an RR malfunction on the sampling date, the backcalculated Eri values seem reasonable. Note in Figure 9 that the laboratory Eri (deviator stress of 6 psi) is variable. The average of four laboratory values is 5.4 ksi with a standard deviation of 1.07 ksi (coefficient of variation of 20 percent). Note in Table 9 that the coefficient of variation of D0 never exceeded 12.3 percent.

The resilient moduli of AC core samples determined in indirect tensile tests at 77°F ranged from 550 to 600 ksi (Figure 9). The backcalculated Eac values ranged from 40 to 1000 ksi and seem to follow a logical trend with surface pavement temperature and testing dates.

The heterogeneity of the subgrade soil is evident from the Shelby tube sample results (Figure 9). Depending on the location of the sample in the vertical soil profile (up to 24 in), it is not rare to find different moistures and densities and even different soil types corresponding to different horizons. From this perspective, the backcalculated Eri value is probably a better characterizing parameter of the subgrade soil mass.

Table 9. Summary of deflection-basin values for Sherrard section.

Testing Date	Pavement Temperature (°F)	Measurement	RR Values at 8 Kips and 15 Hz D0 (mils)	Area (in)	F1	F2	Predicted FWD Values at 8 Kips[a] D0 (mils)	Area (in)	F1	F2	D0 for ILLI-PAVE Interpretation[b] (mils)
5/16/78	67	Mean	20.4	21.5	0.82	0.84	21.3	18.0	1.27	1.35	24.0
		SD	2.5	0.7	0.07	0.07					
		CV (%)	12.3	3.4	8.1	8.9					
7/17/78	98	Mean	22.2	18.8	1.10	0.90	23.5	14.8	1.75	1.44	26.4
		SD	1.5	0.6	0.08	0.09					
		CV (%)	6.7	2.9	7.0	10.1					
11/9/78	68	Mean	13.2	21.7	0.81	0.75	12.6	18.2	1.25	1.21	14.2
		SD	0.5	0.8	0.08	0.09					
		CV (%)	4.0	3.9	10.1	12.1					
9/4/79	110	Mean	19.5	20.5	0.91	0.85	20.2	16.8	1.42	1.36	22.7
		SD	0.7	0.5	0.05	0.07					
		CV (%)	3.8	2.6	5.8	8.4					
10/17/79	83	Mean	16.2	22.3	0.74	0.80	16.2	18.9	1.13	1.29	18.2
		SD	0.6	0.70	0.06	0.07					
		CV (%)	3.8	3.2	8.0	8.6					

[a]By using regression equations in Table 1. [b]D0(FWD) x 1.125.

Figure 9. Summary of laboratory data for Sherrard materials.

SECTION: SHERRARD

DATE OF SAMPLING: 5/9/79
STATION SAMPLED: 3

TYPICAL CROSS SECTION

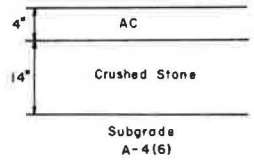

SUBGRADE SOIL PROPERTIES (Upper 6 to 8 inches)

GRAIN SIZE			ATTERBURG LIMITS		CLASSIFICATION		G_s
%S	%Si	%C	LL	PL	TEXTURE	AASHTO	
18.4	59.2	22.4	39.0	44.9	SiCL	A-4(6)	2.54

MOISTURE-DENSITY-CBR RELATIONSHIPS (AASHTO T-99)

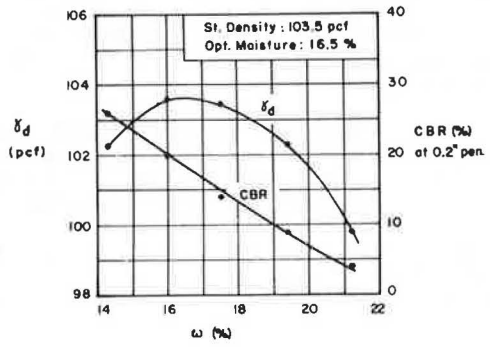

RESILIENT PROPERTIES OF SUBGRADE SOIL FROM SHELBY TUBE SAMPLES

Shelby Tube #	Depth (in.)	γ_d (pcf)	ω (%)	q_u* (psi)	E_s** (ksi)	E_R (ksi) σ_d = 6 psi	E_R (ksi) σ_d = 12 psi
1	0-4	--	20.0	--		--	--
2	1-5	--	19.1	--		5.9	5.0
1	4-8	--	18.9	24.3	0.49	--	--
2	5-9	--	29.2	34.8	0.70	--	--
1	8-12	--	25.3	--		6.2	5.0
2	9-13	--	28.1	--		3.8	2.8
1	12-15	--	25.9	30.4	0.81	--	--
2	13-17	--	28.1	10.9	0.29	--	--
1	16-20	--	25.7	--		--	--
1	20-24	--	28.4	--		5.5	3.6
2	17-21	--	26.5	--		--	--

*Rate of Loading 1.25%/min
**Secant E at 5% deformation - Rate of loading 1.25%/min

NUCLEAR MOISTURE AND DENSITY

	γ_d (pcf)	ω (%)
Top of Base	138.0	5.9
Top of Subgrade	104.1	19.5

CRUSHED STONE INDICATIVE PROPERTIES

GRAIN SIZE			ATTERBERG LIMITS		CLASSIFICATION		G_s
%S	%Si	%C	LL	PL	TEXTURE	AASHTO	
87.3	10.5	2.2	73.0	29.7	Sand	A-1-a(0)	2.71

AASHTO T-99 COMPACTION

Standard density: 143 pcf
Optimum Moisture: 6.0 %
CBR at ω = 5.5% (0.2" penetration): 140%

ASPHALT CONCRETE; Indirect Tensile Test

Resilient Modulus; Temperature: 77°F

Stress Level	# of Samples	Mean E_s ($x10^6$ psi)	St. Dev. ($x10^6$ psi)	C.V. (%)
15	7	.542	.122	23
30	7	.581	.118	20
45	7	.590	.115	19

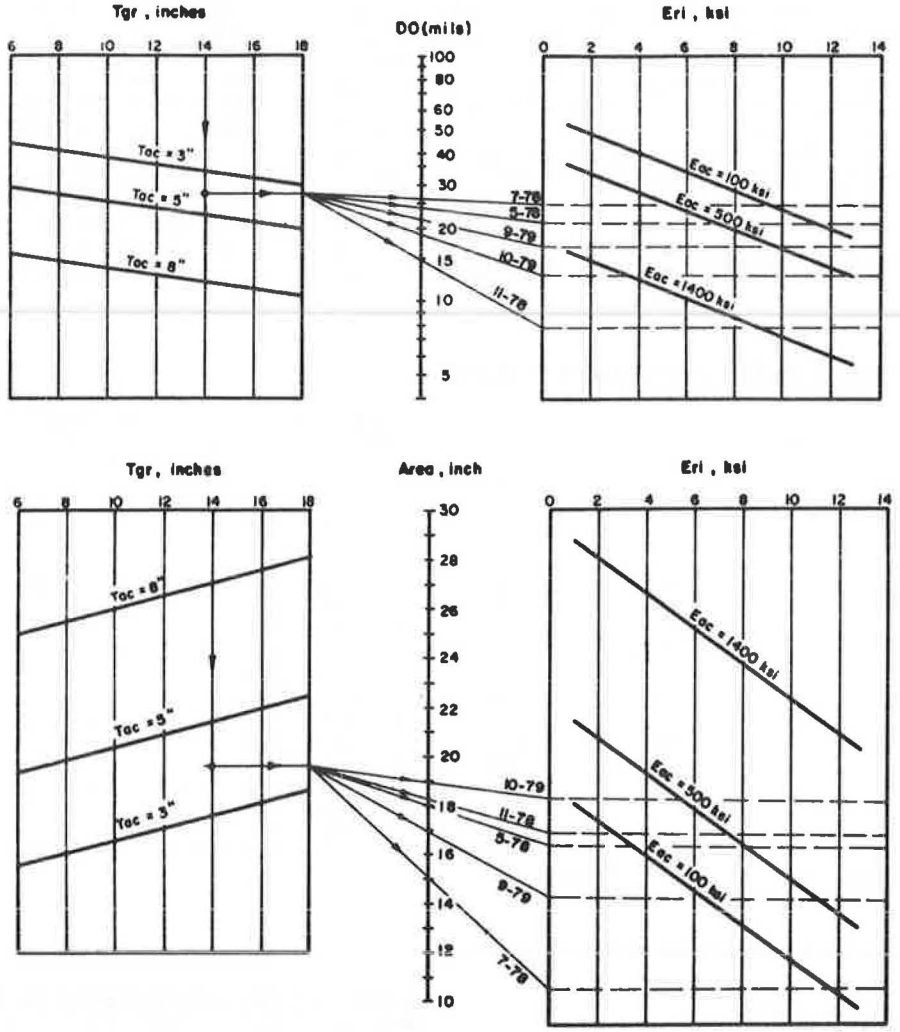

Figure 10. Illustration of Sherrard solutions for different testing dates.

Table 10. Backcalculated parameters for Sherrard section.

	Backcalculated Parameters[a]		F1		F2	
Testing Date	Eri (ksi)	Eac (ksi)	Measured[b]	Predicted[c]	Measured[b]	Predicted[c]
5/16/78	7.5	450	1.27	1.24	1.35	1.31
7/17/78	10.0	40	1.75	1.53	1.44	1.59
11/9/78	13.1	1000	1.25	1.23	1.21	1.33
9/4/79	10.2	430	1.42	1.36	1.36	1.44
10/17/79	9.3	820	1.13	1.18	1.29	1.23

[a] From Figure 8. [b] From Table 9. [c] By using the backcalculated parameters and equations in Table 4.

APPLICATIONS AND LIMITATIONS OF PROPOSED METHOD

The proposed flexible pavement evaluation method provides a rational yet simple procedure for backcalculating in situ material properties based on the interpretation of measured deflection basins. The mechanistic pavement model used (ILLI-PAVE) directly incorporates nonlinear material model characterizations.

Once the material properties have been backcalculated, the ILLI-PAVE model can be used to compute additional response parameters (stresses, strains, etc.) at selected locations in the pavement structure. These additional pavement response parameters are input to appropriate performance models (transfer functions), and proper action can then be recommended (overlay thickness design). The stress-state change caused by a change in the pavement cross section (overlay) is adequately accounted for by the stress-dependent material models. Algorithms and nomographs for ILLI-PAVE stress and strain computations for flexible pavements have been developed for "low-volume" pavements (14). Some of the limitations are as follows:

1. Current ILLI-PAVE calculations and NDT interpretation are only for stress-softening (cohesive) subgrades. It is an easy task, however, to develop algorithms for granular-type (stress-stiffening) subgrades.
2. The NDT algorithms presented are for a typical crushed-stone granular material ($E_r = 9000\theta^{0.33}$) of specified shear strength. Addi-

tional algorithms can be developed for other granular materials as desired.

3. ILLI-PAVE can accommodate only single-wheel loading conditions.

SUMMARY AND CONCLUSIONS

A method (ILLI-CALC) has been presented for the backcalculation of nonlinear resilient moduli from NDT data. ILLI-PAVE, a stress-dependent finite-element program, was used to develop algorithms and nomographs for the interpretation of selected measured deflection-basin parameters. The method was illustrated for two different flexible pavement sections. Method validation included comparison of measured and predicted deflection basins and comparison between backcalculated material properties and properties determined at the laboratory. Applications and limitations of the proposed method were discussed.

The algorithms and nomographs presented in this paper provide a fast, reliable, and economical means for interpreting measured deflection basins for structural flexible pavement evaluation. Expensive and frequently unavailable computer analyses can be replaced by these algorithms and nomographs.

Reasonable agreement was obtained between backcalculated material properties and properties determined at the laboratory. Agreement was also obtained between measured and predicted deflection basins. The backcalculated nonlinear moduli can be directly incorporated into the stress-dependent ILLI-PAVE model for overlay design.

ACKNOWLEDGMENT

This paper is based on the results of Project IHR-508: Load Response Characteristics of Flexible Pavements. Project IHR-508 is a cooperative study. Project planning and development were joint efforts of IDOT and the University of Illinois. IDOT (P. Dierstein, J.S. Dhamrait, and K.W. Wicks) assumed responsibility for all NDT testing. Various IDOT districts aided in the field sampling. The Soils Laboratory of the Bureau of Materials and Physical Research under the supervision of T.S. Lewis conducted routine soil tests. Specialized soils and materials tests were conducted by the University of Illinois. V.J. McDonald, Research Engineer at the University of Illinois, and the IDOT Instrumentation Development Group of the Physical Research Section were responsible for accelerometer data acquisition and data processing. Data reduction, structural modeling analyses, and the development of procedures for analyzing NDT data were activities conducted by the University of Illinois.

Special thanks are extended to the various IDOT districts, County Superintendents of Highways, and Township Commissioners who willingly agreed to provide test pavement sites and general aid.

IHR-508 was sponsored by the Illinois Department of Transportation (Division of Highways) and the Federal Highway Administration, U.S. Department of Transportation.

REFERENCES

1. H.J. Treybig, B.F. McCullough, F.N. Finn, R. McComb, and W.R. Hudson. Design of Asphalt Concrete Overlays Using Layer Theory. Proc., 4th International Conference on the Structural Design of Asphalt Pavements, Univ. of Michigan, Ann Arbor, 1977, pp. 589-621.
2. G.W. Sharpe, H.F. Southgate, and R.C. Dean. Pavement Evaluation by Using Dynamic Deflections. TRB, Transportation Research Record 700, 1979, pp. 34-45.
3. G. Wiseman, J. Uzan, M.S. Hoffman, I. Ishai, and M. Livneh. Simple Elastic Models for Pavement Evaluation Using Measured Surface Deflection Basins. Proc., 4th International Conference on the Structural Design of Asphalt Pavements, Univ. of Michigan, Ann Arbor, Vol. 2, 1977, pp. 416-426
4. R.C. Koole. Overlay Design Based on Falling Weight Deflectometer Measurements. TRB, Transportation Research Record 700, 1979, pp. 59-72.
5. W.D.O. Paterson and D.J. Van Vuuren. Diagnosis of Working Strains in a Pavement Using Deflection Profiles. Proc., Australian Road Research Board, Vol. 7, Part 6, 1974, pp. 128-144.
6. Resource International, Inc. Flexible Pavement Overlay Design Procedures. FHWA, Rept. FHWA-RD-79-99, 1980, Vols. 1 and 2.
7. A.J. Bush III. Nondestructive Testing for Light Aircraft Pavements: Phase II, Development of the Nondestructive Evaluation Methodology. Federal Aviation Administration, Final Rept. FAA-RD-80-9-II, 1980.
8. M.S. Hoffman and M.R. Thompson. Mechanistic Interpretation of Nondestructive Pavement Testing Deflections. Univ. of Illinois at Urbana-Champaign, Transportation Engineering Series 32, Illinois Cooperative Highway and Transportation Research Program Series 188, June 1981.
9. M.S. Hoffman and M.R. Thompson. Nondestructive Testing of Flexible Pavements--Field Testing Program Summary. Univ. of Illinois at Urbana-Champaign, Transportation Engineering Series 31, Illinois Cooperative Highway and Transportation Research Program Series 188, June 1981.
10. R.D. Barksdale and R.G. Hicks. Material Characterization and Layered Theory for Use in Fatigue Analysis. HRB, Special Rept. 140, 1973, pp. 20-48.
11. M.R. Thompson and Q.L. Robnett. Resilient Properties of Subgrade Soils. Univ. of Illinois, Urbana, Final Report, Civil Engineering Studies, Series 160, June 1976.
12. G.L. Dehlen. The Effect of Non-Linear Material Response on the Behavior of Pavements Subjected to Traffic Loads. Univ. of California, Berkeley, Ph.D. thesis, 1969.
13. J.J. Allen. The Effects of Non-Constant Lateral Pressures on the Resilient Response of Granular Materials. Univ. of Illinois, Urbana, Ph.D. thesis, May 1973.
14. J.L. Figueroa. Resilient Based Flexible Pavement Design Procedure for Secondary Roads. Univ. of Illinois, Urbana, Ph.D. thesis, 1979.
15. L. Raad and J.L. Figueroa. Load Response of Transportation Support Systems. Transportation Engineering Journal of ASCE, Vol. 106, No. TE1, Proc. Paper 15146, Jan. 1980, pp. 111-128.
16. L.P. Suddath and M.R. Thompson. Load-Deflection Behavior of Lime-Stabilized Layers. U.S. Army, Construction Engineering Research Laboratory, Champaign, IL, Tech. Rept. M-118, 1975.
17. M.L. Traylor. Nondestructive Testing of Flexible Pavements. Department of Civil Engineering, Univ. of Illinois, Urbana-Champaign, Ph.D. thesis, 1979.
18. BISAR (Bitumen Structures Analysis in Roads), Computer Program: User's Manual (abbreviated version). Koninklikje/Shell-Laboratorium, Amsterdam, Netherlands, July 1972.
19. J.L. Figueroa and M.R. Thompson. Simplified Structural Analyses of Flexible Pavements for Secondary Roads Based on ILLI-PAVE. TRB, Transportation Research Record 766, 1980, pp. 5-10.
20. M.R. Thompson and J.L. Figueroa. Mechanistic Thickness-Design Procedure for Soil-Lime Layers. TRB, Transportation Research Record 754, 1980, pp. 32-36.

Publication of this paper sponsored by Committee on Strength and Deformation Characteristics of Pavement Sections.

Effective Moduli and Stress Dependence of Pavement Materials as Measured in Some Heavy-Vehicle Simulator Tests

J.H. MAREE, N.J.W. VAN ZYL, AND C.R. FREEME

The purpose of this paper is to describe a method for determining field-effective moduli of pavement materials and to demonstrate stress dependence, especially of unbound materials. The effective moduli were determined from resilient deflections measured with a multidepth deflectometer at different depths within pavement structures. The results of measurements on four structures are reported. These structures cover light, unbound pavements to stronger inverted structures. The heavy-vehicle simulator was used to determine the moduli at different wheel loads and at various stages of trafficking. The ELSYM5 linear elastic-layered program together with the measured depth deflections were used in an iteration technique to determine effective moduli. The stress-stiffening behavior of granular materials and the stress-softening behavior of subgrade materials were clearly demonstrated. The constants in the models normally used to describe the behavior of these materials could be determined from the field results at various stages of trafficking and under changing moisture conditions. Laboratory and field values of stress-dependent moduli for granular materials were compared and a shift factor was determined. The effect of subgrade support on the effective moduli was also illustrated.

Linear elastic-layered mechanistic models for analyzing pavement structures are currently used to predict pavement behavior under assumed conditions of traffic loading and environment (1-3). In these models, each layer is characterized by a resilient modulus (E_R) and Poisson's ratio (ν_R). The accuracy of the input values influences the reliability of the answers, and considerable research has been done on material characterization (4). The resilient properties (E_R, ν_R) of pavement materials may be determined in the laboratory by various tests in which field stress and environmental conditions are simulated. The resilient moduli may also be determined from measured field deflections. For the latter technique, input moduli are selected so that the calculated deflection corresponds to the measured deflection (5,6). Such moduli are termed "effective" moduli.

In recent years, it has become evident that it is difficult or even impossible to predict the behavior of road pavements solely from laboratory test data. Accordingly, there has been considerable interest worldwide in the development of methods for the accelerated testing of full-scale road pavements. Equipment for accomplishing this has been developed in such diverse countries as the United States, Denmark, Australia, Germany, Japan, and South Africa. The South African contribution, the heavy-vehicle simulator (HVS) (7) developed by the National Institute for Transport and Road Research (NITRR) of the Council for Scientific and Industrial Research (CSIR), is perhaps the most versatile of the various test rigs developed to date because it is the only equipment that is mobile and that can be used on normally constructed road pavements. Material properties to be used as inputs to mechanistic models can be determined from actual field measurements. The purpose of this paper is to describe effective field moduli and the stress dependence of some pavement materials (granular base layers and typical subgrades) as measured in HVS tests. It is beyond the scope of this paper to describe the performance of the pavement structures tested. It will be shown that stress dependence could be important when pavement structures are analyzed under varying wheel loads.

DEPTH DEFLECTION MEASUREMENTS

The resilient deflection on the road surface has been used as an input parameter for many evaluation models (8). The shape of the deflection bowl together with the peak deflection can be used to determine the properties of the pavement layers. At NITRR, a technique has been developed for determining layer properties by measuring the resilient deflections at various depths within the pavement structure. The device developed for this purpose is called the multidepth deflectometer (MDD) (9). Three MDDs are normally installed in an existing pavement structure to be tested by the HVS. A special technique has been developed to drill a hole 38 mm in diameter to a depth of 2 m (9) without major disturbances to pavement layers. The hole is lined with a thin rubber lining, which does not influence deflection measurements but prevents moisture and loose material from damaging the transducers. At the end of an HVS test, the structure is opened and the MDD holes are inspected for any abnormalities. Measurements of resilient deflections with depth are taken throughout the test under various wheel loads and these yield a very good record of the change in structural response of the pavement. The MDD uses a reference point at a depth of 2 m, and up to six modules can be installed in one hole (Figure 1). The MDD modules are normally placed at the interfaces of the layers. Figure 2 shows typical depth-deflection curves measured by an MDD. The surface deflection is usually also independently measured with a deflection beam and correlates very well with the deflection measured by the MDD module just below the surface cap. The deflection beam has also been used to verify that the MDD hole does not significantly influence the resilient deflection of the pavement structure.

DETERMINATION OF EFFECTIVE RESILIENT MODULI

The surface and depth deflections discussed in the previous section can be used to determine the effective elastic moduli of the various pavement layers by using linear elastic theory (5,6) and (according to G. Ahlborn of the University of California at Berkeley) a linear elastic-layered program such as ELSYM5. An iteration technique is normally followed. The initial values of the various moduli are estimated and depth deflection curves similar to those given in Figure 2 are calculated by the program. The calculated values are compared with the measured ones and the moduli are adjusted until measured and calculated values agree. With experience, this iteration technique converges within a few iterations. Initially, a modulus is assigned to the subgrade so that the calculated deflection agrees with the measured deflection on the subgrade. Thereafter, the moduli of the other pavement layers are determined. The slope of the depth deflection curve at any point is an indicator of the modulus of the material at that depth. When the measured slope is steeper than the calculated one, the modulus of the material has to be increased, and vice versa.

Figure 1. MDD installed in pavement structure.

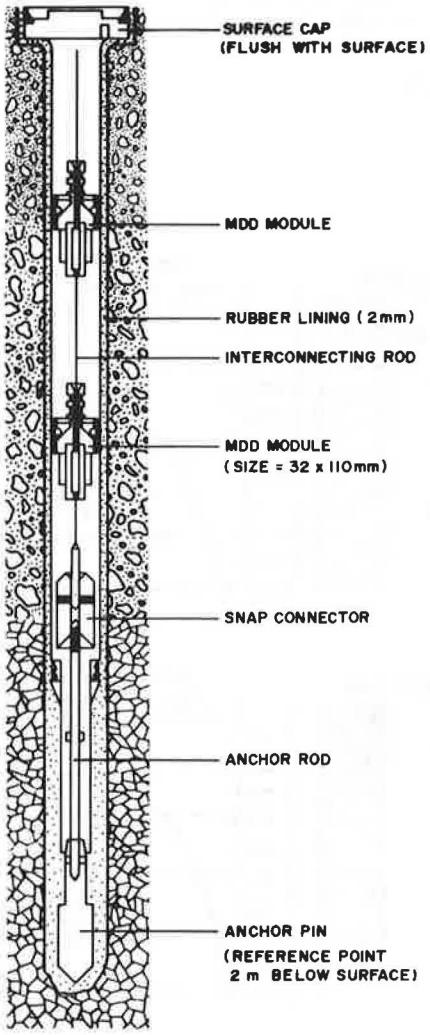

FIGURE NOT TO SCALE, ONLY TWO MODULES SHOWN, UP TO SIX MODULES CAN BE INSTALLED, HOLE DIAMETER = 38 mm

(The depth below the surface will also influence the value of the modulus.) The elastic modulus calculated in this way is called the effective modulus (5).

Figure 2 shows typical deflection curves fitted through the mean MDD deflections under a 40-kN and a 70-kN dual wheel. The dual wheel of the HVS was approximated by two circular loaded areas with contact stress equal to the measured contact stress in the field. This approximation is reasonable at low wheel loads but less accurate at high loads, because the actual contact area is of a long rectangular shape at high loads.

By determining the effective moduli of the different layers at various stages of trafficking, the behavior of the different layers can be monitored throughout the test. The stress dependence of the various pavement materials can also be established by measuring deflections at different wheel loads. These measurements can be used to determine the nonlinear effective moduli. In HVS tests, the wheel load normally varies between 20 and 100 kN. The deflections are therefore measured under real or overloaded road conditions (equivalent axle loads of 40-200 kN).

Figure 2. Measured and calculated depth deflections (Road P157/1).

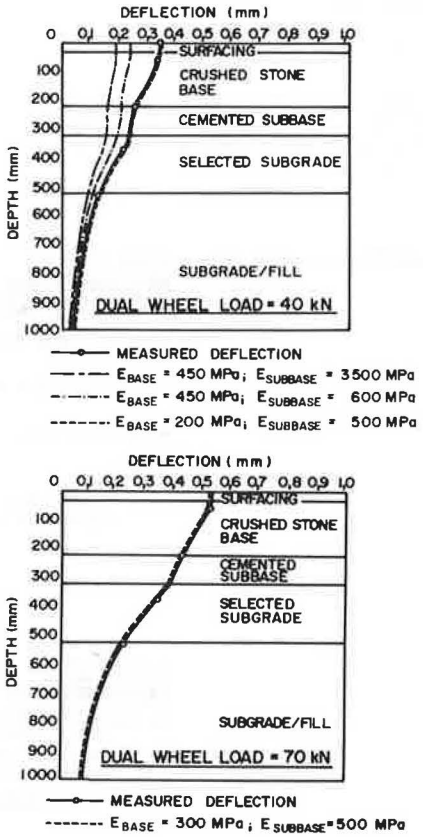

The moduli determined from the depth deflections can be used as input values for further detailed mechanistic analyses of the structures tested. The confidence in the calculated stresses and strains will be higher because the models have been calibrated according to actual measured depth deflections. It is also possible to draw meaningful conclusions from the values of the determined moduli. For example, a cement-stabilized subbase layer may exhibit an initial effective modulus higher than 3000 MPa (3). However, in the postcracked phase, the modulus may drop below 500 MPa. The state of the layer can therefore be determined from the measured resilient depth deflections.

STRUCTURES TESTED BY HVS AND TYPICAL DEPTH DEFLECTION CURVES

Four typical pavement structures will be considered. Two structures represent the light unbound pavements that were used for two-lane rural roads in the 1950s. The other two structures have crushed-stone bases with cemented subbases (so-called inverted designs) and are currently used for the more important routes and for some freeways in the Transvaal Province. Figures 3 and 4 show the structures as well as their typical depth deflection curves. The material qualities are indicated by the material codes currently used in national pavement design documents (10,11). The key to these codes is given in Figure 5. As expected, the light pavements (Figure 3) show much greater deflections than the heavy pavements (Figure 4).

Only the initial depth deflections (at the start of the HVS test) could be measured on the light pavement structures, because the MDD holes collapsed

during the tests. On the heavy structures, the deflections could be monitored throughout.

FIELD EFFECTIVE MODULI

The effective elastic moduli determined from the measured resilient depth deflections are shown in Tables 1 and 2. The material codes for the different pavement layers are also given.

Granular materials, showing stress-stiffening behavior, are most often described by a model that gives the modulus as a function of the first stress invariant:

$$M_R = K_1 \theta^{K_2} \quad (1)$$

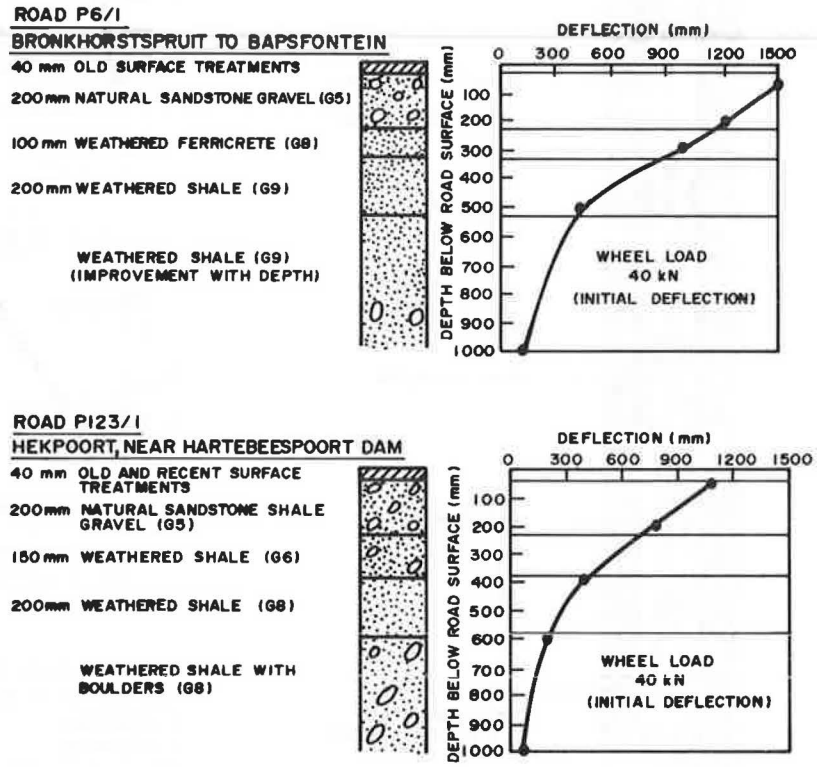

Figure 3. Light pavements and their depth deflection curves.

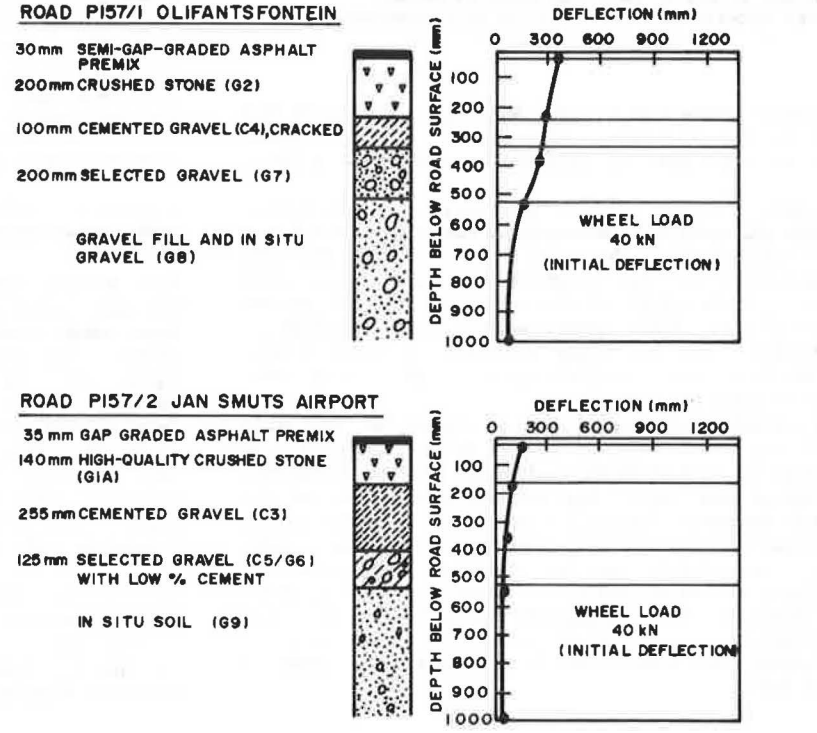

Figure 4. Heavy pavements and their depth deflection curves.

Figure 5. Key to material codes and symbols.

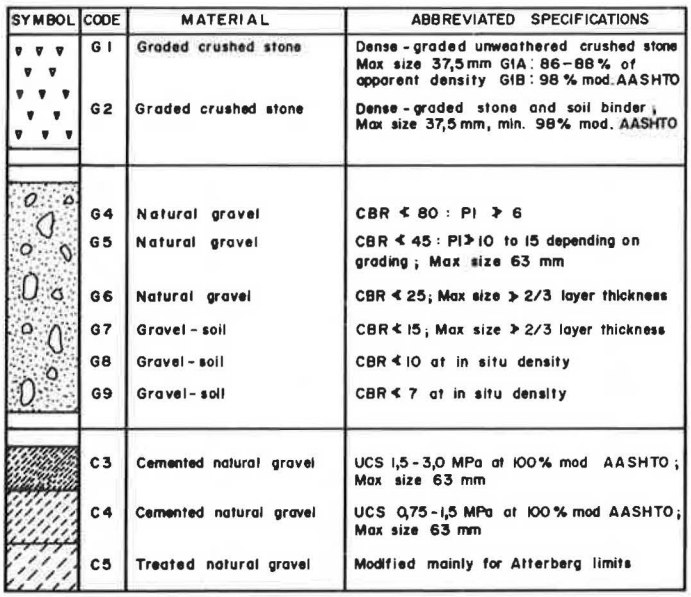

SYMBOL	CODE	MATERIAL	ABBREVIATED SPECIFICATIONS
	G1	Graded crushed stone	Dense - graded unweathered crushed stone Max size 37,5 mm G1A: 86-88% of apparent density G1B: 98% mod. AASHTO
	G2	Graded crushed stone	Dense - graded stone and soil binder; Max size 37,5 mm, min. 98% mod. AASHTO
	G4	Natural gravel	CBR ≤ 80 : PI ≥ 6
	G5	Natural gravel	CBR ≤ 45 : PI ≥ 10 to 15 depending on grading; Max size 63 mm
	G6	Natural gravel	CBR ≤ 25; Max size ≥ 2/3 layer thickness
	G7	Gravel - soil	CBR ≤ 15; Max size ≥ 2/3 layer thickness
	G8	Gravel - soil	CBR ≤ 10 at in situ density
	G9	Gravel - soil	CBR ≤ 7 at in situ density
	C3	Cemented natural gravel	UCS 1,5 - 3,0 MPa at 100% mod AASHTO; Max size 63 mm
	C4	Cemented natural gravel	UCS 0,75 - 1,5 MPa at 100% mod AASHTO; Max size 63 mm
	C5	Treated natural gravel	Modified mainly for Atterberg limits

Table 1. Effective elastic moduli and stress states: Roads P6/1 and P123/1 (light structures).

Dual-Wheel Load (kN)	Effective Elastic Moduli				Calculated Stress States	
	E_{Base} (MPa)	E_{SB} (MPa)	E_{SL} (MPa)	E_{SG} (MPa)	θ_{Base} (kPa)	$(\sigma_1 - \sigma_3)_{SG}$ (kPa)
Road P6/1[a]						
20	60	25	30	70	87	22
40	60	20	25	65	148	45
60	70	20	20	60	183	58
80	85	45	15	55	272	71
100	110	60	15	50	321	80
Material code	G5	G8	G9	G9		
Road P123/1[b]						
20	40	50	60	110	131	23
40	50	50	50	100	238	44
60	55	65	80	90	364	61
80	70	60	60	70	434	75
100	80	60	70	70	519	91
Material code	G5	G6	G8	G8		

Note: SB = subbase; SL = selected layer; SG = subgrade.

[a] Surfacing (multiple old brittle surface treatments) was assumed to have a modulus of 1000 MPa for all wheel loads.
[b] Surfacing (multiple old and recent flexible surface treatments) was assumed to have a modulus of 500 MPa for all wheel loads.

where

$\theta = \sigma_1 + \sigma_2 + \sigma_3$,
$\sigma_1, \sigma_2, \sigma_3$ = principal stresses, and
K_1, K_2 = laboratory-derived regression constants.

By calculating the stress states in the crushed-stone layer, the average sum of the principal stresses can be determined. This average can be compared with the effective elastic modulus in order to determine the constants in the above equation. The principal stresses were calculated at three depths within the crushed-stone layer, which corresponded to the top, middle, and lower parts of the layer. These stress states were determined at the center of the dual-wheel load and under one of the wheels of the dual-wheel load. In Tables 1 and 2, the average calculated stress state (θ) in the base has been included for each wheel load. The actual value of θ is dependent on the wheel load, the pavement structure, and the way in which θ is calculated. The support provided by the subbase and subgrade clearly influences the value of θ (compare Table 1, top, with Table 2, bottom). HVS testing and experience have shown that, of the four structures tested, the structure of Road P157/2 (Figure 4, bottom) can carry the largest number of standard axles. This structure, which has a rather thick cemented subbase, shows the highest values of θ.

Cohesive materials showing stress-softening behavior can be described by a model that gives the modulus as a function of the deviator or vertical stress:

$$M_R = K_1 + K_3(K_2 - \sigma_d) \quad \text{if } K_2 > \sigma_d \tag{2}$$

or

$$M_R = K_1 + K_4(-K_2 + \sigma_d) \quad \text{if } K_2 < \sigma_d \tag{3}$$

where σ_d is the difference in principal stresses $(\sigma_1 - \sigma_3)$ and K_1, K_2, K_3, and K_4 are material constants (K_3 and K_4 describe the rate of change of M_R with σ_d). The maximum calculated deviator stress (under the center of the dual-wheel load) has been included in Tables 1 and 2.

The effective moduli of the subbases and selected subgrade layers have also been determined; they,

Table 2. Effective elastic moduli and stress states: Roads P157/1 and P157/2.

Repetitions of 70- and 100-kN Wheel Load	Dual-Wheel Load (kN)	Effective Elastic Moduli				Calculated Stress States	
		E_{Base} (MPa)	E_{SB} (MPa)	E_{SL} (MPa)	E_{SG} (MPa)	θ_{Base} (kPa)	$(\sigma_1 - \sigma_3)_{SG}$ (kPa)
Road P157/1[a]							
10	40	200	500	80	160	264	29
	70	300	500	80	160	403	46
1×10^6	40	162	230	47	119	266	39
	70	290	350	50	115	366	56
1.75×10^6	40	178	365	37	105	247	33
	70	225	460	45	105	411	55
1.94×10^6	40	195	180	51	109	210	27
	70	235	235	57	103	353	48
	100	263	260	71	110	490	61
Material code		G2	C4	G7	G8		
Road P157/2[b]							
10	40	335	1100	750	230	370	32
	70	520	1400	600	140	618	40
	100	725	1650	500	90	879	41
0.48×10^6	40	250	900	500	150	370	30
	70	420	1400	350	115	625	39
	100	600	1300	500	87	848	44
1.42×10^6	40	260	1100	750	115	379	23
	70	380	950	400	75	592	34
	100	425	1100	500	72	846	43
1.70×10^6	40	190	900	95	90	371	24
	70	230	1250	65	70	630	31
	100	275	1500	45	55	884	33
Material code		G1A	C3	C5/G6	G9		

[a]Semi-gap-graded asphalt premix (30 mm) was assumed to have a modulus of 4000 MPa.
[b]Gap-graded asphalt premix (35 mm) was assumed to have a modulus of 3000 MPa.

too, show stress-dependent behavior. It is of special interest to note that the cemented subbase in Road P157/1 (Table 2, top) has very low effective moduli and that the values are eventually similar to the granular base modulus. At 1.94×10^6 repetitions, the cemented subbase acted like a stress-dependent granular layer. At the end of the test when the subbase was recovered, it was found to be fully cracked into small pieces, which confirmed the moduli measured. The cemented subbase on Road P157/2 (Table 2, bottom) also showed stress-stiffening behavior, although its effective modulus was much higher. At the end of the test this layer was not fully cracked.

The selected layers of Roads P6/1 and P157/2 showed stress-softening behavior. No clear trends were established for the selected layer of Road P123/1, and the selected layer of Road P157/1 showed stress-stiffening behavior.

SUMMARY OF STRESS-STIFFENING BEHAVIOR OF GRANULAR BASE LAYERS

Figures 6-8 show the effective resilient moduli of the granular base layers as functions of either the dual-wheel load or the sum of the calculated principal stresses. These figures show the pronounced stress dependence of granular base layers.

The values of the effective moduli of the low-quality bases for the light structures are very low. For both pavements, there seems to be a lower limit of 40-60 MPa and a marked increase in modulus for wheel loads above 60 kN. It is interesting to note that the actual value of the modulus of the base may be lower than that of the subgrade (refer to Table 1). The ratio of the base modulus to the underlying subbase modulus ranges from 3.5 to 1.8 for Road P6/1 and from 1.3 to 0.8 for Road P123/1. This ratio therefore changes from structure to structure and also changes with wheel load.

The base and subbase layers in the light structures eventually showed spectacular shear failures in the HVS tests, which indicated that the shear stresses and strains in these layers were high and that near-failure conditions existed at the time of the measurements. The low moduli can therefore also be attributed to the unfavorable stress states.

The heavy structures, with better-quality bases (Roads P157/1 and P157/2), show typical stress-dependent behavior (Figures 7 and 8). Very neat straight-line relationships on log-log scales were determined. In these tests the influence of repetitions and environmental changes was also investigated. The value of the modulus decreased throughout the test, although no apparent physical changes (e.g., degradation) took place. A gradual decrease in soil suction due to the repeated loading of the HVS could explain this behavior. In the final stages, when the bases became wet, the modulus showed a further decrease and also became less stress dependent (the slope of the line decreased). In the test on Road P157/2 (Figure 8) the moisture caused a greater change in the modulus than the repetitions of the wheel load.

Figures 7 and 8 also show the moduli as measured in repeated-load triaxial tests done at constant confining pressures. The laboratory tests completely overestimated the actual value of the modulus. The slope of the line (K_2) determined in the laboratory was reasonably close to the field-determined slope, but the position of the line (abscissa K_1) was much lower in the field. The difference between laboratory and field moduli could be attributed to a difference in stress states, a Poisson's-ratio effect, or a difference in soil suction. The laboratory constants were determined in constant confining pressure triaxial tests, which do not accurately simulate true field conditions. The way in which θ was calculated (see previous section) may overestimate the value of θ, which could also lead to the observed difference. A constant value of 0.35 was assumed for Poisson's ratio; this ratio is actually also stress dependent and could also change during the test. Laboratory

tests have shown (4) that the soil suction in the unsoaked condition primarily influences K_1. The soil suction in the laboratory may have been higher than the suction in the field during the dry part of the HVS test, which led to the overestimation of the modulus in the laboratory.

Tests with the road rater (8) that used low dynamic loads (2-7 kN) have yielded different results in that the laboratory moduli appeared to be too low. According to this study (8), the field modulus would decrease with increase in shear strain. It appears that at higher wheel loads (high shear strain) the laboratory measurements overestimate field moduli, although no clear trends could be established from Figures 7 and 8. Table 3 shows the field-determined constants in $M_R = K_1\theta^{K_2}$. It can be concluded that the trends measured in the laboratory will probably hold in the field but that a shift factor of 0.3-0.5 is necessary to predict field moduli. The laboratory modulus should be multiplied by this shift factor. In the dry condition, K_2 is of the order of 0.9-1.0 for both pavements and K_1 of the order of 0.5-2.0. In the wet state, K_2 dropped to a value of 0.3-0.4 and K_1 increased to a value of 15.0-27.0.

The ratio of the base modulus to the subbase modulus ranges from 0.4 to 1.1 for Road P157/1 and from 0.2 to 0.5 for Road P157/2. Apparently, the ratio is always less than 1.0 for structures with cemented subbases unless the subbase is completely cracked. For Road P157/2 the ratio is always less than 0.5.

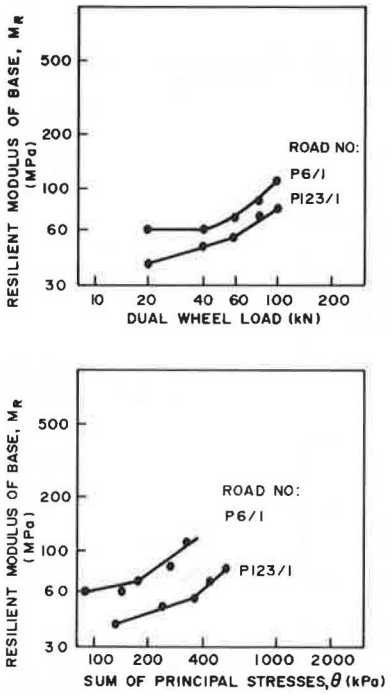

Figure 6. Stress dependence of granular-base resilient modulus as measured in HVS test on Roads P6/1 and P123/1.

SUMMARY OF STRESS-SOFTENING BEHAVIOR OF SUBGRADE MATERIAL

Figures 9-11 show the effective resilient moduli of the subgrades as functions of either the dual-wheel load or the calculated deviator stress on the subgrade. In most cases there is a decrease in the modulus as the wheel load or the deviator stress on the subgrade increases.

The subgrades of the light structures are clearly stress dependent and stress softening, but the actual change in the modulus is not very large (Figure 9). For Road P6/1 a change in wheel load from 20 kN to 100 kN causes a change in subgrade modulus of less than 30 percent. For Road P123/1 the change is less than 40 percent. These changes are smaller than the changes in the base modulus. However, because the subgrade is a much thicker layer, the effect of these changes on the total deflection is probably just as pronounced as the effect of the stress stiffening of the base. The cohesive material model [M_R = f (deviator stress)] has been applied to slightly idealized lines put through the calculated values in Figure 9. The regression constants thus determined by using Equa-

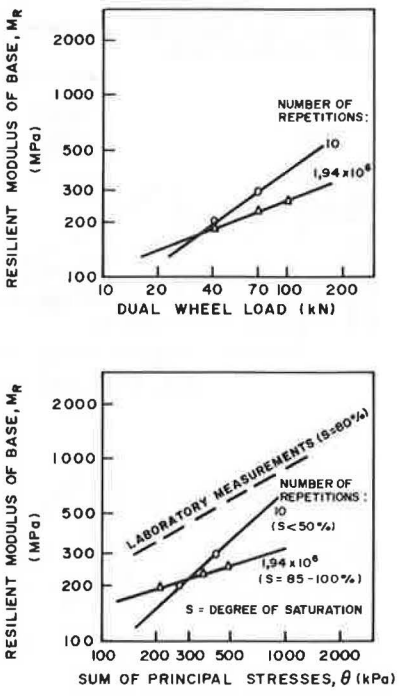

Figure 7. Stress dependence of granular-base resilient modulus as measured in HVS test on Road P157/1.

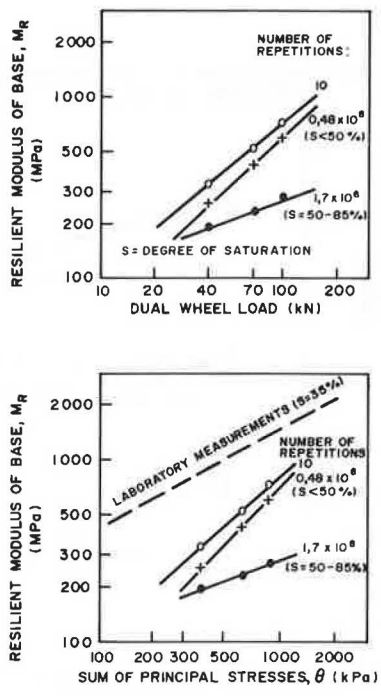

Figure 8. Stress dependence of granular-base resilient modulus as measured in HVS test on Road P157/2.

tion 2 or 3 are shown below (M_R in MPa; σ_d in kPa):

	Regression Constants			
Road	K1 (MPa)	K2 (kPa)	K3	K4
P6/1	65	45	+0.24	-0.43
P123/1	70	75	+0.94	0

The subgrade of Road P6/1 became more stress dependent at deviator stresses above K_2. Normally the slope K_4 is less than the slope K_3, as in the case of Road P123/1. The K_1-values are very similar for the two roads.

The subgrade for Road P157/1 showed very little stress dependence (Figure 10). At high loads this subgrade even exhibited slightly stress-stiffening behavior, but this could be attributed to the granular nature of the subgrade at this site. The value of the modulus changed from 160 MPa to 103 MPa during the test. Table 4 shows the regression constants determined at the end of the test. The effective modulus of the subgrade for Road P157/2 showed typical stress-softening behavior when compared with the dual-wheel load (Figure 11). However, the calculated deviator stress on the subgrade in this complex pavement structure does not necessarily reflect the wheel load, and when the modulus is compared to the calculated deviator stress, a somewhat different relationship emerges (Figure 11). The regression constants are shown in Table 4. As in the case of Road P157/1, the modulus (and K_1) decreased during the test. The value of K_1 dropped from 140 MPa initially to 55 MPa at the end. The moisture conditions play an important role and may override the stress conditions. Toward the end of the test and under wet conditions, the subgrade behaved in the typical stress-softening way. The regression constants determined at 1.42×10^6 repetitions could be typical wet values.

Table 3. Field-determined constants in $M_R = K_1\theta^{K_2}$.

		Regression Constants[a]	
Road	No. of Repetitions	K_1	K_2
P157/1	10	1.1	0.93
	1 940 000 (wet)	27.0	0.32
P157/2	10	1.8	0.89
	480 000	0.6	1.02
	1 700 000 (wet)	15.0	0.43

[a] M_R in MPa, θ in kPa.

Figure 9. Stress dependence of subgrade resilient modulus as measured in HVS test on Roads P6/1 and P123/1.

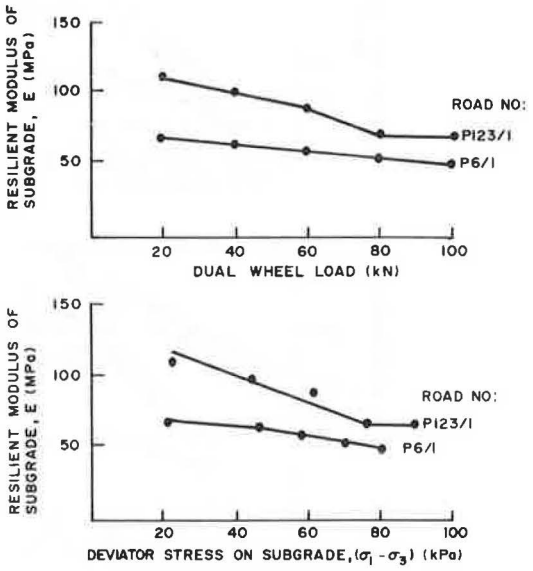

DISCUSSION OF RESULTS

The South African mechanistic design method (3) includes tabulated input moduli of typical road pavement materials. These values correspond to the standard legal dual-wheel load of 40 kN. The previous paragraphs have shown that effective moduli are very dependent on the applied wheel loads. The

Figure 10. Stress dependence of subgrade resilient modulus as measured in HVS test on Road P157/1.

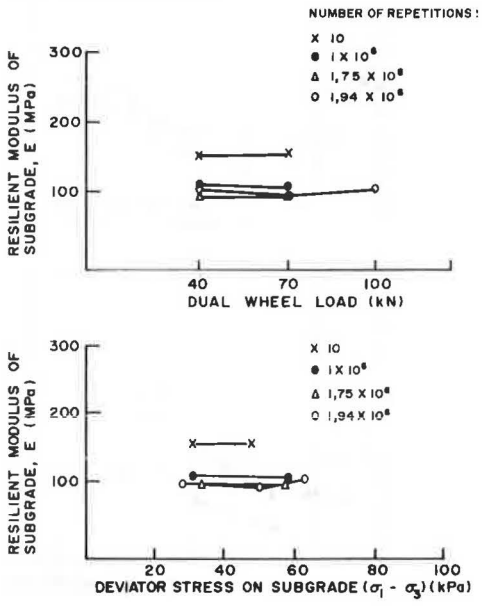

Figure 11. Stress dependence of subgrade resilient modulus as measured in HVS test on Road P157/2.

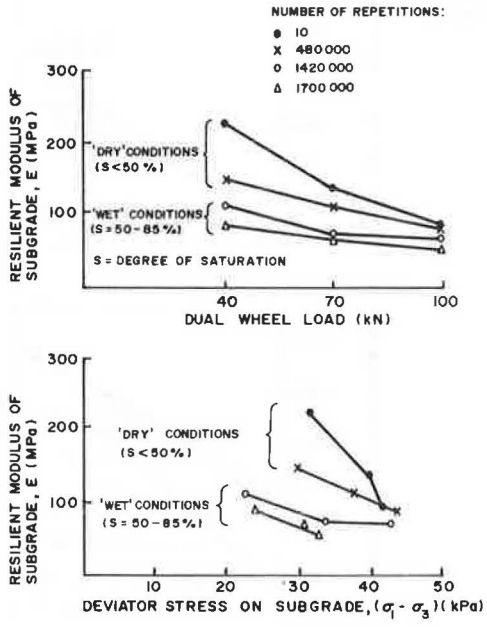

Table 4. Field-determined constants in Equation 2 or 3 for stress-dependent subgrades in Roads P157/1 and P157/2.

Road	Moisture Conditions in Subgrade	No. of Repetitions	Regression Constants[a]			
			K_1 (MPa)	K_2 (kPa)	K_3	K_4
P157/1	Normal	10	160	-	-	-
	In situ	1.94×10^6	103	48	+0.21	+0.60
P157/2	Normal	10	140	40	+11.2	-43.8
	In situ	0.48×10^6	115	39	+4.0	-5.2
	Wet	1.42×10^6	75	34	+3.5	-0.29
		1.7×10^6	55	34	-	-

[a] M_R in MPa; σ_d in kPa.

mechanistic design method (3) is often applied to other situations such as the design of airport pavements or the design of railway track and foundation structures. Enough evidence has been obtained to suggest that the mechanistic method should be applied with care and that the values of the input moduli should be adjusted according to the stress conditions.

The field data of the stress dependence of unbound pavement materials once again confirm the importance of a nonlinear approach to the analysis of pavement structures containing such materials.

SUMMARY AND CONCLUSIONS

A method for determining the effective moduli of different pavement layers has been presented. The method was found to be practical and of great value in interpreting the state of the pavement layers. The multidepth deflectometer functioned well and provided reliable measurements of deflection with depth.

The effective moduli of granular layers, cemented subbase layers, and also subgrade soils have been determined for materials from very light old structures as well as materials from structures currently used by the Transvaal Provincial Administration. On the heavy structures, the effective moduli could be determined throughout an HVS test, and a very good record of the change in structural response of the pavement could be obtained.

The stress-dependent behavior of the different pavement materials has been demonstrated very clearly from field data. Granular materials behave in a stress-stiffening way, and most subgrade soils show stress-softening behavior. The stress-dependent models for granular and cohesive materials could be applied to the effective moduli, especially to the moduli of the unbound crushed-stone bases. The regression constants could be determined for different moisture conditions and at various stages of trafficking.

Environmental factors such as moisture have an important influence and can change the basic behavior of the material. The moisture conditions could be as important as the stress states. The regression constants in the stress-dependent models are very dependent on the moisture conditions.

Laboratory constant confining-pressure triaxial tests overestimate the modulus of the crushed-stone bases, and a shift factor of 0.3-0.5 needs to be applied. Although there is a difference in the actual values, the trends apparent in the laboratory were also apparent in the field. The deviator stresses (or the shear strains) in the field could contribute toward the observed differences. The actual wheel load could therefore influence the shift factor.

The modulus of the base depends on the modulus of the underlying subbase, and for the light structures with unbound subbases, ratios of 0.8-3.5 have been determined. This ratio depends on the pavement structure and also on the wheel load. In pavements with cemented subbases, the ratio is always less than 1.0 unless the cemented subbase is completely cracked. In some cases the ratio may be as low as 0.2. The stress states in the base layers of these inverted designs are more favorable (higher values of θ) and the resulting effective moduli are higher.

The stress dependence of the subgrade moduli is generally less than that of the base, but the effect on the total deflection is probably just as pronounced. Not all subgrades exhibit stress-softening behavior.

Where the mechanistic design method is applied to other pavement structures such as airport pavements, the effective resilient moduli should be adjusted to correspond to the stress conditions.

ACKNOWLEDGMENT

The HVS project in the Transvaal is sponsored by the Transvaal Roads Department. We would like to thank the Director of Roads of the Transvaal as well as G.P. Marais and E.G. Kleyn for their cooperation, the latter especially for many fruitful discussions. We also thank the Director of the National Institute for Transport and Road Research for his permission to publish this paper.

REFERENCES

1. R.N. Walker, W.D.O. Paterson, C.R. Freeme, and C.P. Marais. The South African Mechanistic Design Procedure. Proc., 4th International Conference on the Structural Design of Asphalt Pavements, Univ. of Michigan, Ann Arbor, Vol. 2, 1977.
2. W.D.O. Paterson and J.H. Maree. An Interim Mechanistic Design Method. CSIR, Pretoria, South Africa, NITRR Tech. Rept. RP/5/78, April 1978.
3. J.H. Maree and C.R. Freeme. The Mechanistic Design Method Used to Evaluate the Pavement Structures in the Catalogue of the Draft TRH4 1980. CSIR, Pretoria, South Africa, NITRR Tech. Rept. RP/2/81, March 1981.
4. J.H. Maree. Design Parameters for Crusher Run in Pavements. Univ. of Pretoria, M.Sc. dissertation (in Afrikaans), Oct. 1978.
5. W.D.O. Paterson and D.J. Van Vuuren. Diagnosis of Working Strains in a Pavement Using Deflection Profiles. Proc., 7th Conference of Australian Road Research Board, Vol. 7, Part 6, 1974, pp. 128-144.
6. J.H. Maree and N.J.W. Van Zyl. The Heavy Vehicle Simulator Test on Freeway P157/1, near Jan Smuts Airport. CSIR, Pretoria, South Africa, NITRR Tech. Rept. RP/11/80, 1980.
7. C.R. Freeme, R.G. Meyer, and B. Shackel. A Method for Assessing the Adequacy of Road Pavement Structures Using a Heavy Vehicle Simulator. Presented at International Road Federation World Meeting, Stockholm, June 1-5, 1981.
8. P.A. D'Amato and M.W. Witczak. Analysis of In

Situ Granular-Layer Modulus from Dynamic Road-Rater Deflections. TRB, Transportation Research Record 755, 1980, pp 20-30.
9. J.E.B. Basson, O.J. Wijnberger, and J. Skultety. The Multi-Depth Deflectometer: A Multistage Sensor for the Measurement of Resilient Deflections and Permanent Deformation at Various Depths in Road Pavements. CSIR, Pretoria, South Africa, NITRR Tech. Rept. RP/3/81, Feb. 1981.
10. National Institute for Transport and Road Research. Structural Design of Interurban and Rural Road Pavements. CSIR, Pretoria, South Africa, Draft TRH4, 1980.
11. National Institute for Transport and Road Research. Standards for Road Construction Materials. CSIR, Pretoria, South Africa, Draft TRH14, 1980.

Publication of this paper sponsored by Committee on Strength and Deformation Characteristics of Pavement Sections.

Sulphlex Pavement Performance Evaluations from Laboratory Tests

JAMES A. SHERWOOD AND WILLIAM J. KENIS

New types of energy-saving materials are being developed for use in test sections within the U.S. road network. One of these materials, Sulphlex, has recently received a great deal of attention and is being developed as an alternative binder to asphalt and portland cement. Mechanical tests were conducted on specimens of asphalt concrete and Sulphlex 233 mixes. The mechanical tests conducted are those necessary to provide the material characterizations for input to the VESYS structural subsystem. The long-term predicted behavior of Sulphlex pavements was compared with that of conventional asphalt pavements for five different structural designs, on two different subgrades, and for three levels of temperature. A set of design criteria was selected to allow an analysis of the performance of each pavement.

In order to reduce the risk of unsatisfactory pavement performance to an acceptable level, engineers must be able to reliably predict pavement behavior over time. Current methods for predicting such behavior for different types of pavements, environments, and traffic loads are limited to what are known today as rational or, more precisely, mechanistic design procedures. The Federal Highway Administration (FHWA) has developed one such procedure called the VESYS structural subsystem, which predicts the pavement's behavior over time based on the mechanical properties of the layer materials, the anticipated traffic loads, and the local environmental conditions. Mechanistic design procedures are so called because they are in fact developed from the laws of mechanics in which the prescribed actions of forces on bodies of material elements are related to the resulting stress, strain, deformation, and failure of the total pavement structure. The properties of the material elements are determined by subjecting specimens of a given material to a series of laboratory load tests and applying the laws of mechanics for the prescribed geometry and environmental conditions. There are both advantages and disadvantages associated with mechanistic-type procedures. One of the most important advantages is that such procedures permit the use of completely new materials and/or new types of pavement structures.

Today, many new types of energy-saving materials are being developed, and test sections are being placed within the U.S. road network. For instance, improved technology and the energy crisis have provided the impetus for new binders, some of which are asphalts modified with sulfur (1) and other chemicals to improve their durability and performance. Polymer portland cement concretes (2) and concretes that use super water-reducing agents (3) are also being produced with properties quite different from those of conventional paving types. Recycled pavements conserve materials and, depending on the types, the quantity and quality of additives can be expected to perform as well as high-quality conventionally designed mixtures (4,5). Sulphlex (plasticized sulfur) is another new material that might be made to behave similarly to asphalt or portland cement concrete (6,7).

The purpose of this paper is to evaluate the results of a limited number of laboratory tests conducted by FHWA on Sulphlex and asphalt paving mixtures and to predict the performance of selected structural sections under simulated real-world conditions.

SULPHLEX AS BINDER AND MIX

The primary objectives of an initial FHWA study with Southwest Research Institute were to develop a system to modify sulfur so that it would serve as a binder replacement for asphalt and portland cement and to prepare mixtures of the developed binder with aggregates and measure their properties (6). To be used as a pavement binder, sulfur must be modified to exhibit more plastic characteristics. When elemental sulfur is heated to above its transition temperature of about 320°F and rapidly quenched at 68°F, it exhibits a plastic characteristic; hence, it may be called plasticized sulfur. If the material is allowed to return to room temperature, it quickly hardens and brittle sulfur crystals are formed; such a physical change does not lend itself to practical application in the preparation of binders for highway paving. The intent in this study was the conversion of sulfur to a plastic through a chemical reaction, a mechanical change, or a combination of these so that the resulting material at room temperature might have viscosity, penetration, and other characteristics similar to those of asphalt. During the course of the study, more than 450 different formulations were prepared by using combinations of 80 different modifiers. The most promising binders were selected to be evaluated for their behavior when mixed with a select aggregate. The results of laboratory tests conducted on

Table 1. Mix properties.

Mix Property	AC-20 (wt. %)		Sulphlex 233 (wt. %)		
	6.4	6	10.3	6	9
Air voids (%)	3.1	4.0	3.0	11.0	5.0
Stability (lb)	2600	2625	1850	1375	1880
Flow (0.01 in)	12.0	10.0	15.0	9.5	12.0
Voids in mineral aggregate (VMA) (%)	17.0	17.1	18.6	20.0	19.1
VMA filled (%)	83.5	77.5	84.0	42.5	72.5

both the Sulphlex binders and their mixes have been given elsewhere (6).

Further investigations of the behavior of Sulphlex 233 (a binder possessing intermediate properties) were undertaken by the Materials Division of FHWA's Office of Research (7). The objectives of this study were as follows:

1. To develop mixture design methods and establish mix design criteria for flexible Sulphlex paving mixtures and
2. To examine the chemical properties and behavior of Sulphlex binders that affect the engineering performance of the binders and their safe use in construction.

Work continued at FHWA through the efforts of the Pavement Systems Group of the Structures and Applied Mechanics Division. This effort is discussed in detail in this paper with the objective of predicting the in-service behavior of Sulphlex as compared with that of asphalt concrete pavement sections.

MATERIAL PROPERTIES

In order to determine the feasibility of using Sulphlex as a paving material, it is necessary that two different series of laboratory tests be conducted. The first series are those tests dealing with mix design, and the second series are those dealing with the mechanical properties used to predict the integrity of the materials when subjected to traffic loads in pavement structures. Each series, as applied to Sulphlex 233 mixes and AC-20 mixes, is discussed below.

Mix Design Tests

Two mix design methods were used to evaluate Sulphlex 233 mixes: the Marshall test (AASHTO T245) and the immersion-compression test (AASHTO T165). The aggregate used was a 3/8-in top-size trap rock (diabase) from Chantilly, Virginia, that had the gradation and other characteristics given by Leutz and Harrigan (7). The temperature-viscosity curves for Sulphlex 233 and AC-20 have also been given by Leutz and Harrigan (7). The Marshall test results (2) are summarized below:

Marshall Criterion	Optimum Weight Percent	
	AC-20	Sulphlex 233
Maximum density	6.9	11.4
Maximum stability	6.3	10.0
4 percent air voids	6.1	9.6
Avg	6.4	10.3

The mix properties at the optimum binder contents for the Marshall criteria and at the binder contents used for the test series are given in Table 1.

Results of the immersion-compression test series given elsewhere (7) suggested that the 9 percent by weight Sulphlex mix would require an antistripping agent. All Sulphlex mix specimens tested contained 1 percent hydrated lime as the antistripping agent.

The series of tests discussed above suggest that Sulphlex might be a practical paving material, based on stability and durability, provided an antistripping agent is used.

Mechanical Tests

The series of tests discussed here were performed specifically to provide input to the VESYS structural design subsystem. In VESYS three basic mechanical properties are required (8):

1. Relaxation (elastic) modulus or creep compliance: the elastic or viscoelastic parameters necessary for solutions to problems of stress-strain or deflection boundary values in a layered pavement system,
2. Fatigue properties: the coefficient and exponent of the fatigue equation for use in Miner's law to predict the occurrence of fatigue cracking in a layered pavement system, and
3. Permanent deformation properties: coefficient and exponent of the permanent deformation equation for use in the accumulative permanent deformation law to predict rutting of a layered pavement system.

Beam and cylindrical specimens were prepared in accordance with procedures defined in ASTM D3202 and ASTM D3496, respectively. The levels of Sulphlex binder evaluated were on an equal weight and volume basis by using 6 weight percent AC-20 as a control in comparison with 6 and 9 weight percent Sulphlex 233.

The beam specimens as molded were sawed in half, which yielded specimens approximately 1.70 in deep, 3.25 in wide, and 15 in long. A total of 54 beam specimens were available for test.

Preliminary testing, on trial 4x8-in cylinders without caps, showed that the strains on opposite sides were nearly the same. For this reason, the cylindrical specimens were tested as received, i.e., without capping. A total of 27 cylindrical specimens were available for testing.

Equipment

Equipment for testing beams in fatigue and cylindrical specimens for modulus and permanent deformation properties is described. The equipment developed for fatigue testing consisted of a non-servo-air arrangement capable of testing up to six beam fatigue specimens at one time. Six Bellofram arrangements were fabricated on a steel channel in a temperature-controlled chamber. Based on the work of Barksdale (9), five 1-in thick pieces of 50-durometer rubber (20 in long by 4 in wide) glued together and simply supported over a 10-in span provided an elastic foundation for each specimen (the modulus of reaction for this system was 448 pci at 70°F when loaded with a 1.25-in-diameter steel disk). The rubber was used to minimize permanent strains to simulate resilient responses associated in fatigue-type failures. Load was applied to a specimen that rested on the rubber at midspan through a 3x1.25-in steel bar. Load frequency in the form of square-wave pulses was controlled by an electronic pulsing circuit that operated a four-way solenoid valve for applying and releasing pressure (10). Figure 1 shows the FHWA multiple fatigue-testing system developed for this study. Dynamic strains in the lower fibers of the beams were measured by a 2-in active strain gage glued to the side of the beam at the center and near the bottom. A three-dummy bridge arrangement completed the cir-

cuit, and strains were recorded on oscillographs.

The equipment used to test cylindrical specimens was a servohydraulic system contained in a temperature-controlled cabinet. Measurements of vertical strain were made by two linear variable differential transformers (LVDTs) on opposite sides of the specimens. Vertical strain from each LVDT plus the load were recorded on oscillographs. Load was applied by a steel disk 4 in in diameter through a ball-bearing interface. Figure 2 is a photograph of the system to test cylinders by static and dynamic compressive loads at various temperatures.

Test Procedures

The beam and cylindrical specimens were tested at three temperatures: 40, 75, and 90°F. In the fatigue tests, different levels of constant dynamic load were applied to the beams so as to induce different peak-to-peak underside tensile strains. In this manner, various fatigue lives could be attained. Load duration was set at 0.1 s with a 0.9-s rest period. The beam specimens were placed on the rubber with strain gage attached and allowed to reach test temperature.

Cylinders were brought to test temperature with LVDTs mounted. Typically, three 5-min creep tests were run at the specified load to condition the specimen. Then a 1000-s creep test was run, which served as a basis for the creep compliances presented in this report. In the creep tests the load was applied in a quick ramp fashion, with full load in 0.01 s. On rebound of the 1000-s creep test, the repeated-load tests were conducted, usually for at least 100 000 cycles. Haversine load pulses were applied once per second with a duration of 0.1 s. A 2-psi preload was used throughout all tests to keep the load disk and specimen in contact. Figure 3 shows a typical load history used to test cylindrical specimens. The cylinders were tested at 10, 20, 30, and 50 psi load levels, depending on temperature.

Laboratory Test Results

In the beam fatigue tests, dynamic and permanent tensile strains near the bottom were recorded versus the number of repetitions to failure. Compressive strains with time were measured in the sustained-load tests on cylindrical specimens. In the repeated-load tests on cylindrical specimens, the

Figure 1. FHWA multiple fatigue-testing apparatus.

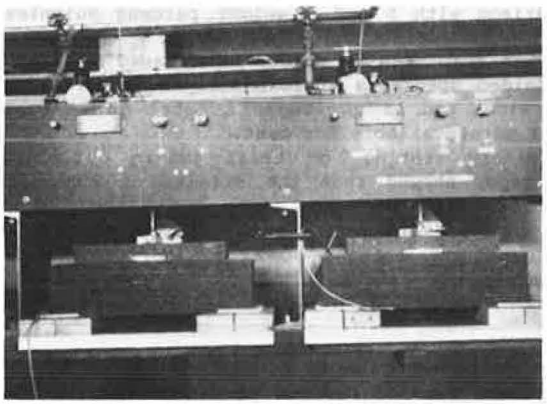

Figure 2. Equipment for compression testing of cylinders.

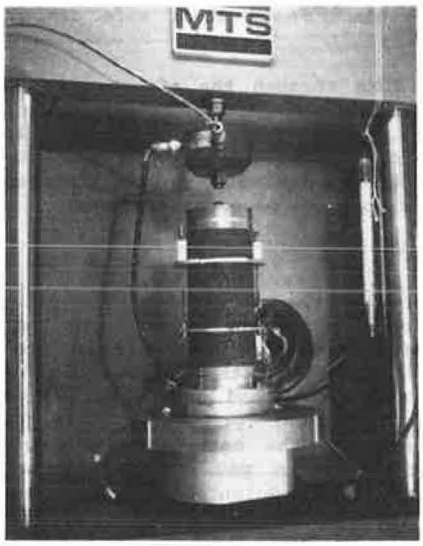

Figure 3. Typical loading for testing cylindrical specimens.

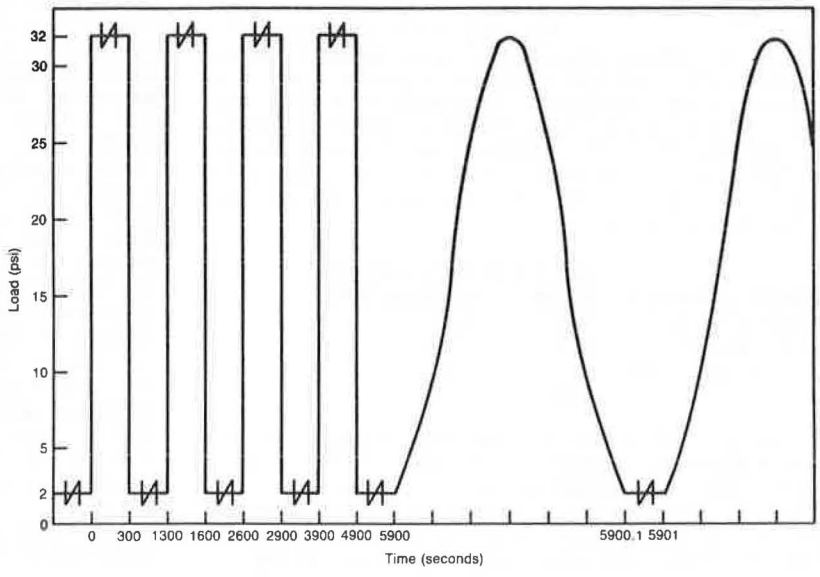

dynamic and permanent compressive strains were recorded versus load repetitions.

Fatigue Properties of Beams

The peak-to-peak or dynamic strain (e) for each specimen was measured at the 2000th repetition, since this was typically the minimum value that lasted until the failure stage. This value for each beam was plotted versus the number of loads to failure (the only exception was whether the beam was in the failure stage prior to 2000 repetitions, in which case the minimum strain was plotted). The results of the fatigue tests are shown in Figures 4-6. There is a clear separation between the Sulphlex and asphalt fatigue lives at each temperature. The fatigue coefficient K_1 and exponent K_2 representing each curve are given in Table 2. Definition of the fatigue equation is given as follows:

$$N_f = K_1 (1/e)^{K_2} \quad (1)$$

where

N_f = number of cycles to failure,
e = peak-to-peak dynamic strain experienced at underside of beam,
K_2 = absolute value of inverse of slope of fatigue line,
$K_1 = N_0 e_0^{K_2}$, and
N_0, e_0 = number of repetitions and strain at the vertical reference axis.

Note that at a given strain level, the asphalt mix possesses the greatest resistance to fatigue, whereas the 6 percent Sulphlex possesses the least. Conclusions regarding field fatigue behavior should not be drawn from these determinations, since the interactions of layer moduli and thickness play an important role in the design process.

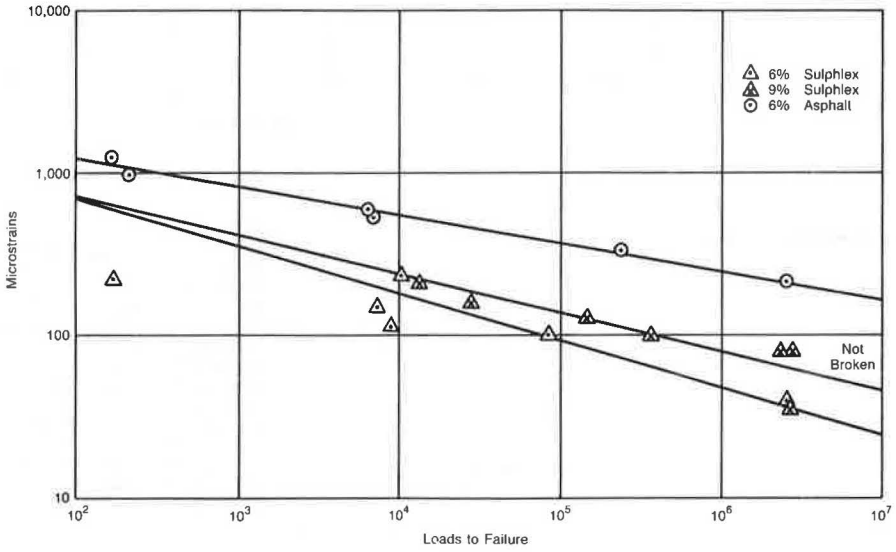

Figure 4. Fatigue tests at 40° F.

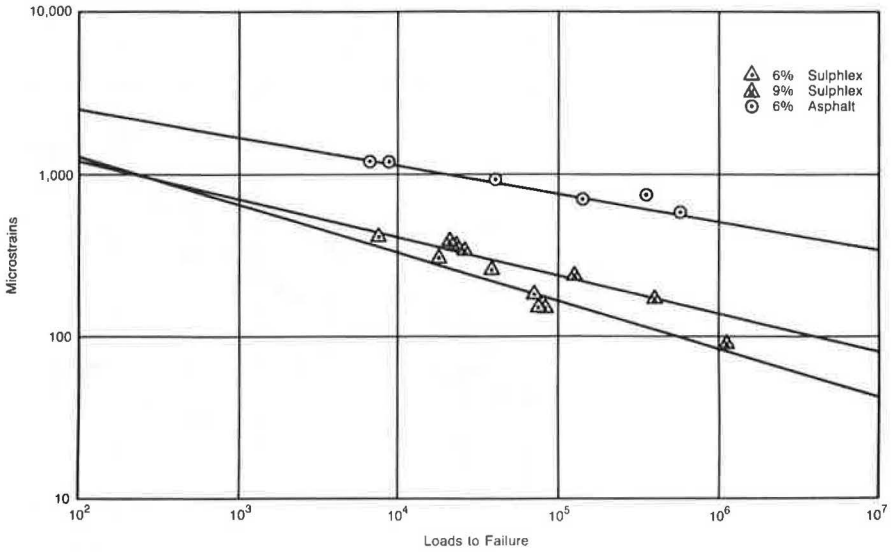

Figure 5. Fatigue tests at 75° F.

Creep Properties of Cylinders

Creep compliance is defined as follows:

$$D(t) = e(t)/\sigma \quad (2)$$

where σ is the applied sustained compressive stress and e(t) is the resulting time-dependent strain.

Creep compliance curves are given in Figures 7-9 for each mix at the three different temperatures.

Figure 6. Fatigue tests at 90° F.

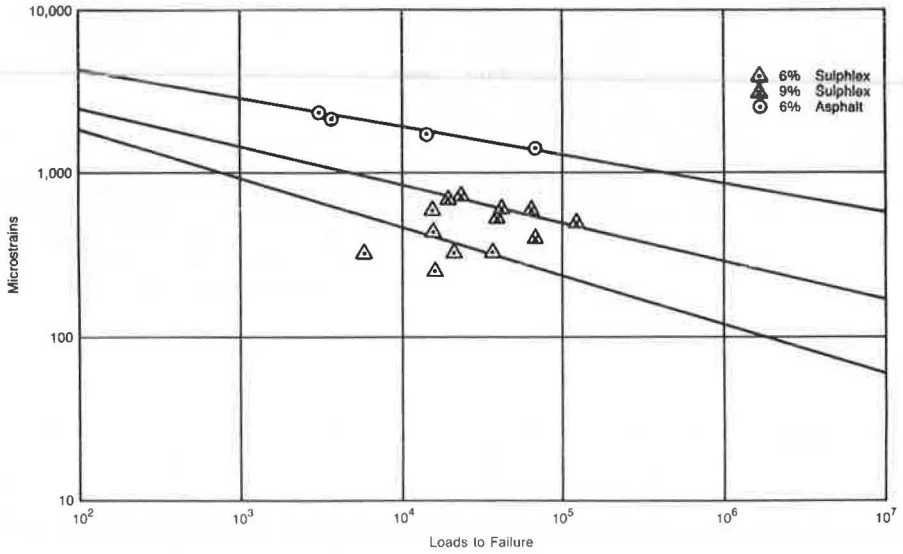

Table 2. Surface materials characterization.

Binder	Temperature (°F)	Fatigue K_1	Fatigue K_2	Permanent Deformation GNU	Permanent Deformation ALPHA	Modulus (psi)
6 percent Sulphlex	40	1.92×10^{-9}	3.39	0	1	3 000 000
	75	1.49×10^{-8}	3.39	0.032	0.63	1 250 000
	90	4.91×10^{-8}	3.39	0.09	0.76	430 000
9 percent Sulphlex	40	5.08×10^{-12}	4.22	0.035	0.45	5 000 000
	75	4.57×10^{-11}	4.22	0.0236	0.51	1 100 000
	90	9.00×10^{-10}	4.22	0.139	0.57	348 000
6 percent asphalt	40	5.77×10^{-16}	5.92	0.038	0.54	1 730 000
	75	3.75×10^{-14}	5.92	0.057	0.72	337 000
	90	8.56×10^{-13}	5.92	0.111	0.58	124 000

Figure 7. Creep compliance, 6 percent Sulphlex.

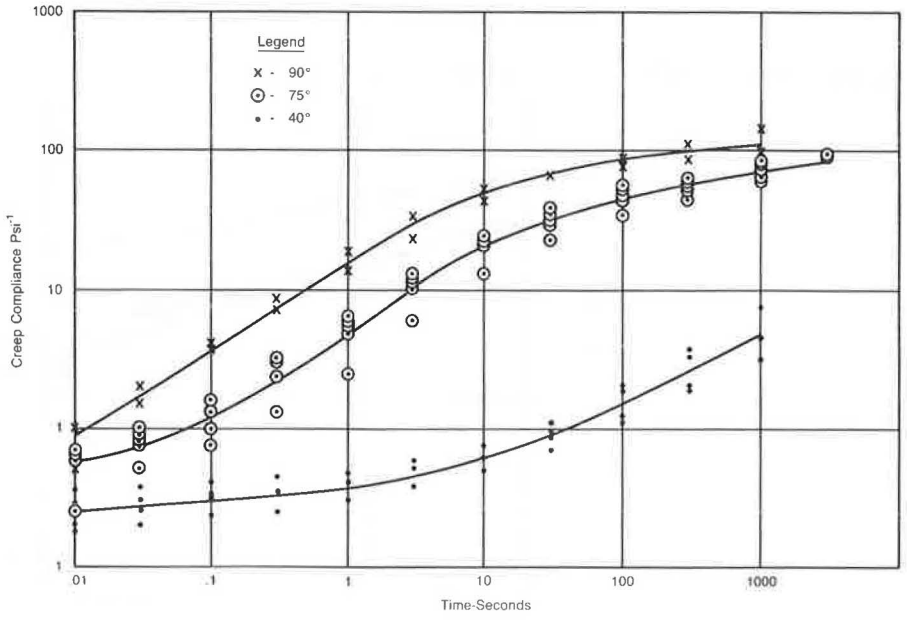

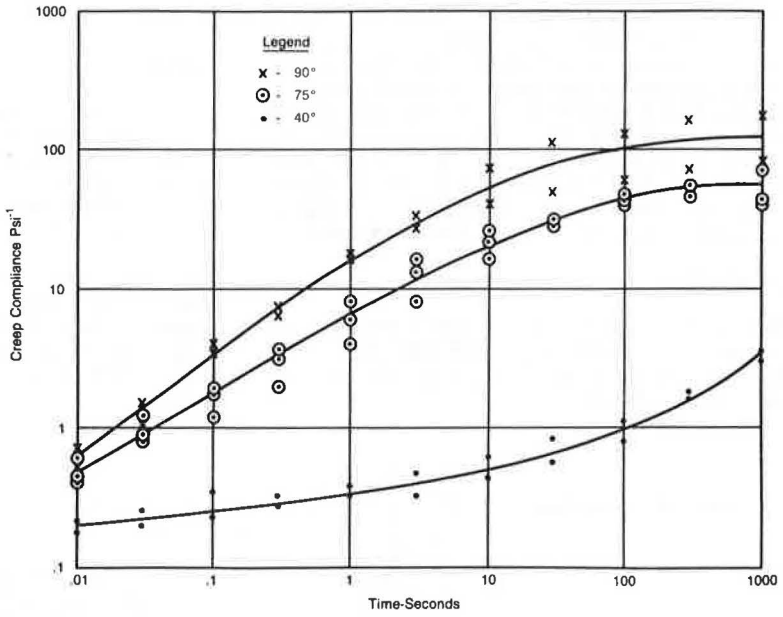

Figure 8. Creep compliance, 9 percent Sulphlex.

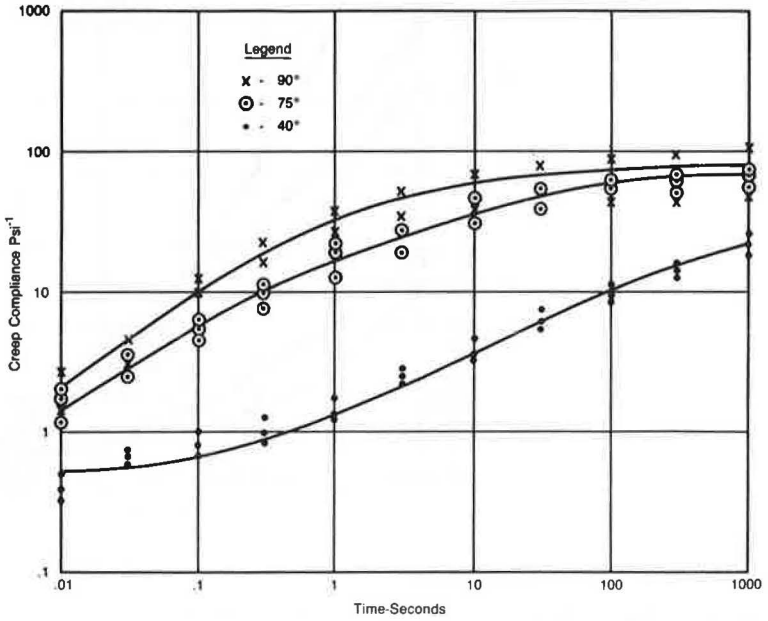

Figure 9. Creep compliance, 6 percent asphalt.

At all temperatures, the mixes are dependent on loading time. In general, the asphalt mix at a given temperature has higher creep compliances (lower moduli) at low loading times. In physical terms, this would mean that under moving traffic, Sulphlex would be the more desirable paving material, i.e., it would have the higher modulus. However, under stationary traffic, Sulphlex would exhibit continued creep and may not be so desirable. There is very little difference between the creep curves for 6 percent and 9 percent Sulphlex.

Modulus Properties

Three different measures of this property are reported:

- $|E^*|$ = magnitude of the complex modulus (dynamic modulus) measured at the 200th repetition in the permanent deformation tests,
- $E(0.03)$ = relaxation modulus taken as the inverse of the creep compliance measured at 0.03 s of the creep compliance curve, and
- M_r = resilient modulus as obtained by using the Schmidt device for 0.1-s loading time (2).

The resilient modulus was obtained from an FHWA report (2). Averages for $|E^*|$ and M_r are given in Figure 10 for each mix, from which it is clear that the Sulphlex mixes exhibit predominantly higher modulus values than the asphalt mixes at all temperatures. The M_r tests (Schmidt) yielded

moduli for 6 percent Sulphlex just slightly greater than those for 9 percent Sulphlex; however, the dynamic tests yielded significantly higher moduli for 9 percent Sulphlex at the lower temperatures.

The relaxation and dynamic moduli were determined on specimens aged up to 35 days, whereas the M_r tests were run on specimens aged up to 75 days; thus no significant aging susceptibility is evident. Figure 10 depicts significant temperature susceptibility (9 percent Sulphlex exhibits the greatest).

Permanent Deformation Properties

Based on the assumed linear relationship between the permanent strain per pulse (e_p) and the number of load repetitions (N) on a log-log plot, the following equation may be stated:

$$e_p = e_\mu N^{-\alpha} \quad (3)$$

where

e = dynamic strain measured at the 200th repetition,
α = 1 - slope(s), and
μ = (Is/e), where I is the permanent strain after the first repetition (intercept on log-log plot).

To determine the permanent deformation properties ALPHA (α) and GNU (μ) for the three mixes, repeated-load tests were conducted at seven combinations of temperature and stress: 40°F (30 and 50 psi); 75°F (10, 20, and 30 psi); and 90°F (10 and 30 psi).

Figure 10. Effect of temperature on modulus.

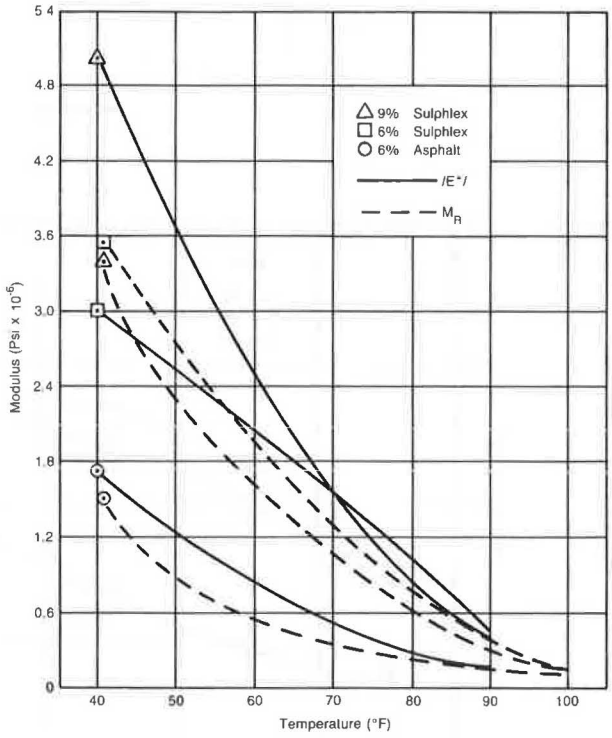

Figure 11. Permanent deformation tests at 40° F.

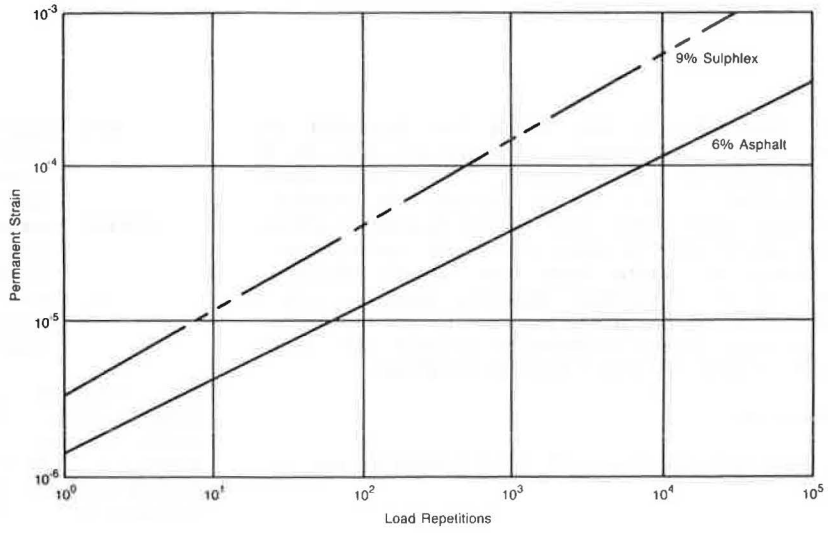

Straight lines on log-log paper of accumulated strain versus N were fitted to the data to define the slope and the intercept. Dynamic strains were measured at the 200th repetition. These numbers were used to calculate GNU and ALPHA in accordance with Equation 3. The permanent deformation properties reported in Table 2 for each binder at the three temperatures are averages of those found at the stress levels tested. These average values were used to plot accumulated strain versus N as shown in Figures 11-13. The dynamic strains (e) used to define these lines were computed for each binder and temperature by using the moduli reported in Table 2 and a stress level of 30 psi.

Six percent Sulphlex experienced the least permanent strain at all temperatures. At 40°F, 6 percent Sulphlex showed no permanent strain before 10 000 repetitions. Sudden periodic increments of accumulated deformation that took place after 10 000 repetitions could possibly be attributed to slippage within the mix instead of plastic flow. Thus, no line is shown in Figure 10 (dynamic tests at 40°F) for 6 percent Sulphlex.

VESYS DESIGN FACTORIAL

The VESYS III-A structural subsystem was used as an analysis method to predict the performance of the three mixes; the properties were tested at the three temperatures given in Table 2. Five structural designs, given in Table 3, were analyzed on a weak and a strong subgrade. The properties of the three base courses are representative of crushed-stone, cement-treated, and cement-concrete materials. The weak subgrade represents clay at 23 percent moisture content (5 ksi), and the strong subgrade represents the same clay at 16 percent moisture (45 ksi). The total factorial consisted of 90 separate analyses. The subgrade properties, load magnitude, traffic rate, and all other data input to the analysis were the same as for the design example in Chapter 6 of the VESYS User's Manual (8).

To evaluate the damage predictions, design criteria over eight years of service (6.6 million axles) were set as follows:

1. Maintain the fatigue damage index below 1 and
2. Maintain rut depth less than 0.60 in.

Figure 12. Permanent deformation tests at 75° F.

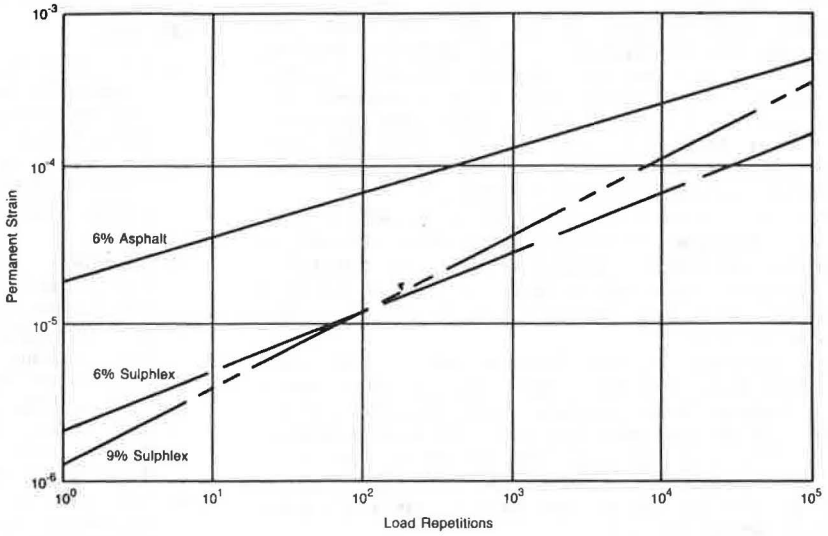

Figure 13. Permanent deformation tests at 90° F.

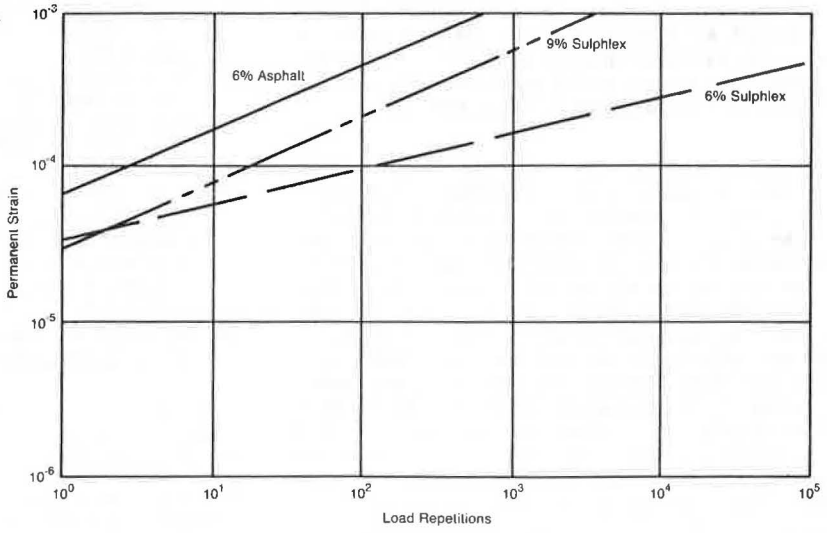

Table 3. Pavement structures for VESYS design factorial.

Pavement Property	Structural Design 1	2	3	4	5
Surface thickness (in)	6	3.5	6	3.5	2
Base thickness (in)	8	18	8	18	12
Base modulus (ksi)	59	59	350	350	1000
Base GNU	0.055	0.055	0	0	0
Base ALPHA	0.73	0.73	1	1	1

Table 4. Evaluation of VESYS design factorial.

Binder	Design Criterion	Structural Design[a] 1 W	1 S	2 W	2 S	3 W	3 S	4 W	4 S	5 W	5 S
6 percent asphalt	Fatigue	*	*	*	*	*	*	*	*	*	*
	Rutting	-	*	-	*	-	*	*	*	*	*
9 percent Sulphlex	Fatigue	-	-	-	-	*	*	*	*	*	*
	Rutting	-	*	-	*	-	*	*	*	*	*
6 percent Sulphlex	Fatigue	-	-	-	-	-	-	-	-	*	*
	Rutting	*	*	*	*	*	*	*	*	*	*

[a]W = weak subgrade; S = strong subgrade. * = satisfies criterion; - = does not meet criterion.

The acceptable designs based on these criteria are indicated in Table 4. A particular design was considered unacceptable if it did not meet the criteria at all temperatures. All pavement designs evaluated with a 6 percent asphalt concrete surface course satisfy the fatigue-cracking criterion (it should also be mentioned that these same pavement designs meet this criterion for 19 years and 20.5 million axles). Designs 1, 2, and 3, however, do not satisfy rutting on the weak subgrade.

The 9 percent Sulphlex designs 3, 4, and 5 satisfy the fatigue criterion; however, design 3 experiences excessive rutting on the wet subgrade. The 9 percent Sulphlex designs 1 and 2 satisfy rutting on the strong subgrade but do not meet the fatigue criterion.

All 6 percent Sulphlex designs satisfy the rutting criterion; however, only design 5 reduces tensile strains in the surface layer sufficiently to maintain the damage index below 1. At high temperatures on the weak subgrade for design 5, the surfaces are always in compression and the tensile stress at the bottom of the base is only 83 psi, thus eliminating fatigue.

An economic evaluation would be required to determine the best alternative design. This would involve comparing the total cost of the acceptable pavements. As an example, a maintenance policy could be adopted to smooth surfaces and to apply a thin overlay to pavement design 2 (3.5-in surface). Such a maintenance policy would restore ride quality and still meet the fatigue-cracking criterion.

CONCLUSIONS

The goal of this research is to provide guidance on Sulphlex pavement design for preliminary construction experiments. In conclusion, 6 percent Sulphlex exhibited the best rutting performance but had the least resistance to fatigue cracking, and 9 percent Sulphlex was similar to asphalt-concrete rutting but had worse fatigue performance. Because the fatigue criterion for the Sulphlex sample pavements analyzed was seldom satisfied, it is recommended that pavement design minimize tensile strains in this material by using thin surfaces over a stiff base course. The sample design procedure presented could serve as a basis on which the state could conduct their own analyses for local materials, traffic, and environment. Each designer should generate feasible alternatives and select the most desirable one by predicting distress and evaluating the economic impacts of construction plus maintenance.

REFERENCES

1. D.E. Pickett, D. Saylak, R.L. Lytton, W.E. Conger, D. Newcomb, and R.A. Shapery. Extension and Replacement of Asphalt Cement with Sulfur. FHWA, Final Rept. FHWA-RD-78-95, March 1978.
2. K.C. Clear and B.H. Chollar. Styrene-Butadiene Latex Modifiers for Bridge Deck Overlay Concrete. FHWA, Interim Rept. FHWA-RD-78-35, April 1978.
3. D. Whiting. Evaluation of Super-Water Reducers for Highway Applications. FHWA, Final Rept. FHWA/RD-80/132, March 1981.
4. R.J. Holmgreen, J.A. Epps, D.N. Little, and J.W. Button. Recycling Agents for Recycled Bituminous Binders. FHWA, Final Rept. FHWA/RD-82/010, Dec. 1980.
5. J.A. Epps, R.J. Holmgreen, D.N. Little, and R.L. Terrel. Guidelines for Recycling Pavement Materials. NCHRP, Rept. 224, Sept. 1980.
6. A.C. Ludwig, B.B. Gerhardt, and J.M. Dale. Materials and Techniques for Improving the Engineering Properties of Sulfur. FHWA, Final Rept. FHWA/RD-80/023, June 1980.
7. H.J. Lentz and E.T. Harrigan. Laboratory Evaluation of Sulphlex-233: Binder Properties and Mix Design. FHWA, Final Rept. FHWA/RD-80/146, Jan. 1981.
8. W.J. Kenis. Predictive Design Procedures, VESYS User's Manual: An Interim Design Method for Flexible Pavements Using the VESYS Structural Subsystem. FHWA, Final Rept. FHWA-RD-77-154, Jan. 1978.
9. R.D. Barksdale and J.H. Miller II. Development of Equipment and Techniques for Evaluating Fatigue and Rutting Characteristics of Asphalt Concrete Mixes. Georgia Department of Transportation, Atlanta, Res. Project 7305, Final Rept., June 1977.
10. W. Bralove. New Fatigue Test Equipment. FHWA Tech. Notes, March 1981.

Publication of this paper sponsored by Committee on Strength and Deformation Characteristics of Pavement Sections.